

# **Macrophytes in estuarine gradients**

## **Flow trough flexible vegetation**

Proefschrift

ter verkrijging van de graad van doctor  
aan de Technische Universiteit Delft,  
op gezag van de Rector Magnificus prof.ir. K.C.A.M. Luyben,  
voorzitter van het College voor Promoties,  
in het openbaar te verdedigen op dinsdag 6 maart 2012 om 15:00 uur

door

Jasper Tjaard DIJKSTRA

civil ingenieur

geboren te Vlissingen

Dit proefschrift is goedgekeurd door de promotoren:

Prof.dr.ir. M.J.F. Stive

Prof.dr.ir. W.S.J. Uijtewaal

Samenstelling promotiecommissie:

Rector Magnificus	voorzitter
Prof.dr.ir. M.J.F. Stive	Technische Universiteit Delft, promotor
Prof.dr.ir. W.S.J. Uijtewaal	Technische Universiteit Delft, promotor
Prof.dr. H.M. Nepf	Massachusetts Institute of Technology, Boston, USA
Prof.dr. P.J.M. Herman	Radboud Universiteit Nijmegen
Prof.dr.ir. H.J. de Vriend	Technische Universiteit Delft
Dr.ir. R.E. Uittenbogaard	Deltares
Dr. M.M. van Katwijk	Radboud Universiteit Nijmegen
Prof.dr.ir. A.E. Mynett	Technische Universiteit Delft

R.E. Uittenbogaard en T.J. Bouma hebben als begeleiders in belangrijke mate aan de totstandkoming van het proefschrift bijgedragen.

Dit onderzoek is ondersteund door de Nederlandse Organisatie voor Wetenschappelijk Onderzoek (NWO) onder nummer 014.27.014 in het kader van het LOICZ-programma.

ISBN 978-90-8570-981-7

Cover design by Edwin Sturm, SturmDesign

Printed by CPI Wöhrmann

Copyright © J.T. Dijkstra, 2012

## Preface

This Ph.D. thesis is one of the products of the research project ‘Macrophytes in Estuarine Gradients’; supported under grant number 014.27.014 from the Dutch science foundation NWO within the LOICZ (Land-Ocean Interactions in the Coastal Zone) program. The project was executed in co-operation with Radboud University Nijmegen, Wageningen University & Research Centre, the Netherlands Institute for Ecological Research – Centre for Estuarine and Marine Ecology (NIOO-CEME) and WL|Delft Hydraulics, later Deltares. Within the same research project another thesis was written by *Van der Heide [2009]*, who focused on stressors and feedbacks in temperate seagrass ecosystems. Next to these studies, there has been a link with the research of *Suzuki [2011]* at TU Delft on wave damping by vegetation.



## Abstract

Aquatic plants –or macrophytes- are an important part of coastal, estuarine and freshwater ecosystems worldwide, both from an ecological and an engineering viewpoint. Their meadows provide a wide range of ecosystem services: forming a physical protection of the shoreline, enhancing water quality and harbouring many other organisms. Unfortunately, these vegetations such as salt marshes, seagrasses or mangroves have been on the decline as a result of anthropogenic pressure and climate change, despite costly conservation and restoration efforts.

The low success rate of these efforts might partially be due to a lack of understanding of the complex bio-physical interactions between plant properties, plant growth, hydro- and morphodynamics and water quality. The capability of plants to alter their abiotic environment via these interactions is referred to as ‘ecosystem engineering’. Many experimental studies, both in the field and in laboratory flumes, have been performed to unravel these interactions. Since such experiments are always hampered by practical limitations such as flume dimensions, available time, or uncontrolled conditions, this knowledge cannot always be generically applied.

Therefore, the primary objective of this study is to develop a generically applicable model for feedbacks between flexible macrophytes and their physical environment. To warrant this general applicability under the various circumstances occurring in estuaries, the model development follows a process based approach; a data-orientated approach is merely applicable to known conditions. Modelling starts out on the scale of one plant to finish at the scale of a meadow. The focus is on seagrass, as seagrasses are well studied, highly flexible, have a relatively simple shape and are among the most productive as well as threatened ecosystems.

The first step was to create the numerical model called ‘Dynveg’, by combining a novel dynamic plant bending model based on a Lagrangian force balance to an existing 1DV  $k-\epsilon$  turbulence model (Chapter 2). The plant bending model is based on measurable biomechanical properties of plants: length, width, thickness, volumetric density and the elasticity modulus. Because very flexible plants can assume a position almost parallel to the flow direction, friction too needed to be incorporated rather than pressure drag alone. Flume measurements on strips of eelgrass-like proportions provided the actual values for drag- and friction coefficients, as well as validation data for predicted strip positions and forces. The effect of multiple plants on hydrodynamics was incorporated by assuming that all plants in a meadow do the same, and by defining two turbulence length scales: One for internally generated turbulence, related to the wakes behind individual stems, and one for larger eddies created in the shear layer above, penetrating the canopy depending on the space between the stems. Dynveg compared favourably with the measurements of hydrodynamic characteristics in mimicked eelgrass by *Nepf & Vivoni [2000]*.

Next, Dynveg was combined with the large-scale hydro- and morphodynamic model Delft3D to simulate two-dimensional spatial processes in and around meadows of flexible macrophytes (Chapter 3). The leading principle for this integration is the conditional similarity between flow characteristics in flexible vegetation and those in rigid vegetation: If the rigid vegetation has *i)* the same height as the deflected vegetation, *ii)* its plant volume redistributed over the vertical

accordingly and *iii*) a drag coefficient representative of the streamlined shape, the flow is practically analogous for a range of plant properties and hydrodynamic conditions. This modelling method was validated by comparing model results with flume experiments on two seagrass species, showing good agreement for canopy height, flow velocity profile and flow adaptation length.

A field measurement campaign in a French macrotidal bay bordered by an eelgrass meadow provided validation data for application to real meadows (Chapter 5). Along with a detailed bathymetry survey by jetski, time-series of flow velocity and sediment dynamics inside a meadow and over a bare adjacent area were measured over two tidal periods. The applied sediment transport formula [van Rijn, 1993] deals with vegetation effects on sediment pick-up and transport via the effects of plants on hydrodynamics. Vegetation-specific interactions such as particle trapping by blades or flow intensification directly around shoots were not taken into account. Nevertheless, the three-dimensional numerical model was able to reproduce the main features of the observations, indicating that the processes of vegetation bending in non-stationary flow and sediment transport through vegetated areas are incorporated correctly.

Thus, the objective of making a model for feedbacks between flexible macrophytes and their physical environment has been met. The model can be applied as a tool in conservation and restoration studies or in long-term biogeomorphological feedback studies. Recommended extensions are the incorporation of plant-wave interactions, more intricate plant morphologies and a vegetation-specific transport formula.

The second objective of this thesis was to use the developed model(s) as a tool to learn more about biophysical interactions under different conditions. In Chapter 4, Dynveg and the two-dimensional model were used to assess the ecosystem engineering capacities of three plant species that partly co-occur in temperate intertidal areas: the stiff *Spartina anglica*, the short flexible seagrass *Zostera noltii* and the tall flexible seagrass *Zostera marina*. The flow velocity inside the canopy, the canopy flux and the bed shear stress were used as proxies for the species' ability to respectively absorb hydrodynamic energy, the supply of nutrients or sediment and the ability to prevent erosion.

This analysis showed that a species' eco-engineering capacities depend on its spatial density, its size, its structural rigidity and its buoyancy, but also on environmental conditions. Therefore, biomass, leaf area index or other lumped parameters that neglect structural properties are no good generic indicators of ecosystem engineering capacities.

Rigid plants have more potential to trap sediment due to a higher canopy flux than flexible plants. This canopy flux showed to be inversely related to spatial density along the entire natural range. For flexible plants, the canopy flux is only related to density in relatively sparse meadows; in denser meadows the canopy flux is constant with increasing density. Flexible plants are better at preventing erosion because they are more efficient in reducing bed shear stresses than rigid plants. For very thin plants, buoyancy is the most important determinant of position in given flow conditions. For intermediate flexible plants, the structural rigidity is the most influential parameter, whereas for (nearly) rigid plants, the spatial density is dominant.

In Chapter 6, the three-dimensional model of the macrotidal bay was used to study the effects of different types of macrophytes on (residual) sediment transport and light availability. The effects of the real, relatively sparse eelgrass meadow were compared to those of a meadow with rigid plants of the same spatial density, with a dense eelgrass meadow, and with a bare bed. Though the differences between these four vegetation scenarios were small –only a few percent– the consequences on long timescales can be considerable.

In deep water, sparse flexible vegetation kept more sediment inside the bay than rigid or denser plants. When vegetation only occupies a small part of the water column, plants prevent erosion rather than promote deposition and they have more effect on bed-load transport than on the transport of suspended sediment. Stiff and denser plants affect the bed-load more than sparse flexible vegetation, thereby blocking the transport from outside to inside. The presence of dense or stiff macrophytes increased the light availability at the bed over a tidal cycle up to 7% with respect to a bare bed. The increase of light availability was less pronounced for the relatively open eelgrass meadow: up to 3%.

Overall, this study has resulted in a widely applicable model for the interactions between flexible aquatic plants, flow and sediment transport and in more insight in some of these interactions. Other researchers are encouraged to use this tool complementary to fieldwork and laboratory experiments, and to extend it with other functionalities, e.g. for wave attenuation or vegetation development.



## Samenvatting

Waterplanten –ook wel aquatische macrofyten genoemd– spelen zowel in ecologisch als in waterbouwkundig opzicht een belangrijke rol in natte ecosystemen. Een veld waterplanten levert verschillende ecosysteem diensten: fysieke oeverbescherming, verbetering van de waterkwaliteit en huisvesting van vele andere organismen. Echter, zeegrasvelden, schorren en mangrovebossen nemen af onder druk van menselijke invloeden, ondanks kostbare inspanningen voor bescherming en herstel.

Het beperkte succes van deze inspanningen is deels te wijten aan een beperkt begrip van de complexe bio-fysische interacties tussen planteigenschappen, de groei van planten, hydro- en morfodynamica en waterkwaliteit. Planten die hun abiotische omgeving door deze interacties kunnen veranderen worden ‘ecosysteemingenieurs’ of ‘eco-ingenieurs’ genoemd. Zulke interacties zijn het onderwerp van veel experimentele studies, zowel in het veld als in laboratoria. De kennis die deze experimenten opleveren kan echter niet altijd breed toegepast worden vanwege praktische beperkingen, zoals oncontroleerbare omstandigheden, tijd en afmetingen van stroomgoten.

Het hoofddoel van deze studie is daarom het ontwikkelen van een breed toepasbaar model voor terugkoppelingen tussen flexibele macrofyten en hun fysieke omgeving. Om deze brede toepasbaarheid onder de vele in estuaria voorkomende condities te waarborgen, volgt de ontwikkeling van dit model een proces-gebaseerde aanpak; een data-gebaseerde aanpak is vooral geschikt voor bekende omstandigheden. De schaal van modelleren is in het begin die van één enkele plant, later is dit uitgebreid naar een heel veld. De nadruk ligt op zeegras, omdat zeegrassen goed bestudeerd en gedocumenteerd zijn, ze zijn erg flexibel, hebben een simpele vorm en ze vormen één van de meest waardevolle maar ook bedreigde ecosystemen.

De eerste stap was het combineren van een bestaand eendimensionaal  $k-\epsilon$  turbulentiemodel met een nieuw numeriek model voor dynamische plantbuiging, gebaseerd op een Lagrangiaanse krachtenbalans (hoofdstuk 2). Het resulterende model, ‘Dynveg’ genaamd, is gebaseerd op meetbare fysieke eigenschappen van planten: lengte, breedte, dikte, soortelijk gewicht en elasticiteitsmodulus. Omdat zeer flexibele planten een oriëntatie parallel aan de stromingsrichting aan kunnen nemen was het nodig niet alleen krachten als gevolg van een drukverschil te modelleren, maar ook als gevolg van wrijving. Metingen in een stroomgoot aan stroken materiaal vergelijkbaar met zeegras leverden exacte waarden voor deze druk- en wrijvingscoëfficiënten, en validatiedata voor berekende krachten en posities van nepplanten. Het effect dat meerdere planten op de hydrodynamica hebben is meegenomen onder de aanname dat alle planten in een veld zich hetzelfde gedragen, en door twee lengteschalen voor turbulentie te definiëren: Eén voor intern gegenereerde turbulentie, gerelateerd aan de wervels achter individuele bladen, en één voor grotere wervels die het veld binnendringen vanuit de bovenliggende waterlaag, afhankelijk van de ruimte tussen de bladen. De berekeningen van Dynveg waren goed vergelijkbaar met metingen in kunstmatig zeegras van *Nepf & Vivoni [2000]*.

In de volgende stap (hoofdstuk 3) werd Dynveg gecombineerd met het grootschalig hydro- en morfodynamisch model Delft3D om tweedimensionale ruimtelijke processen in en rondom velden

van flexibele macrofyten te kunnen simuleren. Als leidend principe voor deze integratie is de conditionele overeenkomst tussen stroming in flexibele en stijve vegetatie: Als stijve vegetatie *i)* dezelfde hoogte heeft als de gebogen vegetatie, *ii)* dezelfde verdeling van plantvolume heeft over de verticaal en *iii)* een wrijvingscoëfficiënt heeft representatief voor de gestroomlijnde vorm, is de stroming praktisch gelijk voor een veelheid aan planteigenschappen en stromingscondities. Deze methode is gevalideerd door modelresultaten te vergelijken met metingen aan twee zeegrassoorten in een stroomgoot, en gaf een goede overeenkomst in planhoogte, stroomsnelheidsprofiel en aanpassingslengte van de stroming.

Veldmetingen in en rond een veld *Zostera marina* in de getij-gedomineerde Baie de l'Écluse (Frankrijk) leverde validatiedata voor een toepassing van dit gecombineerde model in een echt macrofytenveld (hoofdstuk 5). Naast het gedetailleerd inmeten van de bathymetrie met een jetski, werden gedurende twee getijperioden tijdreeksen van stroomsnelheid en –richting en sedimentconcentratie gemeten in een begroeid en in een naastgelegen kaal transect. De gebruikte sedimenttransportformule [van Rijn, 1993] houdt rekening met de effecten van vegetatie op resuspensie en transport via de hydrodynamica. Specifieke plant-sediment interacties zoals het botsen van deeltjes met bladen of versnelling van de stroming direct naast de plant, zijn hier niet in verwerkt. Desondanks was het driedimensionale model in staat de belangrijkste patronen uit de metingen te reproduceren, wat er op wijst dat plantbuiging in niet-stationaire omstandigheden en sedimenttransport door vegetatie juist gesimuleerd worden.

Daarmee is het eerste doel van dit onderzoek –het maken van een model voor terugkoppelingen tussen flexibele waterplanten en hun fysieke omgeving- behaald. Dit model kan gebruikt worden om te bestuderen hoe toekomstige beschermings- en herstelinspanningen het effectiefst uitgevoerd kunnen worden, of voor studies naar biogeomorfologische terugkoppelingen op langere termijn. Het is aan te raden dit model uit te breiden met formuleringen voor de interactie tussen planten en golven, mogelijkheden om planten met een gecompliceerdere vorm te simuleren en een sedimenttransportformule die expliciet rekening houdt met vegetatie.

Het tweede doel van dit onderzoek was het toepassen van de ontwikkelde modellen om zo meer te weten te komen over biofysische terugkoppelingen in verschillende omstandigheden. In hoofdstuk 4 zijn Dynveg en het tweedimensionale model gebruikt om de eco-ingenieurscapaciteiten van drie plantsoorten die in intergetijdegebieden in gematigde streken voorkomen: het stijve slijkgras *Spartina anglica*, het korte flexibele zeegras *Zostera noltii* en het lange flexibele zeegras *Zostera marina*. De stroomsnelheid binnenin het veld, de flux door het veld en de bodemschuifspanning zijn gebruikt als maatstaf voor de mogelijkheid van een soort om respectievelijk energie uit stroming te absorberen, sediment of nutriënten in te vangen en erosie te voorkomen.

Uit deze analyse bleek dat de eco-ingenieurscapaciteit van een soort afhangt van zijn ruimtelijke dichtheid, zijn afmetingen, zijn buigstijfheid en zijn drijfvermogen, maar ook van de omstandigheden. Daarom zijn biomassa, een bladoppervlakteindex of andere parameters die structurele eigenschappen negeren geen goede indicatoren van eco-ingenieurscapaciteiten.

Stijve planten hebben een groter potentieel voor het invangen van sediment dan flexibele planten, als gevolg van een grotere flux door het veld. Deze flux bleek omgekeerd evenredig met het aantal planten per vierkante meter over het gehele scala aan natuurlijke dichtheden. Bij flexibele planten is deze flux alleen bij schaarse bedekkingen gerelateerd aan de ruimtelijke dichtheid; in dichtere velden blijft de flux constant bij toenemende dichtheid. Flexibele planten zijn beter in het voorkomen van erosie doordat ze de bodemschuifspanning sterker reduceren dan stijve planten. Voor zeer dunne, dus zeer flexibele, planten, is, gegeven de stromingscondities, drijfvermogen de belangrijkste factor voor de oriëntatie en daarmee het stromingspatroon. Voor gemiddeld flexibele planten is de buigstijfheid de belangrijkste factor, terwijl bij vrijwel stijve planten de ruimtelijke dichtheid dominant is.

In hoofdstuk 6 is het driedimensionale model voor de Baie de l'Écluse gebruikt om de effecten van verschillende macrofyten op (residueel) sedimenttransport en de beschikbaarheid van licht voor fotosynthese te bestuderen: De effecten van het echte, vrij dun begroeide *Zostera marina* veld werden vergeleken met een veld van stijve planten bij dezelfde ruimtelijke dichtheid, met een dicht begroeid zeegrasveld en met een kale bodem. Hoewel de verschillen tussen deze vier scenario's slechts een paar procent bedroegen, kunnen de gevolgen op lange termijn groot zijn.

In dit diepe water hield de vrij open flexibele vegetatie meer sediment binnenin de baai vast dan stijve planten of een dichter veld. Als planten slechts een klein deel van de waterkolom innemen hebben ze vooral invloed op het transport nabij het bed, en minder op het suspensief transport. Ook voorkomen ze dan vooral erosie, in plaats van depositie te vergroten. Stijve planten en dichte velden hadden een grotere invloed op het transport nabij het bed, waardoor het transport van zand van buiten naar binnen vrijwel geblokkeerd werd. De aanwezigheid van stijve of dicht bij elkaar staande macrofyten vergrootte de beschikbaarheid van licht aan de bodem, gemiddeld over een getijperiode, met 7% ten opzichte van een kale bodem. De toename in lichtbeschikbaarheid was minder duidelijk in het geval van de open natuurlijke vegetatie: 3%.

Deze studie heeft een breed toepasbaar model voor terugkoppelingen tussen flexibele waterplanten, stroming en sedimenttransport opgeleverd, en meer inzicht in deze terugkoppelingsmechanismen. Anderen worden aangemoedigd om dit model te gebruiken in aanvulling op experimenten in het veld of in stroomgoten, en om het uit te breiden met functionaliteiten voor bijvoorbeeld golfdemping of ontwikkeling van vegetatie.



# Table of Contents

<b>Preface</b>	<b>i</b>
<b>Abstract</b>	<b>iii</b>
<b>Samenvatting</b>	<b>vii</b>
<b>Table of Contents</b>	<b>xi</b>
<b>1 Introduction</b>	<b>1</b>
1.1 The importance of macrophytes .....	3
1.2 Seagrasses: occurrence and properties .....	4
1.3 Flow, sediment transport and vegetation: processes and models.....	6
1.4 Research approach .....	7
<b>2 Developing ‘Dynveg’: a small-scale model for the interaction between flow and highly flexible aquatic vegetation</b>	<b>9</b>
2.1 Introduction.....	11
2.2 Methods .....	12
2.2.1 The vegetation model .....	12
2.2.2 The hydrodynamic model.....	15
2.2.3 Setup of flume experiments .....	18
2.2.4 From forces to coefficients.....	20
2.2.5 Validation experiments: flexible strip positions .....	20
2.2.6 Validation experiments: hydrodynamics .....	21
2.3 Results .....	21
2.3.1 Model verification runs .....	21
2.3.2 Forces and values of coefficients .....	22
2.3.3 Validation with flexible strips .....	23
2.4 Discussion and Conclusions .....	26
2.4.1 Performance of the model: forces and positions .....	26
2.4.2 Performance of the model: hydrodynamics .....	26
2.4.3 Comparison to other work .....	28
2.4.4 Interaction between plants properties and flow.....	29
2.4.5 Applicability and further work.....	30
2.5 Conclusions.....	30
<b>3 Creating and testing a two-dimensional model for flow through flexible aquatic vegetation</b>	<b>33</b>
3.1 Introduction.....	35
3.2 Methods .....	35
3.2.1 Step 1: Modelling flexible vegetation in one dimension .....	35
3.2.2 Step 2: Modelling flexible vegetation as short rigid rods .....	36
3.2.3 Step 3: Developing a fast iterative method to relate $k_{veg}$ and $C_{Deq}$ to hydrodynamics .....	38
3.2.4 Step 4: Modelling flexible vegetation in more dimensions .....	38

3.2.5	Model validation .....	39
3.3	Results and Discussion .....	40
3.3.1	Model validation against flume measurements .....	40
3.3.2	Limitations and scope for applications .....	41
3.4	Conclusions .....	42
<b>4</b>	<b>Assessing ecosystem-engineering capacities of aquatic vegetations of contrasting flexibility: a model study</b> .....	<b>43</b>
4.1	Introduction .....	45
4.2	Methods .....	45
4.2.1	Parameters used as proxy for ecosystem engineering capacity .....	45
4.2.2	Dependence of ecosystem engineering capacity on species properties .....	46
4.2.3	Dependence of ecosystem engineering capacity on hydrodynamics .....	47
4.3	Results .....	47
4.3.1	Effects of hydrodynamic conditions - 1D simulations .....	47
4.3.2	Effects of plant solidity - 1D simulations .....	49
4.3.3	Comparing model predictions of 1D vs. 2D simulations .....	51
4.3.4	Spatial patterns generated by 2D simulations .....	52
4.4	Discussion .....	53
4.4.1	Ecosystem engineering capacity: effects of conditions .....	53
4.4.2	Ecosystem engineering capacity: effects of plant properties .....	55
4.4.3	Leading edge effects and other spatial processes .....	56
4.4.4	Other processes and other organisms: possible consequences .....	57
4.5	Conclusions .....	58
<b>5</b>	<b>Effects of a seagrass meadow on flow and sediment transport</b> .....	<b>59</b>
5.1	Introduction .....	61
5.2	Materials and Methods .....	62
5.2.1	Location choice and description .....	62
5.2.2	Instrument set-up .....	62
5.2.3	Environmental conditions .....	63
5.2.4	Model description .....	64
5.2.5	The model grid .....	64
5.2.6	Model boundaries, bed roughness and eddy viscosity .....	65
5.2.7	Vegetation modelling .....	66
5.2.8	Model calibration .....	66
5.3	Results .....	67
5.3.1	Flow measurements .....	67
5.3.2	Sediment concentration .....	68
5.3.3	Sediment transport .....	70
5.3.4	Model calibration and validation .....	70
5.3.5	Model results: sedimentation and erosion .....	71
5.4	Discussion .....	71
5.4.1	Observations .....	71
5.4.2	Model calibration and validation .....	72
5.4.3	Sediment transport formulations .....	72

5.4.4	Model applicability .....	73
5.5	Conclusions .....	74
<b>6</b>	<b>Modelling effects of diverse vegetation meadows on flow, sediment transport and light availability</b>	<b>75</b>
6.1	Introduction .....	77
6.2	Materials and Methods .....	77
6.2.1	Modelling scenarios .....	77
6.2.2	Light availability .....	78
6.3	Results .....	78
6.3.1	Spatial flow patterns .....	78
6.3.2	Flow and transport time-series .....	80
6.3.3	Sedimentation and residual sediment transport .....	82
6.3.4	Light availability .....	85
6.4	Discussion .....	87
6.4.1	Effects of vegetation on flow and sediment transport .....	87
6.4.2	Effects of vegetation on light availability .....	88
6.4.3	Possible applications .....	89
6.5	Conclusions .....	90
<b>7</b>	<b>Synthesis</b>	<b>91</b>
7.1	Model development .....	93
7.1.1	Small-scale modelling: individual plants .....	93
7.1.2	Two-dimensional modelling: plants in laboratory flumes .....	94
7.1.3	Three-dimensional modelling: a natural meadow .....	94
7.2	Bio-physical feedbacks .....	95
7.2.1	Individual plants and small meadows .....	95
7.2.2	Large meadows and their surroundings .....	96
7.3	Recommendations .....	96
7.3.1	Model development and application .....	96
7.3.2	Ecological aspects .....	97
	<b>References</b>	<b>99</b>
	<b>Appendix A Dynveg-Delft3D coupling verification</b>	<b>109</b>
	<b>Appendix B Sediment transport and vegetation</b>	<b>113</b>
	<b>Dankwoord</b>	<b>117</b>
	<b>Curriculum Vitae</b>	<b>119</b>



A black and white photograph of a sandy beach. In the foreground, there are several large, dark, wet rocks. Scattered across the sand and rocks are various types of seaweed, including long, thin blades and some more complex, branching structures. The sand is light-colored and appears slightly damp. The overall scene is a natural, coastal environment.

## **1 Introduction**



## 1.1 The importance of macrophytes

### Macrophytes as eco-engineers

Aquatic plants –or macrophytes- are an important part of coastal, estuarine and freshwater ecosystems worldwide, both from an ecological as well as an engineering viewpoint [Costanza *et al.*, 1997]. These vegetations provide a wide range of ecosystem services such as forming a physical protection of the shoreline by attenuating waves and currents and by stabilizing sediments [Fonseca & Cahalan, 1992; Möller *et al.*, 1999; Barbier *et al.*, 2008], enhancing water quality by filtering, oxygen production and nutrient recycling and providing a habitat to many other (including commercially important) organisms [Peterson *et al.*, 1984; Hemminga & Duarte, 2000; Koch, 2001; Orth *et al.*, 2006a; Hughes *et al.*, 2009]. In other areas, the presence of vegetation in rivers and lakes can be problematic as the hydraulic resistance caused by plants can increase water levels [Stephan & Gutknecht, 2002; Järvelä, 2002, 2005]. Most of these ecosystem services depend on the capacity of plants to alter their abiotic environment via bio-physical (feedback) interactions, which is often referred to as ecosystem engineering [cf. Jones *et al.*, 1994].

### Conservation and restoration

Unfortunately, areas with coastal and estuarine vegetation such as salt marshes, seagrasses or mangroves are rapidly declining due to anthropogenic pressure (eutrophication, pollution, hydropower, dredging, coastal engineering works, etc.) and climate change [Orth *et al.*, 2006a; Waycott *et al.*, 2009]. Attempts to restore seagrass vegetations in different areas around the world have often limited success, despite large efforts [e.g., see Zimmerman *et al.*, 1995; Orth *et al.*, 2006b; van Katwijk *et al.*, 2009]. One of the reasons for this low success rate may be our limited knowledge of the complex bio-physical feedbacks between vegetation and hydrodynamics-driven processes that govern seagrass ecosystems. For example, it was recently demonstrated that bio-physical feedbacks may lead to alternative stable state behaviour in seagrass meadows by causing thresholds for (re)establishment [van der Heide *et al.*, 2007; Carr *et al.*, 2010]. Hence, management and restoration of seagrass meadows would benefit from in-depth understanding of bio-physical interactions governing plant growth, hydrodynamics and water quality.

### Knowledge gap: flow trough flexible vegetation

In order to assess the eco-engineering ability of macrophytes and to enhance the prospects of success of restoration and protection efforts, more insight is needed into the interaction between vegetation, currents, waves, sediment transport and water quality. Many empirical [e.g., Kouwen & Unny, 1970, 1973; Järvelä, 2002; Wilson *et al.*, 2003; Sukhodolov & Sukhodolova, 2006] as well as modelling work [e.g., Nepf, 1999; López & García, 2001; Neary, 2003; Baptist *et al.*, 2007; Stoesser *et al.*, 2009] studied the effect of vegetation on flow structure and hydraulic resistance, i.e. from an engineering background. These studies have provided very useful insights, however they mostly focused on rigid or moderately flexible vegetation, whereas aquatic vegetation systems in estuaries usually consist of very flexible seagrasses. Numerous more ecologically oriented studies (see Madsen *et al.* [2001] for a review) both in laboratory flumes

[e.g., Gambi et al., 1990; Folkard, 2005; Morris et al., 2008] and in the field [e.g., Fonseca et al., 1982; Ackerman & Okubo, 1993; Orth et al., 1994; Vermaat et al., 1997; Koch, 1999; Bouma et al., 2009] have aimed at quantifying the effect of biomechanical properties of flexible plants on the bio-physical interactions between vegetation and hydrodynamic processes. Such experiments are always hampered by practical limitations such as flume dimensions, available flume time, or, in the field, by uncontrolled hydrodynamic conditions and limited number of co-occurring species.

## Objective

Generically applicable computational models that describe the interaction between flexible plants and their environment would be greatly beneficial to obtain a more universal insight in the effects of *i)* species properties (e.g., morphology, height, flexibility, buoyancy, etc.), *ii)* meadow properties (e.g., density, size, etc.) and *iii)* abiotic conditions (e.g., current velocity, water depth, turbidity, etc.) on such bio-physical interactions. Moreover, such models would be valuable assets in practical management and conservation issues.

The objective of this study is to develop, test and apply such a generic model. Although essentially suitable for other plant species, the focus during these three modelling phases will be on seagrass, for multiple reasons: Seagrasses are well studied; seagrasses are highly flexible; seagrasses have a relatively simple shape compared to other macrophytes and seagrasses form an important –but threatened– part of estuarine ecosystems.

## 1.2 Seagrasses: occurrence and properties

### Occurrence and requirements

Seagrasses are aquatic flowering plants, occurring in brackish and marine waters in temperate and tropic areas [Hemminga & Duarte, 2000; Green & Short, 2003]. In total, 55 species exist in four families. Seagrass meadows are found in intertidal and subtidal areas and can consist of multiple species or be monospecific. Hydrodynamic stress, especially from waves, and desiccation set the upper depth limit for their occurrence, whereas the lower limit is determined by light availability [Duarte, 1991; van Katwijk & Hermus, 2000; Koch, 2001; van der Heide et al., 2009]. This lower limit ranges from 1 m in turbid waters to several tens of meters in clear waters, depending on photosynthetic requirements (i.e., species), latitude and turbidity. Eutrophication, as a result of agricultural runoff, is an important factor for light availability: Not only does the abundance of algae increase the light attenuation in the water column, the seagrass blades can become covered with epiphytes that decrease light availability even further. Factors like toxic substances (e.g., ammonium, sulphide; Brun et al., 2002; Pedersen et al., 2004), diseases like *Labyrinthula zosterae* (wasting disease; Giesen et al., 1990) and physical disturbance [Orth et al., 2006a] also play a role in the decline of seagrasses.

### Morphology, growth and reproduction

Seagrasses are clonal plants, connected by rhizomes belowground [Hemminga & Duarte, 2000]. Aboveground, the shoot consists of a number of leaves where photosynthesis occurs; thus

taking up carbon from the water and producing oxygen. The rhizome allows for transport and storage of resources and for vegetative expansion of the plants, whereas the other belowground components –the roots- are responsible for nutrient uptake from the soil and securing the plants in the bed. Besides clonal expansion through the rhizome system, seagrasses can also reproduce sexually by means of flowering shoots. Whereas single seagrass seeds usually spread nearby, the floating seed-carrying shoots can cover large distances [Erftemeijer et al., 2008].

## Properties of seagrasses in NW Europe

*Zostera marina* and *Zostera noltii* are the two species endemic to North-West Europe [Green & Short, 2003]. While most seagrasses are perennial, these species can have a yearly growth cycle: they lose their leaves in fall and survive the winter as an underground rhizome mat or in some cases just a seed bank, to return for the next growing season in spring [Vermaat & Verhagen, 1996].



Figure 1.1 (left) An individual eelgrass plant [Picture Kristian Peters, CC]; (right) An eelgrass meadow

*Z. marina* (eelgrass) usually occurs subtidally, down to depths of 15 m, though typically less deep. Varying per location, a shoot consists of an optional short stiff sheet and 2-7 buoyant leaves of 20-200 cm length (Fig. 1.1). The width and thickness of the leaves roughly scale to the length, ranging between 3-20 mm and 0.35-2 mm, respectively. The spatial density of eelgrass can be as low as a couple of plants per square metre [Bos et al., 2007] or be well over a thousand shoots. The dwarf eelgrass *Z. noltii* occurs in very high densities -up to 10.000 shoots per square metre are not uncommon- in the intertidal. Its leaves are generally 5-15 cm long, 1-3 mm wide and 0.15-0.25

mm thick. Both species have in common that their leaves are very thin, and rely on buoyancy rather than stiffness to remain upright.

## **1.3 Flow, sediment transport and vegetation: processes and models**

### **Drag and bending of plants**

The feedbacks between plants and their physical environment are mainly governed by hydrodynamic drag: This drag determines turbulence production and dissipation, the flow structure, the position of the plants, the force experienced by the plants and ultimately, the stresses acting on the bed [Nepf & Vivoni, 2000; Ikeda et al., 2001; Carollo et al., 2005; Bouma et al., 2009]. Through these processes, the transport of sediment and other constituents are also influenced by plants [López & García, 1998; Morris et al., 2008]. Because the drag of flexible macrophytes depends on their bending [Kouwen & Unny, 1973; Vogel, 1981; Kutija & Hong, 1996], it is of major importance to account for this bending when modelling the interaction between plants and their environment [Nepf & Vivoni, 2000; Abdelhrman, 2003].

Other biophysical processes are the trapping of sediment particles against blades [Hendriks et al., 2008] and the stabilisation of the soil by a root system, possibly enhanced by accelerated consolidation as a result of evapotranspiration in the intertidal. As the former process seems of less importance to the environmental conditions than drag and flow patterns, and because the latter process is a matter of soil mechanics and biogeochemistry rather than hydrodynamics, these process are not subject of this modelling study. Neither is biogeochemistry itself.

### **Vegetation in flow and sediment transport models**

Modelling flow and sediment transport at the scale of estuaries has become common engineering practice, as the widespread use of models such as Delft3D shows [Lesser et al., 2004]. Delft3D is based on a three-dimensional finite difference solution of the Navier-Stokes equations, allowing for the simulation of free surface flow over complex topographies. Traditionally, the effect of vegetation on flow in hydrodynamic models is parameterized by means of an empirically determined bed roughness coefficient [e.g., Kouwen & Unny, 1973; Klaassen & van Zwaard, 1974; Wu et al., 1999]. This method has the crucial limitation that it cannot represent the vertical flow velocity profile correctly. As a consequence, the velocity near the bed and the bed shear stress are overestimated in a vegetated area, which would lead to more erosion than in a bare area, whereas in reality the flow inside a canopy is lower than in the overlying water column, resulting in a lower bed shear stress and less erosion.

The current version of Delft3D has the capability to deal with vegetation in a different, more realistic way: Using a  $k-\epsilon$  turbulence model, plants are represented as rigid elements that have a diameter, drag coefficient and a spatial density that can vary over the vertical [Uittenbogaard, 2003; Baptist, 2005], so that the actual flow velocity profile and bed shear stress are simulated. This model was successfully applied by Temmerman et al. [2005, 2007] to reproduce sedimentation patterns in tidal landscapes. Therefore, it is logical to use Delft3D to build on and extend it with a functionality for flexible vegetation.

## 1.4 Research approach

### Objectives

The primary objective of this thesis is to develop a generically applicable numerical model for the interaction of flexible aquatic plants and their physical environment. The second objective is to use this model as a tool to learn more about these interactions in different situations.

A prerequisite for this general applicability is that the model should be based on the knowledge of processes –e.g., the Navier-Stokes equations– rather than empirically derived rules or coefficients. The latter are only valid under specific conditions or at a specific scale, whereas process-based descriptions are valid across multiple scales –provided that they are schematised correctly. However, spatial and temporal scales do determine which processes are the most relevant. Since incorporating all processes is not feasible, a selection needs to be made [de Vriend *et al.*, 1993; Teeter *et al.*, 2001].

To do so carefully, modelling commences on a small scale: That of an individual plant. Gradual up-scaling via a vegetation patch in laboratory flume reveals which parameterisations are essential to represent the biophysical interactions at the scale of a real meadow in an estuary (Fig. 1.2). At each scale, the results of the model are compared to observations.

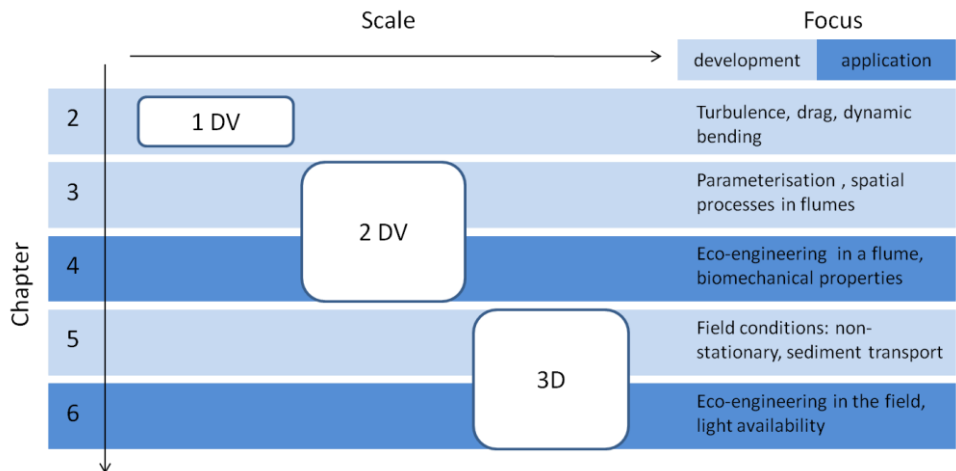


Figure 1.2 Thesis outline. A light background colour indicates a focus on model development; the dark colour indicates a focus on model application.

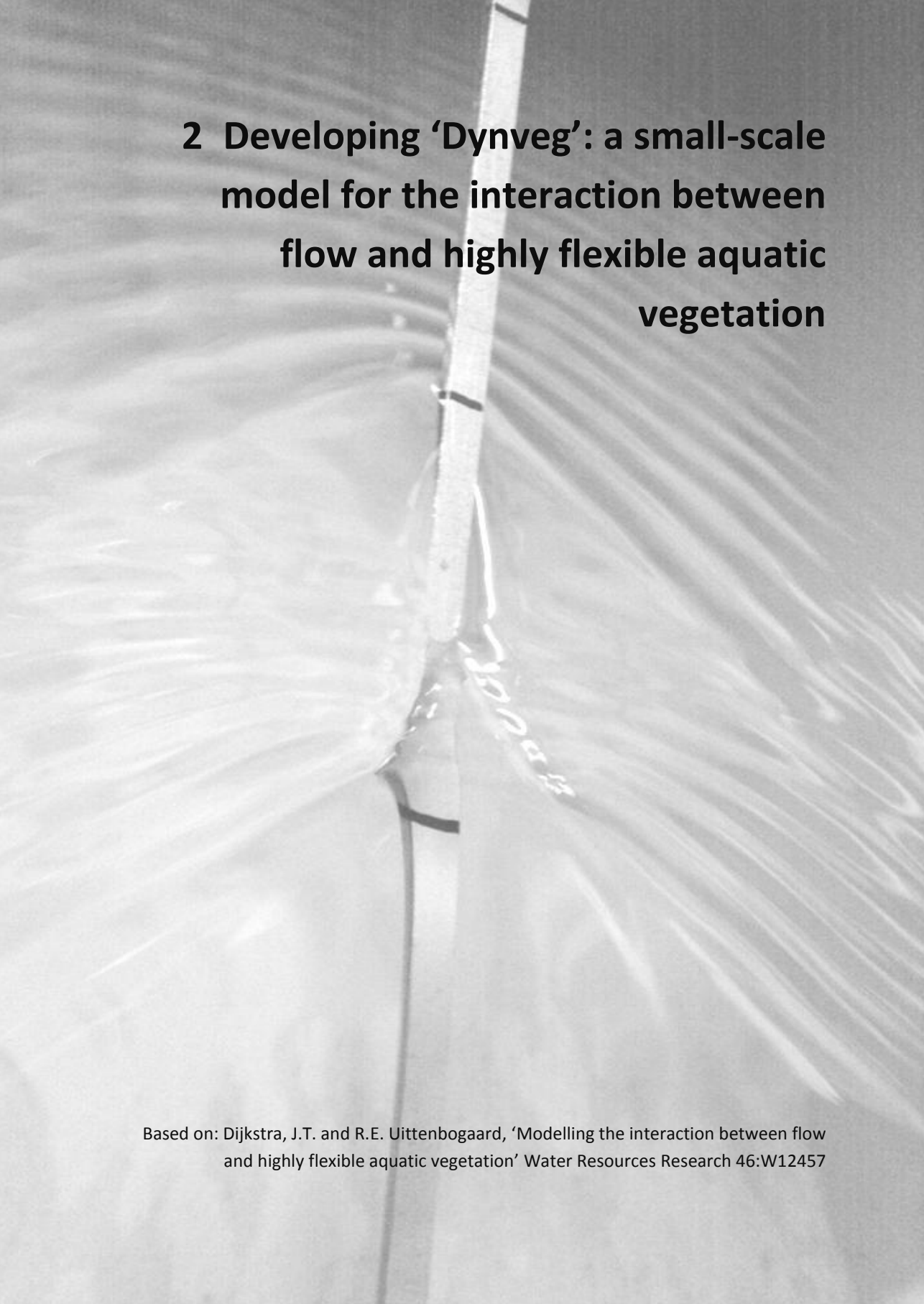
### Outline

First, a model for the dynamic bending of a single plant is developed, based on a force balance that accounts for the real biomechanical properties of leaves: bending stiffness and buoyancy (Chapter 2). This model is merged with a one-dimensional  $k-\varepsilon$  turbulence model with additional terms for turbulence production and dissipation due to vegetation. The model is validated using own observations of positions of flexible plastic strips and of the forces these

strips endure over a range of flow velocities, as well as using hydrodynamic measurements of others.

Next, this detailed plant-flow model is combined with the large-scale hydrodynamic model Delft3D by means of a look-up table for representative vegetation properties along a range of conditions (Chapter 3). This two-dimensional model is validated with flume observations of different seagrass species, paying attention to spatial variations in canopy height and flow structure. Subsequently, this model is used to assess the ecosystem engineering capacities of three plant species with different properties (Chapter 4). The velocity inside the canopy, the canopy flux and the bed shear stress are used as proxies for a plant's ability to absorb hydrodynamic energy, to ascertain nutrient supply and to prevent erosion, respectively.

A measurement campaign in a macrotidal bay home to *Zostera marina* in Dinard, France, provides validation data for a three-dimensional version of the model that, besides flow, also simulates sediment transport through vegetation (Chapter 5). This three-dimensional version is then used to study how different vegetation covers affect the flow and sediment transport patterns in the bay, ultimately affecting the morphological development and light availability in and around the bay (Chapter 6).



## **2 Developing ‘Dynveg’: a small-scale model for the interaction between flow and highly flexible aquatic vegetation**

Based on: Dijkstra, J.T. and R.E. Uittenbogaard, ‘Modelling the interaction between flow and highly flexible aquatic vegetation’ Water Resources Research 46:W12457

## Abstract

Aquatic vegetation has an important role in estuaries and rivers by acting as bed stabilizer, filter, food source and nursing area. However, macrophyte populations worldwide are under high anthropogenic pressure. Protection and restoration efforts will benefit from more insight into the interaction between vegetation, currents, waves and sediment transport. Most aquatic plants are very flexible, implying that their shape and hence their drag and turbulence production depend on the flow conditions.

We have developed a numerical simulation model that describes this dynamic interaction between very flexible vegetation and a time-varying flow, using the seagrass *Zostera marina* as an example. The model consists of two parts: an existing 1DV  $k-\epsilon$  turbulence model simulating the flow combined with a new model simulating the bending of the plants, based on a force balance that takes account of both vegetation position and buoyancy. We validated this model using observations of positions of flexible plastic strips and of the forces they are subjected to, as well as hydrodynamic measurements. The model predicts important properties like the forces on plants, flow velocity profiles and turbulence characteristics well. Although the validation data are limited, the results are sufficiently encouraging to consider our model to be of generic value in studying flow processes in fields of flexible vegetation.

**Keywords:** flexible vegetation, seagrass, turbulence, drag coefficient measurements, modelling

## 2.1 Introduction

When abundant, submerged aquatic vegetation can act as an 'eco-engineer', with plants affecting their environment in such a way that they create more favourable living conditions for themselves and for other organisms [Bouma *et al.*, 2005; Bos *et al.*, 2007; Peralta *et al.*, 2008]. In other areas, the presence of vegetation in rivers and lakes can be problematic as the hydraulic resistance caused by plants might increase water levels. Many empirical [e.g. Kouwen *et al.*, 1970, 1973, 1980; Järvelä 2002, Sukhodolov & Sukhodolova, 2006; Wilson *et al.*, 2003] as well as modelling work [e.g. López & García 2001, Stoesser *et al.*, 2009; Neary, 2003] has studied the effect of vegetation on hydraulic resistance. These studies have provided very useful insights in to the interaction between vegetation, currents, waves, sediment transport and water quality, however they mostly focused on rigid or moderately flexible vegetation, whereas aquatic vegetation in estuaries is very flexible.

These interaction of these vulnerable seagrasses with their environment has been subject of numerous studies in the United States [e.g., Fonseca *et al.*, 2002; Koch & Beer, 1996; Abdelrhman, 2003; Ackerman & Okubo, 1993; Worcester, 1995], in the Venice Lagoon (Italy) [Bocci *et al.*, 1997; Sfriso & Marcomini, 1997; Amos *et al.*, 2004] and in other areas [van Katwijk & Hermus, 2000; Christiansen *et al.*, 1981; Godet *et al.*, 2008; Olesen *et al.*, 2004; Gacia & Duarte, 2001; Tamaki *et al.*, 2002].

Field and laboratory experiments [like Fonseca *et al.*, 1982; Folkard, 2005; Schanz, 2003; Ackerman & Okubo, 1993] provide valuable information, but are often expensive, difficult to conduct and have a limited range of applicability. We therefore decided to construct a numerical simulation model that is based on the processes that determine the interaction between flexible vegetation and its environment. With such a generic model, a wide range of characteristics in respect of currents, waves, water depths and vegetation characteristics can be studied.

The first challenge is to model the water motion through a static vegetation field, since the hydrodynamics determine the transport of sediment and nutrients, as well as the forces acting on plants. Vegetation elements are often modelled as rigid objects [see e.g. López & García 2001; Nepf, 1999], but flow patterns in highly flexible vegetation such as seagrass are very different from flow patterns through rigid vegetation. The bending or reconfiguration of plants reduces drag forces considerably [Vogel, 1981; Gaylord & Denny, 1997; Sand-Jensen, 2008; Bouma *et al.*, 2005]. The bending allows for a greater flow over the canopy ('skimming flow') and for a turbulence maximum closer to the bed, whereas the prone leaves can shield the bed from high shear stresses. A second challenge is modelling the reconfiguration of a plant under time-varying flow, i.e. changes in unidirectional flow velocity or waves. Mechanical interactions between plants as well as the intricate structure of branches and leaves of some macrophyte species form further challenges.

In this study, we set out to deal with the first challenge only: demonstrating a modelling approach for unidirectional flow through flexible vegetation. We strive to build on generic principles, while keeping in mind that the model eventually should be applicable to many species of macrophytes in many flow conditions. These latter two challenges require extensive experimental work however. In order not to make matters overly complicated we focus on flexible plastic strips and one plant species: the seagrass *Zostera marina*. Like most seagrasses, *Z. marina*

(eelgrass) has a relatively simple shape: typically five long ( $>30$  cm), thin ( $<0.5$  mm) leaves with a rectangular cross-section attached to a very short ( $< 1$  cm) stem. This makes eelgrass very flexible, and relatively straightforward to model.

## 2.2 Methods

The aim is to create a generically applicable tool that is useful in studying flow and flow related exchange processes in fields of different kinds of flexible vegetation, as well as hydrodynamic loads on the vegetation and on the seabed. This means that two interacting models are necessary: one to simulate the hydrodynamics and one to simulate the movement of the plants. The former builds on an earlier model for flow through rigid vegetation by the second author that was presented at a symposium but not published in a journal [Uittenbogaard, 2003], the latter is new. Each model works fully implicitly in time and space for stability, whereas their coupling is formulated semi-implicitly.

### 2.2.1 The vegetation model

The crucial difference with earlier rigid vegetation models is that in this model the movement (i.e., the position, orientation and velocity) of a plant is modelled. The non-stationary nature of flow and plant motion in waves requires dynamic modelling. This has consequences for the numerical scheme because some forces depend linearly others quadratically on the velocity or the acceleration of the leaf. Backhaus & Verduin [2008] coupled a canopy model that simulates motions of plant ensembles to a hydrodynamic model, suitable for the simulation of short waves. Their model is based on field observations of maximum deflection of the seagrass *Amphibolis antarctica*. For small excitations the plants just follow the orbital motion, only at their maximum deflection plants exert a drag force. This approach works well for surface waves, although it is very species-specific. Ikeda et al. [2001] used a 'plant grid' within a large eddy simulation grid to model groups of leaves, assuming the movement of the plant can be described by the equations of motion for a flexible cantilever. Kutija & Hong [1996] modelled the effect of flexible reeds on hydraulic resistance, but without calibration and not taking the interaction of plants with flow into account. With the purpose of predicting the stability of plants in lakes, Schutten & Davy [2000] performed a regression analysis that linked hydraulic drag on flexible plants to flow velocity, biomass and species-specific factors. They did not study the effect of plants on flow. The model of Velasco et al. [2008] provides a reasonable approximation of the vegetation position as well as the velocity and shear profiles in flow through barley, but with the use of a large number of tuneable parameters rather than a physical basis.

Abdelhrman [2007] successfully developed and tested a two-dimensional model for the coupling of flow and very flexible eelgrass. His model is applicable to stationary flow and very flexible vegetation only, as blade elasticity is omitted. Otherwise, his approach is partly similar to ours, by modelling a blade as a series of elements.

Because of the need to deal with thin blades that show very large deflections, our method is to follow a Lagrangian approach by setting up a force balance of a plant, consisting of a number of leaf segments; see Figure 2.1. The coordinate measured along the leaf is  $s$ , at  $s=0$  it is connected to the bed,  $s=s_{max}$  is the tip of the leaf. On every leaf segment  $ds$  acts a distributed force  $q$  ( $\text{Nm}^{-1}$ ) as a result of its relative weight and fluid motions relative to the orientation and velocity of the

segment. In addition, the force components  $F$  (N) act on the ends of the leaf segment. These are a combination of internal normal and shear stresses, integrated over the leaf cross section.

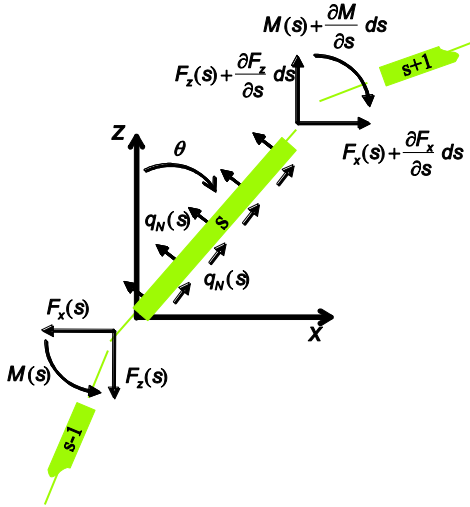


Figure 2.1 The force balance of one vegetation element  $s$  of length  $ds$ , with adjacent elements  $s-1$  and  $s+1$ .

The following limitations apply:

- A leaf moves in a single vertical plane only.
- A leaf cannot fold around itself.
- A leaf can only bend, not elongate.
- Biomechanical properties are assumed constant along the leaf.

This last limitation is not typical of the model: different properties can be assigned along the leaf, but for simplicity this is not tested in this study.

The force balance for an element with solidity  $a$  ( $\text{m}^2$ ) reads:

$$\begin{aligned} q_x + \frac{\partial F_x}{\partial s} &= \rho_t a \frac{\partial^2 x}{\partial t^2} \\ q_z + \frac{\partial F_z}{\partial s} &= \rho_t a \frac{\partial^2 z}{\partial t^2} \end{aligned} \quad (1)$$

Where  $\rho_t$  is the total density of the leaf and the surrounding virtual water mass, based on the volumetric density of the vegetation  $\rho_v$ , the water  $\rho_w$  and a Morison-like virtual mass factor  $m_f$  [Morison et al., 1950]:

$$\rho_t = \rho_v + m_f \rho_w \quad (2)$$

The internal force components  $F_x(s)$  and  $F_z(s)$ , as well as the leaf's positions  $x(s)$  and  $z(s)$  relative to its root connection are unknowns. A first additional equation couples the internal moment on a cross section to the internal forces:

$$\frac{\partial M}{\partial s} = \frac{\partial x}{\partial s} F_z - \frac{\partial z}{\partial s} F_x \quad (3)$$

The internal moment itself is also unknown, but it is related to the leaf's curvature  $\partial \theta / \partial s$  through:

$$EI \frac{\partial \theta}{\partial s} = M \quad (4)$$

with  $E$  ( $\text{Nm}^{-2}$ ) the elastic modulus of the leaf and  $I$  ( $\text{m}^4$ ) the moment of inertia, based on width  $b$  and thickness  $d$ .

The essential unknown here is the angle  $\theta$  that serves in the leaf's position, assuming no elongation of the leaf:

$$\begin{aligned} \frac{\partial x}{\partial s} &= \sin \theta \\ \frac{\partial z}{\partial s} &= \cos \theta \end{aligned} \quad (5)$$

Consequently,  $x(s)$  and  $z(s)$  follow directly from a given angle  $\theta(s)$ . With Equations (1) to (5) the problem is closed and formulated into a single unknown  $\theta(s)$ .

The following set of boundary conditions applies:

$$\begin{aligned} s = s_{mx} : \quad & M = 0; \quad F_x = 0; \quad F_z = 0 \\ s = 0 : \quad & x = 0; \quad \frac{\partial x}{\partial t} = 0; \quad \frac{\partial^2 x}{\partial t^2} = 0; \\ s = 0 : \quad & z = 0; \quad \frac{\partial z}{\partial t} = 0; \quad \frac{\partial^2 z}{\partial t^2} = 0; \\ s = 0 : \quad & \theta = \theta \{M(0)\} \end{aligned} \quad (6)$$

The first condition states that the leaf tip is not loaded; the other conditions fix the position at the bed, but allow for the angle to vary with the total exerted moment  $M(0)$ , i.e. flexibility in the roots and soil.

The most prominent forces acting on the leaf are those due to pressure differences, but when the relative flow direction is nearly parallel to the leaf, also shear stresses need to be considered:

$$\begin{aligned}
q_s &= \frac{1}{2} \rho_w C_s b |\vec{u}_w - \vec{u}_v| u_s \\
q_N &= \frac{1}{2} \rho_w C_N b |\vec{u}_w - \vec{u}_v| u_N
\end{aligned} \tag{7}$$

where  $q_s$  and  $q_N$  are the force components parallel (i.e., friction) and perpendicular (i.e., lift) to the leaf, respectively. On the right hand side,  $\rho_w$  is the specific density of water,  $C_s$  is the friction drag coefficient (actually,  $C_s = f A_w$  with  $f$  a friction factor and  $A_w = 2(b+d)$  the wetted area of a leaf) and  $C_N$  is the coefficient for lift. Further,  $\vec{u}_w$  and  $\vec{u}_v$  are the velocity vectors of respectively water and vegetation, whereas  $u_s$  and  $u_N$  are the local velocity components referring to respectively parallel to and normal to the leaf.

The coefficients  $C_s$  and  $C_N$  are complicated because of their dependency on the orientation with respect to the flow and the shape of the cross-section. Many observations are available for flat strips perpendicular or almost parallel to the flow, but nothing in between. Drag and lift coefficients along a range of angles could only be found for circular cross-sections, e.g. in *Hoerner [1965]*. We removed this uncertainty by performing experiments with strips of eelgrass-like dimensions at different angles with the flow; Section 2.2.3. It is assumed that the coefficients found for a stiff strip under a certain angle, also apply to a series of leaf sections at local angles  $\theta$  ( $s$ ).

### 2.2.2 The hydrodynamic model

This model is an extension of the 1DV flow model as presented by *Uittenbogaard & Klopman [2001]* that is suitable for low-Reynolds number turbulence by incorporation of the closure of *Goldberg & Apsley [1997]*. Dispersive stresses [*Poggi & Katul, 2008; Nikora & Rowinski; 2008*] are not included. Where many models for flow through vegetation have used principles derived from studies on atmospheric boundary layer flow [*Finnigan, 2000; and Poggi et al., 2004*], our model also uses principles of flow through porous media [cf. *Breugem et al., 2006*], solving for the momentum equation for the pore velocity  $u(z)$  ( $\text{ms}^{-1}$ ):

$$\rho_0 \frac{\partial u(z)}{\partial t} + \frac{\partial p}{\partial x} = \frac{\rho_w}{1 - A_p(z)} \frac{\partial}{\partial z} \left( (1 - A_p(z)) (\nu + \nu_T(z)) \frac{\partial u(z)}{\partial z} \right) - \frac{F(z)}{1 - A_p(z)} \tag{8}$$

in which  $\rho_w$  is the fluid density ( $\text{kgm}^{-3}$ ),  $\partial p / \partial x$  the horizontal pressure gradient ( $\text{kgm}^{-2}\text{s}^{-2}$ ),  $\nu$  the kinematic viscosity ( $\text{m}^2\text{s}^{-1}$ ),  $\nu_T$  the eddy viscosity ( $\text{m}^2\text{s}^{-1}$  defined by a turbulence model, and  $A_p$  (-) the solidity of the vegetation across a horizontal plane, i.e. the cross-sectional area  $b(z) \times d(z)$  ( $\text{m}^2$ ) of a leaf times the number of leaves ( $n$ ) per  $\text{m}^2$ . Because we consider a horizontal plane, the thickness  $d$  depends on the angle of the leaf.

$F(z)$  is the resistance imposed on the flow that follows from the vegetation model according to:

$$F(z) = \frac{1}{2} \rho_w C_D a(z) u(z) |u(z)| \tag{9}$$

where  $C_D$  is the drag coefficient (-) and  $a(z)=d(z)n(z)$  ( $m^{-1}$ ) is the solid area projected on the vertical plane perpendicular to the flow, per unit depth and per unit width. Note that a large number of plants is represented by the position of a single plant. Using this approach, all plants are considered to behave alike, which makes the model applicable to a spatially uniform situation inside a vegetation meadow.

The applied two-equation turbulence model estimates the eddy viscosity through:

$$\nu_T = c_\mu \frac{k^2}{\varepsilon} \quad (10)$$

with  $k$  the turbulent kinetic energy or TKE ( $m^2s^{-2}$ ), and  $\varepsilon$  the dissipation rate ( $m^2s^{-3}$ ).

The equation for  $k$  reads:

$$\frac{\partial k}{\partial t} = \frac{1}{1-A_p} \frac{\partial}{\partial z} \left( (1-A_p)(\nu + \nu_T / \sigma_k) \frac{\partial k}{\partial z} \right) + T_k + P_k - \varepsilon \quad (11)$$

The first term in the RHS represents the vertical diffusion of TKE by its own mixing action, corrected for the available horizontal surface.  $T_k$  is the additional turbulence generated by the vegetation ( $Wm^{-3}$ ). The amount of power spent by the mean flow  $u(z)$  working against the plant drag  $F(z)$  depends on the plant Reynolds number  $Re_p$  through the viscous damping function  $f$ , which is  $< 1$  for  $Re_p < 200$  [Goldberg & Apsley, 1997]:

$$T_k = f(Re_p)T ; \quad Re_p = \frac{ud}{\nu} \quad (12)$$

$$T(z) = F(z)u(z)$$

The third term,  $P_k$ , represents the standard expression for turbulence production by shear rates:

$$P_k = \nu_T \left( \frac{\partial u}{\partial z} \right)^2 \quad (13)$$

The last term in Eq.(11) is the dissipation of TKE by its work against viscous stresses, modelled by the following  $\varepsilon$ -equation:

$$\frac{\partial \varepsilon}{\partial t} = \frac{1}{1-A_p} \frac{\partial}{\partial z} \left( (1-A_p)(\nu + \nu_T / \sigma_\varepsilon) \frac{\partial \varepsilon}{\partial z} \right) + P_\varepsilon + c_{2\varepsilon} \frac{T_k}{\tau_{eff}} - c_{2\varepsilon} \frac{\varepsilon^2}{k} \quad (14)$$

Here, the first term on the RHS represents vertical diffusion of small-scale eddies, representing  $\varepsilon$ , by the turbulent eddies. The last term may appear to represent the dissipation of dissipation, but it actually represents the rate at which the energy cascade converts TKE-dissipating eddies into smaller enstrophy-dissipating eddies.

The second term,  $P_\varepsilon$ , is the production of small-scale eddies, scaled to the turbulence production  $P_k$  by:

$$P_\varepsilon = c_{1\varepsilon} \left( \frac{\varepsilon}{k} \right) P_k \quad (15)$$

The third term of (14) corresponds to the enstrophy production (being dissipation due to vegetation), which depends on the effective time scale  $\tau_{eff}$  and the closure coefficient  $c_{2\varepsilon}$ . This time scale is related to the different length scales controlling turbulence in and above vegetation. Internally generated turbulence (IGT) is created at sufficient distance from the bed as well as from the top of the vegetation. Here, the wake turbulence length scale is smaller than the available fluid space. Therefore the time scale of this small scale IGT equals the intrinsic turbulence time scale:

$$\tau_{int} = \frac{k}{\varepsilon} \quad (16)$$

This time scale is used as effective time scale by *Shimizu & Tsujimoto [1994]* and *López & García [2001]*.

However, above the vegetation a shear layer exists that creates eddies at larger length scales. Insight from Direct Numerical Simulation by *Breugem et al., [2006]* shows that these can be advected into the vegetation, thus being squeezed into smaller-scale eddies with a size depending on the available space inside the vegetation. The time scale related to this penetrated flow turbulence (PFT) can be derived by considering a stationary uniform turbulent flow through uniform vegetation, for which –in the absence of diffusion or shear production– dissipation equals TKE production:

$$\frac{Dk}{Dt} = T - \varepsilon \equiv 0 \rightarrow T = \varepsilon \quad (17)$$

$$\frac{D\varepsilon}{Dt} = c_{2\varepsilon} \frac{T}{\tau} - c_{2\varepsilon} \frac{\varepsilon^2}{k} \equiv 0 \rightarrow k = T\tau \quad (18)$$

We can relate the time scale in Eq. 18 to a geometrical length scale by comparing the definition of the eddy viscosity in the  $k$ - $\varepsilon$  equation (Eq. 10) with Prandtl's classical length-scale closure:

$$\nu_\tau = L\sqrt{k} \equiv c_\mu \frac{k^2}{\varepsilon} \rightarrow L = c_\mu \frac{k^{3/2}}{T} \quad (19)$$

Which yields the following expression for the geometry-imposed time scale:

$$\tau_{geom} = \left( \frac{L_p^2}{c_\mu^2 T} \right)^{1/3} \quad (20)$$

Where  $L_p$  is the typical length scale between the vegetation defined as:

$$L_p(z) = c_l \left\{ \frac{1 - A_p(z)}{n(z)} \right\}^{1/2} \quad (21)$$

With  $c_l$  of order unity.

After calculation of both internal and geometrical time scales over the vertical, the effective time scale for enstrophy production is evaluated by:

$$\tau_{eff} = \min(\tau_{int}, \tau_{geom}) \quad (22)$$

The values of the partially inter-related constants  $\sigma_k$ ,  $\sigma_\epsilon$ ,  $c_{\mu}$ ,  $c_{1\epsilon}$  and  $c_{2\epsilon}$  used in Eq. 11-20 are 1, 1.3, 0.09, 1.44 and 1.92 respectively; equal to those used by *López & García [2001]* and based on an extensive examination of turbulent shear flows by *Launder & Spalding [1974]*.

### 2.2.3 Setup of flume experiments

The experiment has two objectives: *i)* to provide drag and lift coefficients for strips under various angles of attack for use in the flexible vegetation model and *ii)* to provide a dataset of forces and positions of flexible strips with well-known properties for use in validating the model.

All measurements were performed in the racetrack flume of NIOO-CEME (Netherlands Institute for Ecology – Centre for Estuarine and Marine Ecology) in Yerseke, the Netherlands (which has also been used by e.g. *Peralta et al. [2008]*; see their article for a picture). The flume is 60 cm wide and can be filled with fresh or salt water to a depth of 40 cm. A conveyor belt with adjustable rpm creates bulk velocities up to approximately  $0.4 \text{ ms}^{-1}$ . Collimators and screens in the bends regulate turbulence and bend effects. For determining the coefficients  $C_N$  and  $C_S$  -these depending on the angle of incidence and on the Reynolds number- the horizontal and vertical forces on inflexible metal strips have been measured with a force transducer. We used strips with a rectangular cross-section of 5.0 mm width and 2.0 mm thickness.

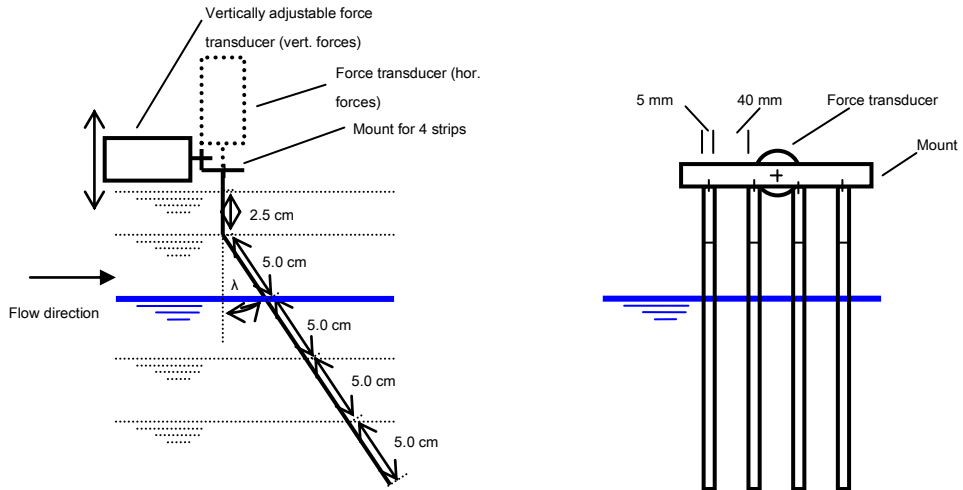


Figure 2.2 The force transducer mounted with four strips; side view (left) and front view (right; upstream)

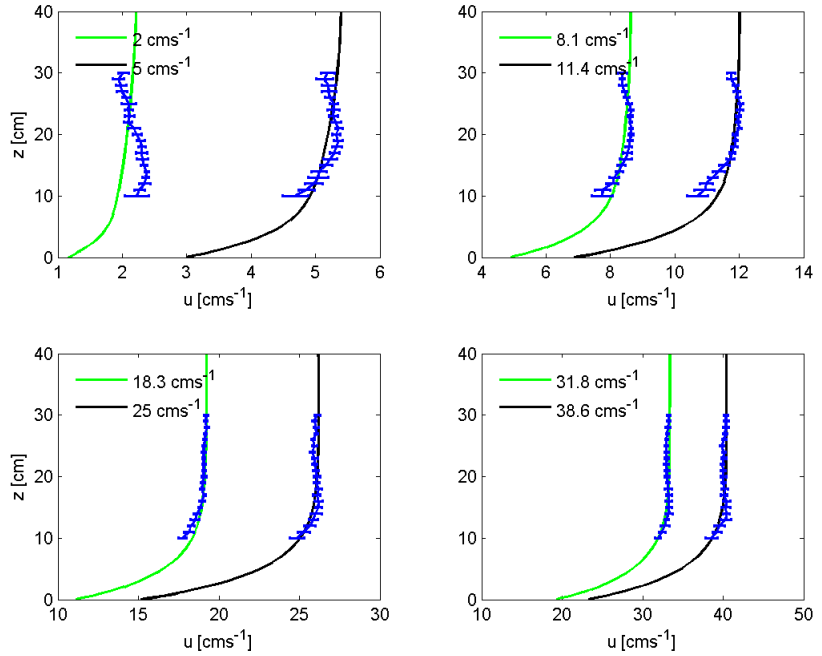


Figure 2.3 Flow velocity profiles of the empty NIOO-flume, averaged over the measurement width. Lines indicate the profiles reproduced by our model, horizontal errorbars the measurements. Note that at low velocities, the velocity profile is not uniform, but decreases near the surface.

The angles ( $\lambda$ ) of the strips ranged from 0 to 90° relative to vertical, with increments of 10°. For each angle, four strips were mounted onto the force transducer, see Figure 2.2. The use of four strips proved necessary because at low velocities the force on a single strip was on the lower detection limit of our equipment. A linear relation between the number of strips and the total force proved that strips do not influence each other in this setup (data not shown).

The forces were recorded at bulk velocities of 5.0, 11.4, 18.3, 25.0, 31.8 and 38.6  $\text{cm s}^{-1}$  (see Fig. 2.3 and Table 2.2). In most cases, measurements were also taken at 2.0 and 8.1  $\text{cm s}^{-1}$  for low-Reynolds number flows, thereby covering Re-numbers from 100 to 1930. Every recording, hence every raw data file, contains one minute of 20 Hz force measurements; i.e. 1200 values to give a good average. Measurements were done at the upper part of the water column with the largest possible depth (40 cm) to get the most uniform velocity profile, thus avoiding the logarithmic velocity profile near the bottom

At the measurement location,  $u$ ,  $v$ , and  $w$  velocities were recorded using an ADV (Nortek) sampling at 25 Hz for 5 seconds in a grid of 21 points over the vertical and 15 points over the width of the flume; starting at 11 cm from the bed and 11.6 cm from the walls. The representative bulk velocity in Figure 2.3 was acquired by subsequent averaging over time and space. Though the sampling time is actually too short according to *Nikora & Goring [1998]* and *Garcia et al. [2005]*,

we feel that the dense spatial cover combined with earlier reports of rather stationary conditions in this flume [Van Duren, pers. comm.] gives a sufficiently accurate bulk velocity for our purposes.

#### 2.2.4 From forces to coefficients

To derive the coefficients  $C_S$  and  $C_N$  as used in the model, the magnitude ( $F$ ) and direction ( $\beta$ ) of the total force are calculated from the measured horizontal ( $F_H$ ) and vertical ( $F_V$ ) force through:

$$F^2 = F_H^2 + F_V^2 \quad (23)$$

$$\beta = \arctan \frac{F_H}{F_V} \quad (24)$$

Subsequently, the angle  $\gamma$  between the force angle  $\beta$  and the strip angle  $\lambda$  was calculated, enabling the decomposition of  $F$  in forces parallel ( $F_S$ ) and perpendicular ( $F_N$ ) to the strip:

$$\begin{aligned} F_S &= F \cos \gamma \\ F_N &= -F \sin \gamma \end{aligned} \quad (25)$$

Then, assuming only a horizontal velocity (i.e.  $w=0$ ,  $u=u_H$ ),  $C_S$  and  $C_N$  are defined as:

$$\begin{aligned} C_N &= \frac{F_N}{\frac{1}{2} \rho_w A u_H u_N} \\ C_S &= \frac{F_S}{\frac{1}{2} \rho_w A u_H u_S} \end{aligned} \quad (26)$$

According to the ‘cross-flow’ principle of *Hoerner [1965]*, the following appears valid for circular cross-sections:

$$\begin{aligned} C_N &= C_D \cos \lambda \\ C_S &= f C_f \sin \lambda \end{aligned} \quad (27)$$

Where  $C_D$  is a coefficient for the form drag and  $C_f$  represents skin friction, multiplied by a factor  $f$  for the ratio between the wetted area and the cross-section. Here,  $f = A_{wet}/A = 2(b+d)/bd = 2.8$  holds.

#### 2.2.5 Validation experiments: flexible strip positions

Three types of plastic strips with different flexural rigidity were used in the same set-up and conditions as the metal strips in Section 2.2.3 (Fig. 2.2) to check whether the position of the plant and the forces acting on it are calculated correctly, see Table 2.1. At various velocities, we measured the force in main flow (i.e. horizontal) direction for a number of strip lengths. For each condition, the positions (Fig. 2.5) have been recorded using two 1-cm coordinate grids stuck to the flume walls to assure a perpendicular view, marking the position on a transparent sheet. The positions of the transparent strips could not be determined reliably.

Table 2.1 Flexible strip properties. The E-modulus has been determined with a Perkin Elmer DMA 7e dynamic tester, the thickness with a micrometer and the width with a digital caliper.

strip	material	E Nm <sup>-2</sup>	thickness mm	width mm	I m <sup>4</sup>	density kgm <sup>-3</sup>
very flexible (FR)	PVC	1.60·10 <sup>9</sup>	0.178	5.0	2.30·10 <sup>-15</sup>	975
tie-wrap (TW)	Nylon 66	1.06·10 <sup>9</sup>	1.009	4.8	4.11·10 <sup>-13</sup>	1080
flexible transparent (FT)	copolyester	1.81·10 <sup>9</sup>	0.540	5.0	6.56·10 <sup>-14</sup>	1380
stiff transparent (ST)	copolyester	1.72·10 <sup>9</sup>	0.981	5.0	3.93·10 <sup>-13</sup>	1290

As boundary conditions for the model, we used the water depth and depth averaged flow velocity. Measured flow velocity profiles (Section 2.2.3, Fig. 2.3) were used to calibrate the bed- and sidewall roughness coefficients. The computational grid consists of 100 computational layers over the vertical that zoom in at the bed and the area around the top of the vegetation while following the canopy top. The grid cell height around the vegetation top is 0.01 mm, at the bed level it is 0.1 mm. Each strip consisted of 40 elements. The verification runs in Section 2.3.1 showed that these numerical settings should be more than adequate, which was confirmed by a small sensitivity test.

## 2.2.6 Validation experiments: hydrodynamics

Experimental results from *Nepf & Vivoni [2000]* were used for validation of the hydrodynamic performance of the model. They applied a 24 m long and 0.38 m wide flume, with a 7.4 m long canopy section consisting of 330 randomly placed 0.16 m high plants per m<sup>2</sup>, each made of six 3 mm wide, 0.25 mm thick vinyl blades attached to a 2 cm high wooden base (6.4 mm diameter). The elasticity modulus of the blades is 2.56·10<sup>9</sup> Nm<sup>-2</sup>, derived from the specified flexural rigidity and the moment of inertia. The volumetric density of the material is not mentioned, but estimated at 975 kgm<sup>-3</sup> because it was slightly buoyant. The best recorded experiment is for a depth of 0.44 m and a depth averaged velocity of 0.10 ms<sup>-1</sup>.

This water depth and depth averaged velocity were used as boundary conditions in the simulation of their experiments. The roughness coefficients were considered similar to those in the NIOO-flume; the numerical settings are equal to those in Section 2.2.5 too.

## 2.3 Results

### 2.3.1 Model verification runs

As a first simple check of the model, we compared the bending of a relatively stiff strip under a uniformly distributed load in our model with the theoretical solutions for cantilevers, see e.g. *Gere & Timoshenko [1999]*. The results were essentially the same.

Further, we verified the behaviour of the model for a number of simple cases with ‘standard’ conditions (water depth  $h=0.5$  m, depth averaged flow velocity  $U=0.2$  ms<sup>-1</sup>, leaf length  $l=0.25$  m, leaf width  $b=5$  mm, thickness  $d=0.3$  mm,  $E=2\cdot10^9$  Nm<sup>-2</sup>,  $\rho_v=920$  kgm<sup>-3</sup>,  $\rho_w=1000$  kgm<sup>-3</sup>,  $n=100$  stems per m<sup>2</sup>, 40 elements per stem) representative of field and laboratory conditions. Without showing data or going into too much detail, we found that:

- Time steps of  $dt=0.01$  to  $dt=1$  s yield similar solutions;
- 50 to 100 layers over the vertical yield the same solutions, the result of 20 layers is very similar but slightly coarser;
- 20 or more elements are necessary to represent the plant position well.

In addition, we varied some properties of the plants, leading to the following observations:

- An increased tissue density (range: 1-2000 kgm<sup>-3</sup>) leads to increased bending, but the effect on flow properties is limited as the chosen number of plants is small;
- An increase in number of plants (range: 1-10000 m<sup>-2</sup>) leads to a more upright position, larger turbulence production and a distinctly different flow profile;
- Short plants (0.05 m) remain almost upright, experience more drag and have more effect on flow than plants of intermediate lengths (0.25 and 0.50 m) that assume a more streamlined position. Longer plants (1-2 m) bend further, but do create more resistance due to skin friction;
- The stiffer the plant ( $E=1\cdot10^2$  to  $10^{14}$  Nm<sup>-2</sup>), the more upright it stays and the more drag it creates. Due to rapid movement, stable simulations on very flexible plants require a smaller time step to remain stable;
- At higher flow velocities (0-2 ms<sup>-1</sup>) plants bend more;
- For increasing water depths (0.05-5 m), the bending of the plants as well as their effect on flow decrease markedly as more flow passes over the plants.

### 2.3.2 Forces and values of coefficients

In Figure 2.4 the values for  $C_S$  and  $C_N$ , determined from the experiments through Equation 23, are plotted against the angle  $\lambda$ . The coefficients seem to be fairly equal at all flow velocities, although at lower velocities measurements were difficult and less accurate. At higher velocities, the strips started to vibrate at low angles relative to vertical, resulting in a higher drag coefficient. Therefore, the values measured at the intermediate  $U=18.3$  cms<sup>-1</sup> are used.

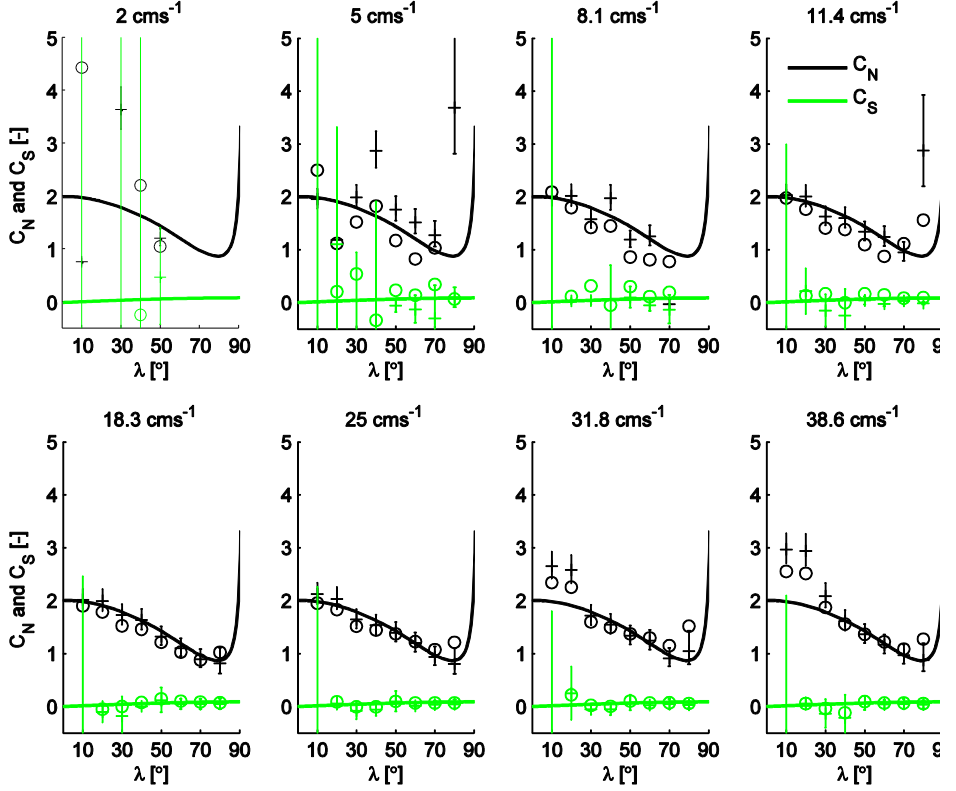


Figure 2.4  $C_N$  and  $C_S$  for various angles with the vertical plane. The circles are values corrected for tip effects, the crosses are uncorrected values with error bars and the lines indicate the relation in Eq. 25.

For a fit, Equation (27) would be an obvious starting point. However, in the case of  $C_N$  this is not possible; especially values at high angles (i.e., a ‘flatter’ orientation) are much higher. To account for these higher values, the following fit was made:

$$\begin{aligned} C_N &= \min(2 \cos \lambda + 0.1 \tan \lambda, 2\pi) \\ C_S &= 0.018 f \sin \lambda \end{aligned} \quad (28)$$

In the model,  $C_N$  is limited to  $2\pi$  for stability reasons, a value often used for plates at small angles of attack, see *Hoerner [1965]*.

### 2.3.3 Validation with flexible strips

Figure 2.5 shows the positions of very flexible and rather stiff plastic strips at different flow velocities and different lengths, whereas Table 2.2 lists the forces. Like the metal strips, the plastic strips started to vibrate at high flow velocities, possibly resulting in a different drag coefficient, which has not been included in the model. Also, measurements at 2.0 and 5.0  $\text{cms}^{-1}$  are less accurate (see Section 2.2.3). Possible errors in equipment, experimental set-up and the measurement of strip properties give an accuracy of 11% for the forces and 1 cm for the positions.

Table 2.2 Forces and relative errors. For measurements marked with # the strips vibrated, ~ means a measurement error, and values marked by \* are too low, probably as a result of a lower flow velocity in the upper part of the water column that could not be measured. These values are considered too low because the maximum increase in force with respect to the other strip lengths exceeds with a linear relation.

U cms <sup>-1</sup>	L M	FR			TW			ST		
		F <sub>model</sub>	F <sub>exp</sub>	error	F <sub>model</sub>	F <sub>exp</sub>	error	F <sub>model</sub>	F <sub>exp</sub>	error
		10 <sup>-2</sup> N	10 <sup>-2</sup> N	%	10 <sup>-2</sup> N	10 <sup>-2</sup> N	%	10 <sup>-2</sup> N	10 <sup>-2</sup> N	%
2.0	0.127	0.03	0.05	-33.9	0.03					
2.0	0.177	0.03	~0.03	28.6						
2.0	0.227	0.03	0.05	-30.0	0.05	0.06	-19.4			
5.0	0.127	0.11	0.12	-2.9	*0.18	0.15	21.6	0.19	*0.11	70.6
5.0	0.177	0.10	0.10	0.9				0.26	0.26	-2.2
5.0	0.227	0.10	0.10	-7.0	0.31	0.34	-7.6	0.33	0.34	-2.7
8.1	0.127	0.19	0.22	-13.5	0.46	0.00				
8.1	0.177	0.18	0.20	-9.4						
8.1	0.227	0.18	0.23	-20.9	0.80	0.79	1.6			
11.4	0.127	0.29	0.28	4.0	*0.89	0.76	17.8	0.93	*0.78	19.7
11.4	0.177	0.28	0.29	-0.2				1.28	1.27	0.9
11.4	0.227	0.29	0.33	-12.3	1.48	1.36	8.9	1.60	#1.65	-3.1
18.3	0.127	0.54	0.48	12.6	2.27	1.74	30.5	2.38	*2.05	15.9
18.3	0.177	0.56	0.49	12.5				3.18	#3.22	-1.5
18.3	0.227	0.58	0.53	9.1	3.08	2.89	6.7	3.62	#4.18	-13.6
25.0	0.127	0.82	0.72	14.4	4.06	3.29	23.3	4.34	*4.26	1.9
25.0	0.177	0.86	0.76	12.9				5.38	#6.32	-15.0
25.0	0.227	0.90	0.80	11.8	4.47	3.57	25.4	5.50	#6.51	-15.4
31.8	0.127	1.16	0.97	19.9	6.17	4.81	28.3	6.80	6.84	-0.6
31.8	0.177	1.22	1.04	17.3				7.63	#9.00	-15.3
31.8	0.227	1.27	1.06	19.3	5.86	4.22	38.8	7.29	#7.33	-0.5
38.6	0.127	1.53	0.98	55.5	8.25	6.48	27.2	9.42	10.24	-8.0
38.6	0.177	1.61	1.07	49.6				9.68	#10.38	-6.7
38.6	0.227	1.67	1.09	53.6	7.28	4.93	47.5	9.02	8.18	10.2

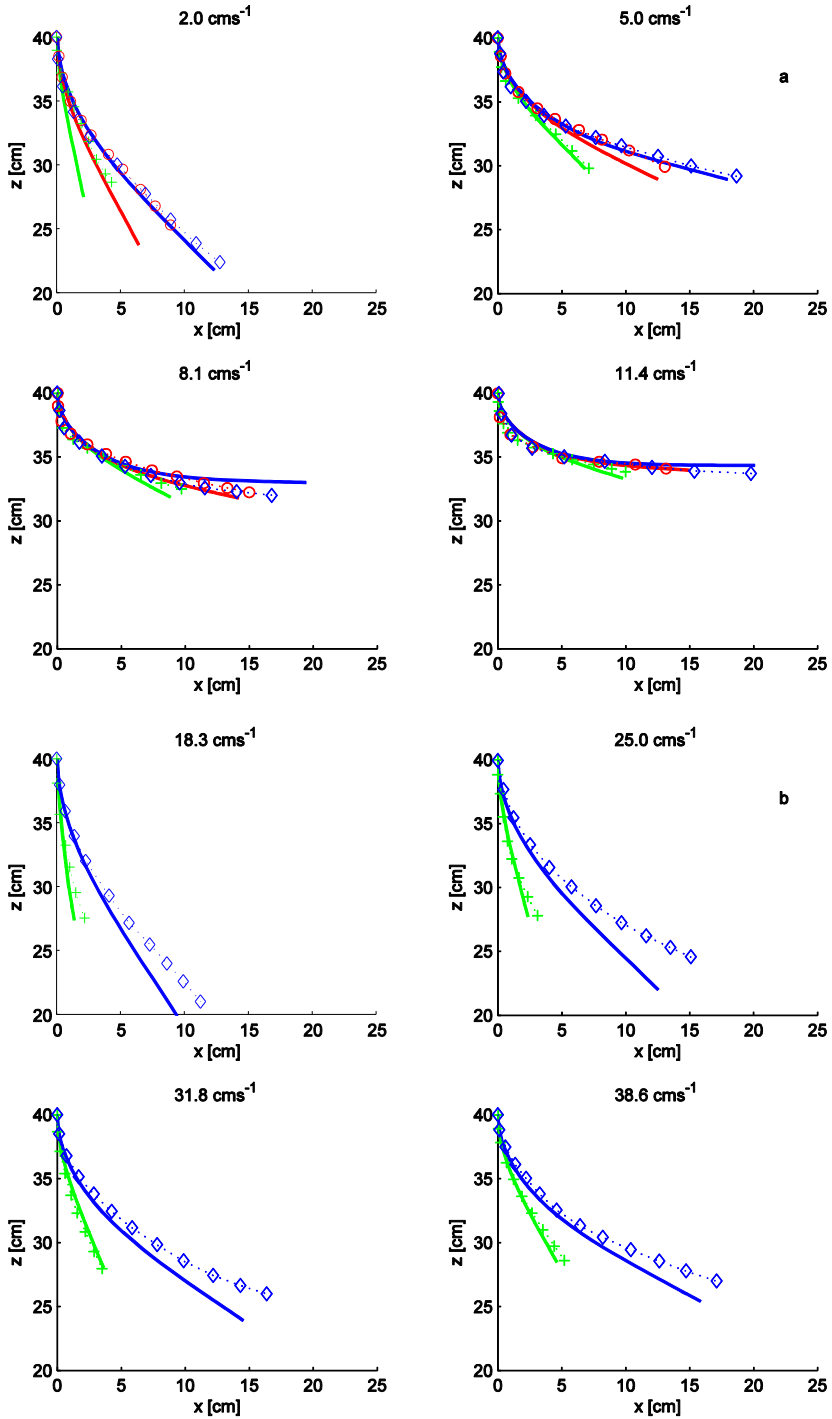


Figure 2.5 Positions of the (a) very flexible strips (FR) and (b) tie-wraps (TW) at four velocities and different lengths. Crosses, circles and diamonds indicate measurements for strips of 12.7, 17.7 and 22.7 cm respectively. The continuous lines are the model predictions.

## 2.4 Discussion and Conclusions

The general behaviour of the model as discussed in Section 2.3.1 matched our expectations as well as observations recorded in literature. Our simulations clearly show that longer plants do not necessarily create more drag, similar to our own observations and those of *Vogel [1981]* and *Bouma et al. [2005]*.

Our model appeared to be very sensitive to the number of stem elements. At the same time, this number affects the computation time negatively, up to a power of four. To alleviate this problem we incorporated a logarithmic distribution of element increments ( $ds$  in Eq. 1-5), concentrating many small elements near the fixation point (where most bending occurs, hence resolution is required) and longer increments towards the free and straight tip.

### 2.4.1 Performance of the model: forces and positions

In many cases, especially at intermediate flow velocities, the predicted forces are fairly close to the measured values (Table 2.2). In some cases model predictions deviate more than the expected measurement precision, but they do show an internal consistency similar to that of the measurements. Therefore, the results are considered to be useful.

At the lowest flow velocities, the performance of the model is difficult to determine, since the forces are close to the lower detection limit of our equipment and the velocity profiles are not uniform along the strip (Fig. 2.3). Nevertheless, the results are not far off, though generally under-predicted. This difference might be explained by the model's drag and lift coefficients' independence of the Reynolds number, whereas at these low Re-numbers the measurements on stiff strips indicated higher values.

Apart from some individual anomalies, the structural differences in both forces and positions between the model and the experiments can be explained by a possible dissimilarity of the velocity profile: in the model, the simulated velocity profile is uniform over the upper part of the water column, whereas in the experiment appears to be slightly lower close to the water level. That close to the fixed end of the strips, this lower velocity hardly affects bending, but it does reduce the force quadratically. On the other hand, if the velocity at the tip is slightly higher, the position will be strongly affected due to the larger leverage, but due to the more streamlined orientation of the strips the resulting increase in force is minimal.

The structural under-prediction of the forces and positions for the stiff transparent strips (ST, Table 2.2, marked by '#') might be attributed to the drag increasing flutter, a phenomenon not incorporated in the model. The measurements on the stiff metal strips clearly show an increase (about 25%) in drag if flutter occurs.

### 2.4.2 Performance of the model: hydrodynamics

Figure 2.6 shows a comparison of the experiment and model simulations. The agreement with the measurements of *Nepf & Vivoni [2000]* is fairly good, especially in the vegetated part of the water column. The discrepancies near the water surface are probably the result of side wall friction in their rather narrow flume causing secondary flows. Another small, but coherent deviation from the measurements is the slight underestimation of the velocity especially just below the top of the canopy, combined with an overestimation of the turbulence intensity in this

area. This indicates that we either underestimate the penetration of momentum from the free flow into the canopy, which would lead to a higher velocity inside the canopy, or that we slightly underestimate the canopy height itself. The latter corresponds to our finding that the plants in our model remain very upright, which is probably due to the very high –but not directly measured- modulus of elasticity.

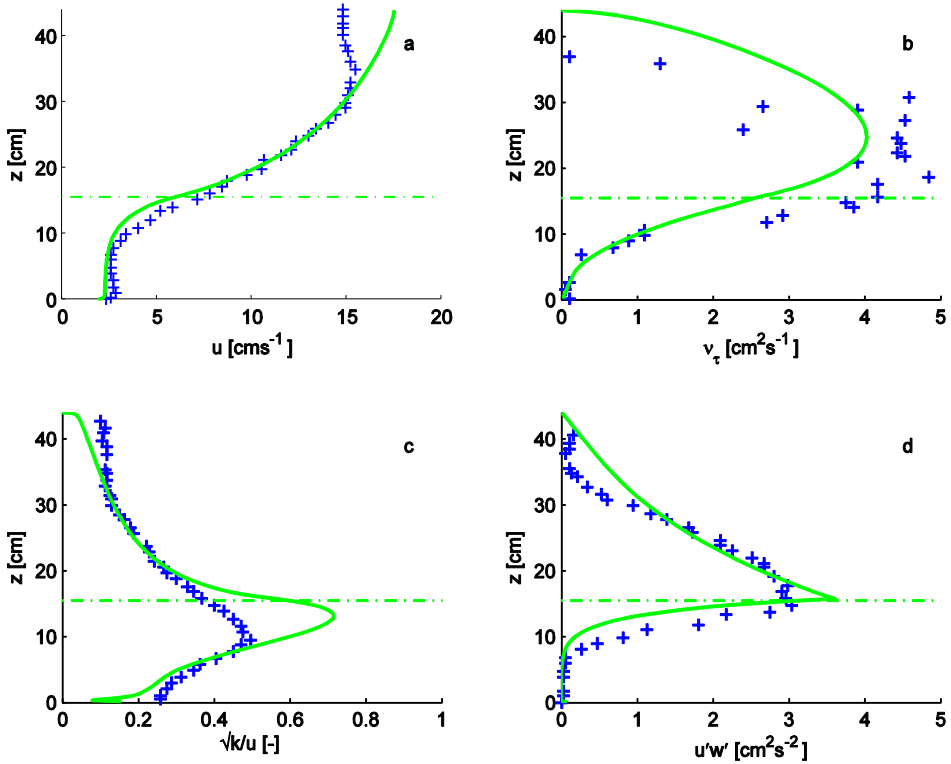


Figure 2.6 Vertical profiles of hydrodynamic properties as predicted by the model (continuous line), measured by *Nepf and Vivoni [2000]* (crosses). The dashed line indicates the height of the canopy. a) horizontal velocity; b) eddy viscosity; c) turbulence intensity; d) Reynolds stress

To study the effect of different canopy heights on flow properties, we compared these validation results with those of simulations based on the same settings, but with completely rigid ( $E=2 \cdot 10^{12} \text{ Nm}^{-2}$ ) and naturally flexible ( $E=2 \cdot 10^7 \text{ Nm}^{-2}$ ) vegetation. Figure 2.7 shows that the experimental results of *Nepf & Vivoni [2000]* and rigid vegetation are very similar, whereas the more flexible vegetation leads to a lower canopy with higher flow velocities inside. For a comparison with more traditional methods of incorporating the effect of vegetation in a hydrodynamic model, we also made a simulation with a smooth bed without vegetation and one in which the vegetation is mimicked by a bed roughness coefficient (in this case a Chézy coefficient of  $8.78 \text{ m}^{1/2} \text{ s}^{-1}$ , based on flume dimensions and water level gradient). Figure 2.7 clearly shows that the flow profiles are very different at the same depth-averaged velocity. Especially the transfer of momentum to the bed –paramount in erosion studies- is greatly overestimated when using the traditional methods of a higher bed roughness factor: the bed shear stress would

amount  $0.26 \text{ Nm}^{-2}$  in that case, whereas our model indicates values of  $0.0024 \text{ Nm}^{-2}$  in case of flexible vegetation,  $0.0025 \text{ Nm}^{-2}$  for rigid vegetation. As a comparison, the computed values in case of very flexible vegetation are  $0.0050 \text{ Nm}^{-2}$  and  $0.013 \text{ Nm}^{-2}$  for a bare bed.

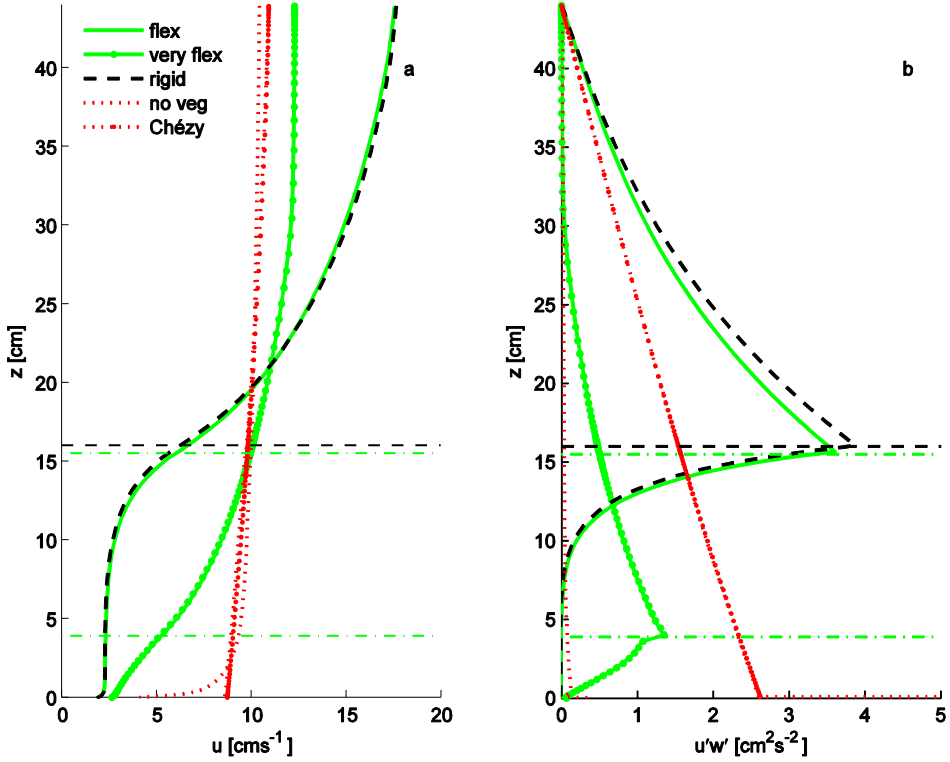


Figure 2.7 Comparison of flow properties for five different scenarios, all at a depth-averaged velocity of  $10 \text{ cm s}^{-1}$ : With the same vegetation as used in Fig. 2.6, with more flexible vegetation, with rigid vegetation of the same size, without vegetation and without vegetation but with a representative bed roughness (Chézy coefficient). a) horizontal velocity; b) Reynolds stress. Horizontal lines indicate canopy height.

### 2.4.3 Comparison to other work

An interesting test of the model's general applicability would be a comparison to other experiments on (artificial) seagrass, like those of *Folkard [2005]*, *Maltese et al. [2007]*; *Abdelrhman [2003, 2007]* and *Gambi et al. [1990]*. However, either their recording of vegetation properties, the complicated shape of their vegetation meadow or the single dimension of our model hampers a good comparison. This indicates the two major drawbacks of our model: it does not deal with spatial variability or complicated plant forms and it requires the input of vegetation properties that are not usually measured such as the modulus of elasticity. At the same time, the reliance on vegetation properties is one of the main advantages of our model: when these physical properties are known, there is no need for estimating 'drag' coefficients like for example in the model of *Velasco et al. [2008]*.

#### 2.4.4 Interaction between plants properties and flow

To show the effects of changes in plant properties on flow properties and vice versa, we made a series of simulations in similar conditions as discussed in Section 2.4.2, though with some small changes: Figure 2.8 shows what happens if from the standard set of parameters (d.a. velocity, depth, plant elasticity or spatial density), one is changed. The standard settings are  $U=20 \text{ cm s}^{-1}$ ,  $h=50 \text{ cm}$ , flume width 38 cm, bed roughness  $C=80 \text{ m}^{1/2} \text{ s}^{-1}$  and 1000 plants per  $\text{m}^2$  with  $l=0.25 \text{ m}$ ,  $b=3 \text{ mm}$ ,  $d=0.35 \text{ mm}$ ,  $\rho_v=920 \text{ kg m}^{-3}$  and  $E=2 \cdot 10^7 \text{ Nm}^{-2}$ . These simulations should be seen as a first exploration, since many combinations are possible in nature. We feel that in some circumstances the one parameter is decisive, whereas in other conditions the effect of this single parameter may be rendered insignificant by others, e.g. in very dense fields the properties of individual plants may not matter anymore. However, a thorough study into all mutual influences is beyond the scope of this article.

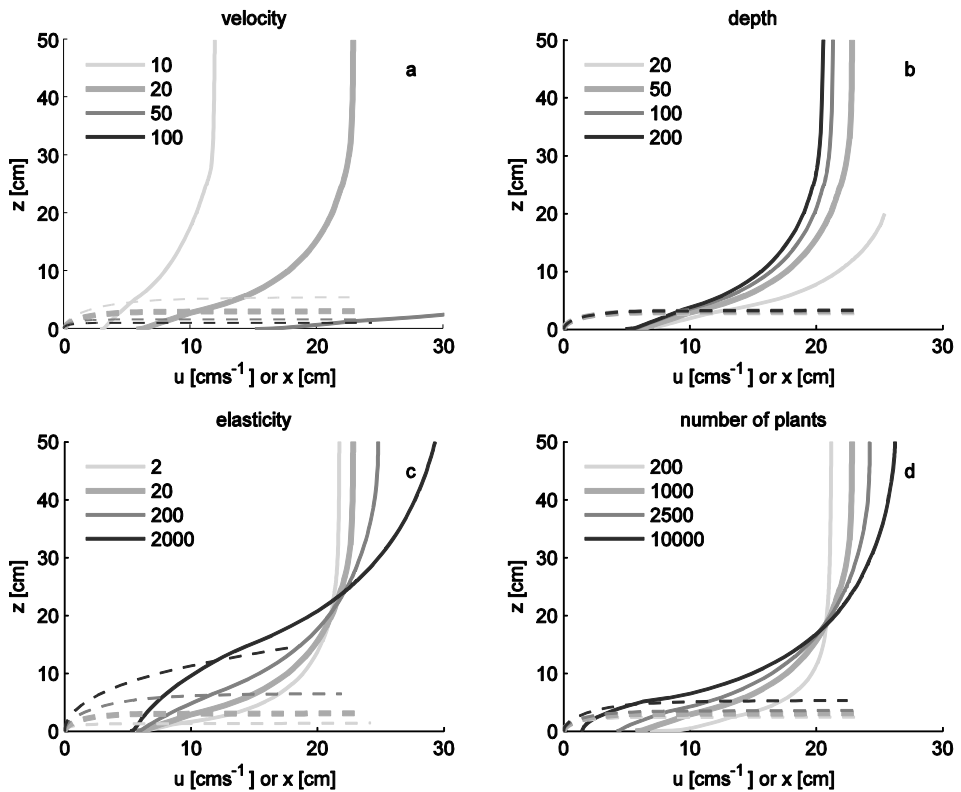


Figure 2.8 Flow velocity profiles (continuous lines) and plant positions (dashed lines) in a flume for a) various depth-averaged velocities ( $\text{cm s}^{-1}$ ); b) various flow depths (cm); c) various elasticities (MPa); d) different plant densities (per  $\text{m}^2$ ). All other properties remained constant, as indicated by the slightly thicker line of the 2<sup>nd</sup> value in each graph: length 25 cm, width 3 mm and thickness 0.35 mm.

An increasing flow velocity means that the plants will bend more and the bed shear stress is higher. For increasing depths there is not much difference because the ratio of free flow to canopy flow is large in most cases, except for the shallowest condition where more water is forced through the canopy. Changes in elasticity seem to have the strongest effect on flow and

plant position: The stiffer the plants, the higher they reach into the water column and the more they divert flow from the canopy towards higher regions. The flow velocity near the bed however is very similar in all cases. A larger plant thickness would do the same, as both thickness and elasticity contribute to flexural rigidity. A denser canopy does lower the velocity close to the bed considerably, but only the highest density has a considerable effect on the plant position.

#### 2.4.5 Applicability and further work

With the model in its current form, one can look in detail at processes in and above a vegetation field, and derive properties that govern the exchange of substances and the survival of plants. This model could also be used as a predictor of bed roughness coefficients for areas with flexible vegetation -such as estuaries and rivers-, thus expanding the possibilities of other hydrodynamic models that do not account for vegetation explicitly.

The inclusion of spatial variability and the possibility to study plants with non-uniform properties along their length are subject of current research. A similar extension into three dimensions has already been successfully made for an earlier rigid version of this model [Temmerman *et al.*, 2005]. Other improvements to the model would be including more natural meadow-related issues like the mechanical interaction between blades, the effect of plants sheltering in each other's wakes [Raupach, 1992; Nepf, 1999] and effects of other organisms, e.g. epiphytes on blades. In our opinion, each of these topics would justify separate studies that require a substantial experimental basis. On a different track, assessing the model's performance in wave conditions is also worthwhile.

### 2.5 Conclusions

In conclusion, our model for flow through very flexible vegetation performs well. Its achievement in determining the position and forces of strips of three different materials, at various lengths and flow velocities, indicates that the model and the drag/lift coefficients are generally applicable. As very flexible plants can assume a position almost parallel to the flow direction, it is not sufficient to take only the drag perpendicular to a leaf into account. The predicted hydrodynamic properties also compare quite well to measurements and are based on measurable physical input parameters rather than estimated tuning coefficients. The incorporation of flexible vegetation gives more realistic results than the use of rigid vegetation or the use of an adjusted bed roughness coefficient. The model is sensitive to plant parameters though; particularly the stem thickness and the elasticity. The latter can be difficult to measure. Another limitation is the fact that the model does not deal with spatial variability, complicated plant shapes or mechanical interactions between plants. The flow velocity has a much stronger effect on the plant position than the depth and the structural rigidity is more influential than the number of plants per area.


Overall, the performance of the model is good. Validation data are limited however and the hydrodynamic performance is validated only against measurements in rather common flow conditions. The model should also be tested against measurements of more extreme situations: higher and lower flow velocities, more flexible vegetation, different relative flow depths and different vegetation configurations.

Because we realistically predict plant positions, forces on plants, hydrodynamic properties and bed shear stress reduction, we consider our model a useful improvement. The basis of physically measurable input parameters provides us with a very useful and generic tool in studying flow and exchange processes in fields of flexible vegetation.

## **Acknowledgements**

We thank NIOO-CEME for the use of their experimental facilities, Luca van Duren for help on flume data, Ben Norder of DelftChemTech for determining the properties of the artificial vegetation and three anonymous reviewers for their valuable comments. The first author is funded by the NWO LOICZ-programme, under grant 014.27.014.



The background of the slide is a grayscale photograph of a river or marshy area. In the foreground, there are several long, thin reeds or grasses leaning at various angles. In the background, a tall, vertical pole or structure is visible, possibly part of a bridge or a measurement station. The overall scene is somewhat hazy, suggesting a misty or overcast day.

### **3 Creating and testing a two-dimensional model for flow through flexible aquatic vegetation**

Based on Dijkstra, J.T. and T.J. Bouma 'Assessing ecosystem-engineering capacities of aquatic vegetations of contrasting flexibility: a model study'; to be submitted

## Abstract

The detailed hydrodynamic/plant motion model Dynveg, developed in the previous chapter, performs very well but is limited to a single spatial dimension. In this chapter, Dynveg was combined with the large-scale hydrodynamic model Delft3D to enable modelling of flexible vegetations at a larger scale. The leading principle for this integration is that flexible vegetation can be simulated as rigid objects, provided that these objects have properties that are representative of the flexible vegetation's position and orientation, and change depending on flow conditions.

This modelling approach was validated by comparing model results with flume experiments on two seagrass species, showing good agreement for canopy height, flow velocity profile and flow adaptation length. The good performance of the model shows that the principle of modelling flow through flexible vegetation by representing it as stiff vegetation with representative properties that change according to flow conditions, works. The model can be applied to study how spatial plant-flow interactions depend on plant properties as well as hydrodynamic conditions, which is done in the next chapter.

**Keywords:** flexible vegetation, two-dimensional modelling, *Zostera noltii*, *Cymodocea nodosa*

### 3.1 Introduction

Flume studies have shown that it is of major importance that models describing the hydrodynamic interaction between plants and their environment, account for both the bending of plants and the reduction of current velocities by the canopy [Nepf & Vivoni, 2000; Abdelrhman, 2003]. The bending of plants determines both the canopy height and the drag force experienced by the plants [Kouwen & Unny, 1973; Kutija & Hong, 1996; Wilson et al., 2003]. Together, plant height, orientation and spatial density determine the flow velocity distribution over the vertical, hence the bending of the plants [Ikeda et al., 2001; Luhar et al., 2008; Carollo et al., 2005]. This implies that vegetation height is the resultant of a highly dynamic feedback between plant bending and flow velocity, and that this feedback eventually determines the flow velocities and bed shear stresses inside the canopy that are relevant for the transport of nutrients and sediment.

Previous attempts to incorporate flexible vegetation in a hydrodynamic model are restricted in various ways: they are either limited to small plant deflections [Kutija & Hong, 1996; Ikeda et al., 2001] limited to buoyant vegetation [Abdelrhman, 2007], limited to a single plant species [Backhaus & Verduin, 2008] or require tuning of multiple parameters [Velasco et al., 2008]. Whereas these limitations are overcome by our Dynveg model [Dijkstra & Uittenbogaard, 2010; previous chapter] that calculates plant bending and the interaction with hydrodynamics based on real biomechanical properties, the application of Dynveg is limited as it is restricted to modelling one dimension (i.e., only height, but without spatial variability).

Delft3D is a spatial three-dimensional model that simulates flow related processes such as sediment transport and water quality in rivers, estuaries and coastal settings [Lesser et al., 2004]. This model can reproduce the effect of rigid vegetation on flow quite successfully over a large spatial scale [Temmerman et al., 2005], but is not yet able to account for flexible vegetation.

This chapter aims at introducing a method to extend Delft3D with a capability for flexible vegetation by combining it with Dynveg. In the next chapter, this combined model is used to study ecosystem engineering capacities of vegetations with contrasting flexibilities.

### 3.2 Methods

#### 3.2.1 Step 1: Modelling flexible vegetation in one dimension

As aquatic vegetation is highly flexible, bending cannot be described with simple engineering formulae applicable to the small deformations of bending cantilever beams [Gere & Timoshenko, 1999]. Therefore, we use a model specifically developed to simulate the dynamic interaction between flow and very flexible plants, called Dynveg. Dynveg calculates the production of drag by plants, resulting in a vertical distribution of stresses, turbulence and flow velocity (for details see previous chapter). In this one-dimensional model –i.e. without spatial variability–, all plants are considered to have the same properties, hence behave the same. This simplification holds for the middle of a sufficiently large and homogeneous, mono-specific meadow, but fails at the edges. If all plants behave the same, the effect of multiple plants can be represented by that of a single plant multiplied by the spatial density of the meadow.

Within Dynveg, a modelled shoot consists of a number of connected elements that exert forces on the water and each other. The drag forces exerted on the water depend on the velocity

difference between the water and an element, and the orientation of the element that determines its drag coefficient. The forces that the elements exert on each other lead to bending moments that, in combination with buoyancy, inertia and the rigidity of the plant, determine the position of the plant. The output of Dynveg consists of a vertical profile of hydrodynamic parameters such as the flow velocity and eddy viscosity, the plant position and deflected height ( $k_{veg}$ ), the equivalent drag coefficient ( $C_{Deq}$ ), the force acting on a plant and the bed shear stress.

Feedback to the hydrodynamic part of the model occurs through the additional production and dissipation of turbulence, which is calculated using a  $k-\varepsilon$  turbulence model. Production of turbulence is related to the force exerted on the plants, whereas dissipation comes from introducing an effective time scale that depends on the spacing between the plants, i.e. the maximum eddy size. Both the plant movement and the hydrodynamics are solved fully implicitly, but the feedback between them is modelled explicitly.

### 3.2.2 Step 2: Modelling flexible vegetation as short rigid rods

The plant motion-algorithm of Dynveg requires too much computation time to be directly used in medium- or long-term hydrodynamic simulations with Delft-3D (i.e., months to years). Fortunately, the flow through flexible vegetation can be modelled as flow through rigid rods, provided that the correct deflected height ( $k_{veg}$ ) and equivalent drag coefficient ( $C_{Deq}$ ) are chosen (Fig. 3.1; Fig. 3.2 defines  $k_{veg}$  and  $C_{Deq}$ ). Within this approach, the redistribution of biomass over the vertical as a result of plant bending is important, as the solidity (i.e., area of obstructions per unit volume of water) of the meadow determines both the drag and the space available to turbulent eddies. This approach is valid for a range of conditions that can occur in nature: depth  $h=0.1\text{-}2$  m, depth averaged flow velocity  $U=0.1\text{-}1$   $\text{ms}^{-1}$ , and number of plants  $np=10\text{-}10.000$   $\text{m}^{-2}$  (Fig. 3.1).

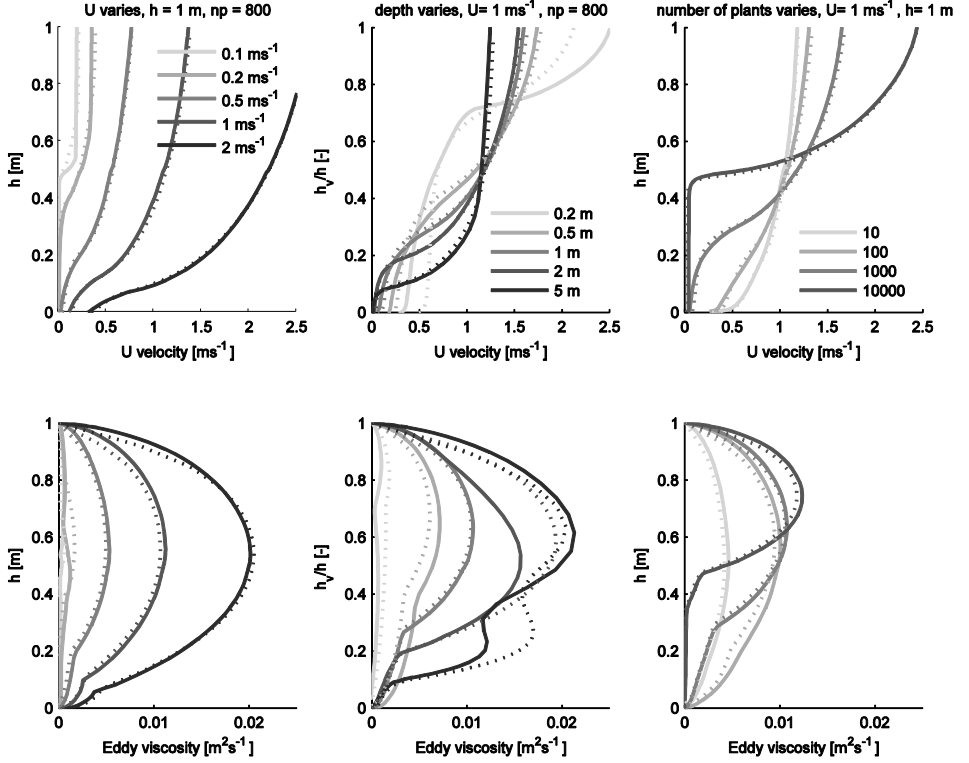


Figure 3.1 Comparison of flow velocity and eddy viscosity profiles for simulations with flexible vegetation (Dynveg model, solid lines) and with rigid rods that have the same height and equivalent drag coefficient (dashed lines). From left to right: variations in depth averaged velocity, in water depth and in spatial density.

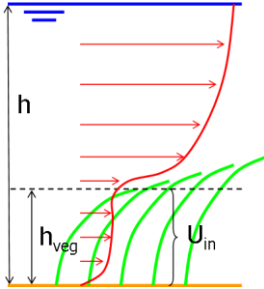


Figure 3.2 Definition of canopy velocity  $U_{in}$  based on flow velocity profile and deflected plant height  $k_{veg}$ .

The hydrodynamic Delft-3D model requires a computational time step in the order of seconds to ascertain the necessary spatial resolution and the matching Courant condition for stability, but  $k_{veg}$  and  $C_{Deq}$  can be adjusted using a much larger time step depending on the nature of the flow. In an estuary, the water depth and the depth averaged flow velocity can be considered as relatively constant over a period of ten minutes [Neumeier & Ciavola, 2004]. Consequently,  $k_{veg}$  and  $C_{Deq}$  also need to be adjusted at this same ten minutes period.

### 3.2.3 Step 3: Developing a fast iterative method to relate $k_{veg}$ and $C_{Deq}$ to hydrodynamics

The actual values of  $k_{veg}$  and  $C_{Deq}$  are on one hand determined by the hydrodynamic parameters water depth and flow velocity, and on the other hand by the plant parameters shoot density, shoot length, leaf area and shoot stiffness. Using Dynveg, we made a species-specific data table for  $k_{veg}$  and  $C_{Deq}$  for a set of realistic hydrodynamic conditions and plant characteristics. To limit the parameter space, plant properties like buoyancy and bending stiffness were assumed to remain constant over time. In its simplest form, when also the plant length and spatial density are considered constant, such a table contains  $k_{veg}$  and  $C_{Deq}$  for a range of realistic water depths and flow velocities (i.e., typically  $h = 0\text{--}2$  m,  $U = 0\text{--}0.5$  ms<sup>-1</sup>, but larger values are possible). As such a table is by definition discrete, “missing values” are found by linear interpolation (Fig. 3.3; interpolated values are bold and encircled). Straightforward linear interpolation is allowable despite the non-linear behaviour, on the condition that the values are sufficiently close together. In practice this meant we used steps of 0.1 m for  $h$  and 0.05 ms<sup>-1</sup> for  $U$ .

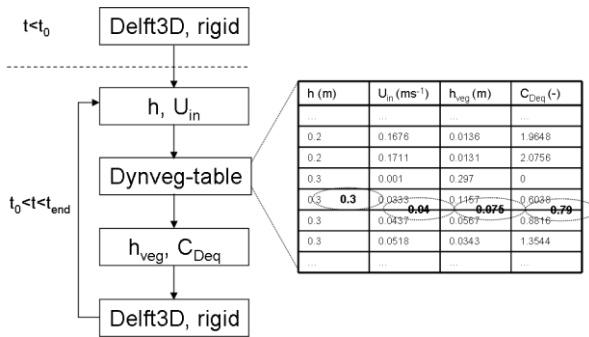


Figure 3.3 Calculation procedure for combined hydrodynamics (Delft3D) and plant position (Dynveg-table). The circles indicate values that are interpolated by the look-up algorithm.

As hydrodynamics and plant position affect each other,  $k_{veg}$  and  $C_{Deq}$  need to be obtained from the table by an iterative procedure (Fig. 3.3). Firstly, a short run with Delft3D is made to have a first estimate of the flow velocity and water depth on the location of the vegetation. Based on these values, secondly a look-up routine –provisionally built in Matlab– searches the representative  $k_{veg}$  and  $C_{Deq}$  in the lookup-table. Thirdly, these values are applied to a subsequent short Delft3D run, in which the flow will be slightly different due to the different vegetation position. This run generates new values of  $k_{veg}$  and  $C_{Deq}$  which are then used for further iteration. The iteration is stopped after twenty steps, which is normally sufficient to reach a stable solution in stationary flow conditions (Fig. A.1).

### 3.2.4 Step 4: Modelling flexible vegetation in more dimensions

Looking at a vegetation field in nature or in a flume, one observes that the plants at the leading edge of the meadow bend further than those in the middle, where all plants assume more or less the same position. As the length of this leading edge zone (LEZ) is relevant for the uptake of nutrients and the transport of sediment (i.e., for ecosystem engineering; *Morris et al., 2008*), a two-dimensional model is required to calculate the adaptation of flow and vegetation position.

As a consequence of this redistribution of flow over the vertical at the leading edge is that the depth averaged velocity ( $U_{da}$ ) cannot be used as a determinant for the plant position. After all, due to conservation of mass,  $U_{da}$  is the same throughout a flume with a constant cross-section, which would lead to the same plant position everywhere. Therefore, the more specific velocity inside the canopy ( $U_{in}$ ; Fig. 3.2), which is a measure for the amount of momentum actually acting on the plants, is used to determine the plant position. The use of  $U_{in}$  however also introduces a source of instability to the model, because  $U_{in}$  is integrated over the deflected vegetation height  $k_{veg}$ : when  $k_{veg}$  increases,  $U_{in}$  decreases, causing  $k_{veg}$  to decrease, leading to an increase of  $U_{in}$ , and so forth, resulting in a flapping plant.

Similar-looking oscillations also occur in nature, probably due to coherent eddies penetrating into a meadow. This phenomenon, called ‘monami’, has been described by various authors [e.g., Ackerman & Okubo, 1993; Ghisalberti & Nepf, 2002; Grizzle et al., 1996], but there is no real consensus about the exact mechanism. Such oscillations are unwanted in our medium- or long-term Delft-3D simulations, because Delft3D is not able to resolve vertical eddies on this scale and morphodynamic calculations over multiple tidal periods require a stable flow field. Therefore, we used temporal and spatial stabilisation methods, with time-averaging occurring before spatial averaging. Both  $k_{veg}$  and  $U_{in}$  are averaged over time, but according to different schemes:

$$U_{in}^t = \theta U_{in}^t + (1 - \theta) U_{in}^{t-1} \quad (29)$$

$$k_{veg}^t = \frac{1}{2} (k_{veg}^t + k_{veg}^{t-1}) \quad (30)$$

with  $\theta$  between 0 and 1. For spatial integration, both parameters are averaged over three cells (upstream, the cell of interest  $i$  and downstream):

$$U_{in}^i = \frac{1}{4} U_{in}^{i-1} + \frac{1}{2} U_{in}^i + \frac{1}{4} U_{in}^{i+1} \quad (31)$$

$$k_{veg}^i = \frac{1}{4} k_{veg}^{i-1} + \frac{1}{2} k_{veg}^i + \frac{1}{4} k_{veg}^{i+1} \quad (32)$$

The procedures for  $C_{Deq}$  are the same as those for  $k_{veg}$ , but  $C_{Deq}$  is only averaged over time. To speed up calculations, plants with similar  $k_{veg}$  and  $C_{Deq}$  values have been put into ‘classes’ with discrete values representative for the whole class: Instead of running calculations for possibly thousands of different plants, the model only has to deal with several classes.

The integration procedures we apply induce numerical damping, implying that our simulation method is not suitable for quickly varying flow or very sharp gradients. For our simulations this is acceptable, as the flow in tidal areas is not likely to change drastically within a couple of seconds; a timescale that can be resolved by the model. Strong spatial gradients however, which may occur at the edges of vegetation meadows, may not be represented well in case large grid cells are used.

### 3.2.5 Model validation

To validate our model, we simulated two contrasting seagrass meadows from which the hydrodynamics were studied in detail in a flume: *Zostera noltii* (Hornem.) and *Cymodocea nodosa* (Ucria) Ascherson. [Morris et al., 2008]. The *Z. noltii* plants have a length of 8 cm, a width of 1.2 mm, a thickness of 0.15 mm and a density of 9815 plants  $m^{-2}$  (equal to 39620 leaves  $m^{-2}$ ). *C. nodosa* has a more open canopy (520 plants or 1820 leaves  $m^{-2}$ ), but longer, wider and thicker

leaves ( $17.5 \text{ cm} \times 3.8 \text{ mm} \times 0.19 \text{ mm}$ ) on  $5.6 \text{ cm}$  long stiff sheaths. The elasticity modulus is notoriously difficult to measure; *Patterson et al. [2001]* measured  $5.6 \cdot 10^6$  up to  $200 \cdot 10^6 \text{ Nm}^{-2}$  for *Z. marina*, *Sarneel [pers. comm.]* found  $20 \cdot 10^6 \text{ Nm}^{-2}$ . *Abdelrhman [2007]* states that due to the small cross-section of the blades, buoyancy is more important than elasticity in restoring their upright position, which corresponds to our own findings during the testing of Dynveg [*Dijkstra & Uittenbogaard, 2010; Chapter 2*]. We considered the elasticity modulus  $E$  and vegetation density  $\rho_v$  similar for both species and used  $E=20 \cdot 10^6 \text{ Nm}^{-2}$  and  $\rho_v=950 \text{ kgm}^{-3}$  (similar to *Sarneel, pers. comm.*) to construct a look-up table using Dynveg.

The experiments were performed in a  $60 \text{ cm}$  wide  $40 \text{ cm}$  deep racetrack flume [*Bouma et al., 2005*] filled with salt water ( $1024 \text{ kgm}^{-3}$ ). The test section with the plants is located near the end of a straight side. In the numerical simulation we use an  $18 \text{ m}$  long rectangular flume, with vegetation from  $x=6 \text{ m}$  to  $x=7.1 \text{ m}$ . The computational grid cells are  $10 \text{ cm}$  long in flow direction,  $60 \text{ cm}$  (= the width of the flume) in  $y$ -direction and  $1 \text{ cm}$  thick ( $40$  cells in a depth of  $40 \text{ cm}$ ). The flow is driven by a velocity boundary upstream ( $U=0.2 \text{ ms}^{-1}$ ) and a water level boundary downstream. The time step in the Delft3D simulation is  $0.001 \text{ min}$  ( $0.06 \text{ s}$ ). After  $100$  Delft3D time steps ( $6 \text{ s}$ ), the vegetation position is updated and a new run starts until the end of the simulation has been reached after  $3 \text{ min}$  ( $30$  iterations).

### 3.3 Results and Discussion

#### 3.3.1 Model validation against flume measurements

A comparison between laboratory measurements by *Morris et al. [2008]* and model results showed that the simulated  $k_{veg}$  was very similar to the measured  $k_{veg}$ : for both *Z. noltii* and *C. nodosa*, the positions were within a few millimetres from each other (Fig. 3.4). Moreover, the gradual transition in bending degree in the first  $0.5$  to  $1 \text{ m}$  of the meadow seemed to be predicted well, too. The largest difference occurred at the edge of the *C. nodosa* meadow, where the real plants bent about  $1 \text{ cm}$  more. The predicted velocity profiles also matched the measured ones quite well: both the velocity inside the canopy and the height of the transition from canopy flow to free flow were similar. At the leading edge of the meadow ( $x=6 \text{ m}$ ), the velocity inside the meadow was somewhat underestimated in case of *Z. noltii*, and somewhat overestimated in case of *C. nodosa*. Similar to the measurements, the modelled canopy flux  $q_{in}$  in *C. nodosa* doubled that of *Z. noltii*, and was substantially higher at the leading edge.

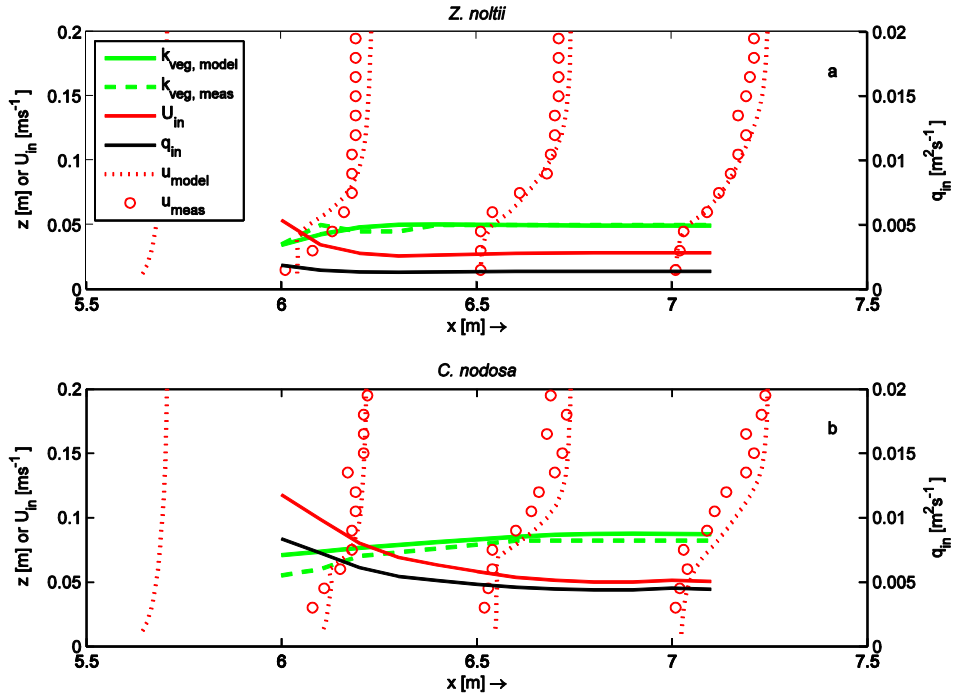


Figure 3.4 Longitudinal cross-section of the flume as used by *Morris et al. [2008]*, with flow velocities and plant deflection predicted by the model compared to measurements. a) *Zostera noltii* b) *Cymodocea nodosa*. Similar to *Morris et al.*, the canopy flux  $q_{in}$  in *C. nodosa* doubles that of *Z. noltii*, and is substantially higher at the leading edge.

### 3.3.2 Limitations and scope for applications

The flow velocity profiles and vegetation positions from modelling runs compared quite well to those from the measurements by *Morris et al. [2008]*. This holds for both *Zostera noltii* and *Cymodocea nodosa*, despite their different dimensions and densities (Fig. 3.4). Also, the patterns of horizontal and vertical velocity as well as turbulent kinetic energy in the simulated *Spartina* meadows were similar to the measurements of *Neumeier [2007]*. Therefore, our combined plant-flow model seems suitable for more general simulations with the aim of understanding how the ecosystem engineering capacity of plants depends on plant flexibility and density along a range of depths and flow velocities.

The possibility of our model to simulate the bending height of the vegetation based on directly measurable biomechanical properties rather than empirical roughness coefficients [e.g. *Kouwen & Unny, 1973; Wu et al., 1999*] is particularly interesting for vegetation that occupies a substantial part of the water column (e.g., estuarine intertidal vegetations & shallow rivers). In deep water where vegetation only occupies a small volume close to the bed, a simpler approach – e.g. using a fixed pre-calculated vegetation height- may be sufficient.

We do realise that the validation remains limited with respect to hydrodynamic conditions, the number of plant species and the transport processes that are incorporated into the model. Moreover, the numeric implementation inherently imposes limits to the model's applicability and

accuracy. For example, vertical exchange of constituents between the meadow and the flow layer on top, caused by large eddies in the mixing layer –a phenomenon that can be observed as a ‘monami’ [Ackerman & Okubo, 1993; Grizzle *et al.*, 1996; Ghisalberti & Nepf, 2002]- was not incorporated in the model. Incorporating this kind of processes requires modelling on a far smaller spatial and temporal scale, which would make it impossible to address the main questions we were interested in; determining how the species characteristics flexibility and density for a range of water depths and flow velocities, affect the biophysical interactions and thereby a species ecosystem engineering capacity.

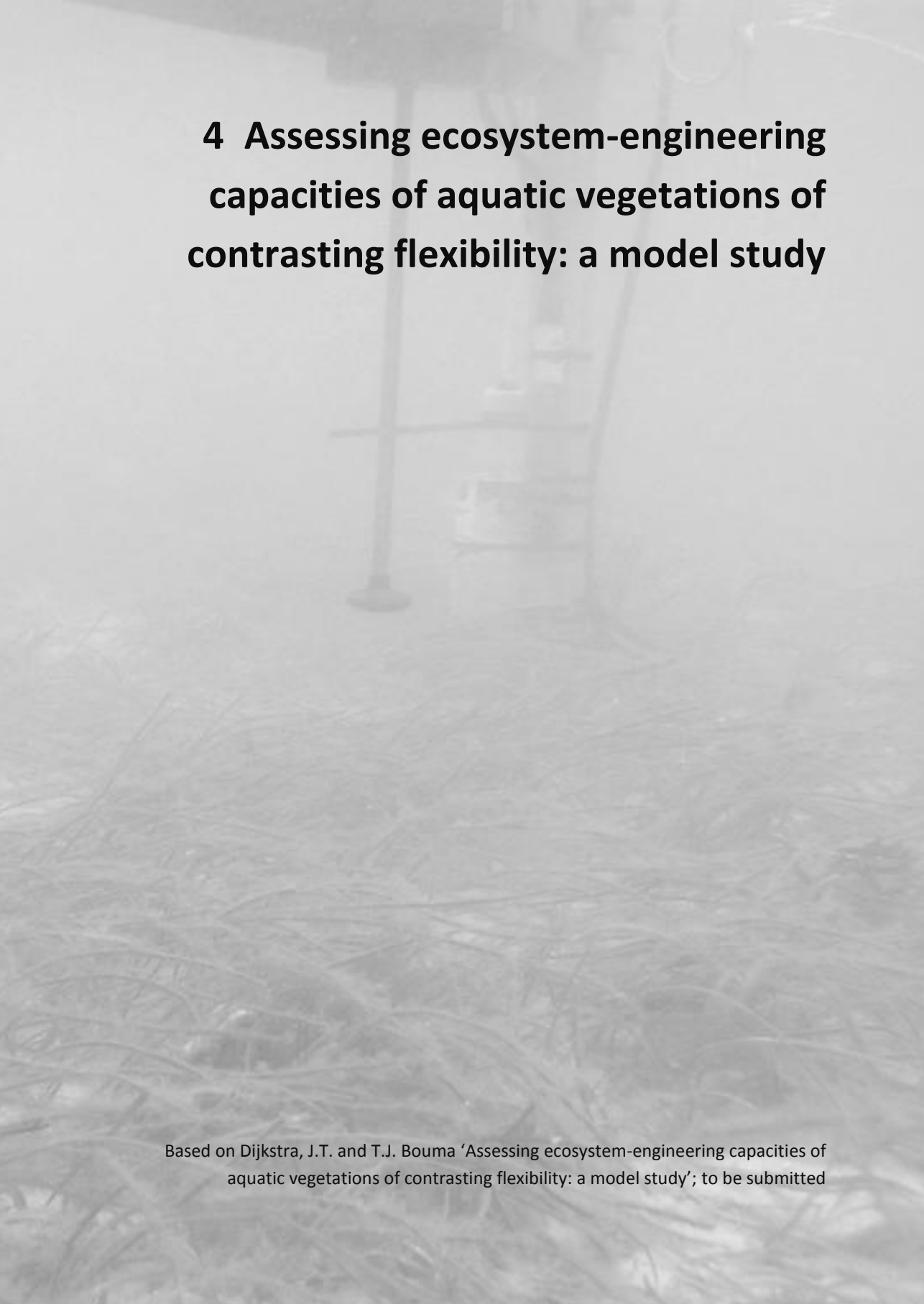
The use of the biomechanical Dynveg model circumvents the need to derive specific analytical formulas or empirical coefficients, although the interpolation of values in a look-up table can cause errors in some circumstances. Simple formulae, cf. Kouwen & Unny [1973], Kouwen & Li [1980] and Vogel [1981], would be preferable. Unfortunately, our attempts to derive such formulae analytically or by means of data mining techniques such as applied by Baptist *et al.* [2007] did not yield any result and primarily showed how complicated the interplay between water depth, flow velocity, plant stiffness, buoyancy, leaf length and spatial density is. Hence we applied a dynamic model that now allows us to account for measurable biomechanical plant properties of simple strip-shaped plants, which is applicable for many estuarine vegetation types. The incorporation of more complexly shaped plants remains to be tested and validated.

Compared to other models for flow through flexible vegetation, our model is more versatile, but also more complex. The basic model of Peterson *et al.* [2004] reproduces flow reduction in the canopy quite well, but only for dense canopies and if the canopy height is known; the drag coefficient remains a fitting parameter like in the model of Velasco *et al.* [2008]. The model of Abdelrhman [2007] is quite advanced and suitable to study two-dimensional flow through meadows of very flexible vegetation. However, because the latter model is based on a force balance of leaves determined by buoyancy rather than elasticity, this model is not suitable to compare plant species varying in shoot stiffness. Furthermore, by using Delft3D as a basis for the hydrodynamics, our model is relatively straightforward extendable to three dimensions and can thus in the future be used to study how canopies affect water quality and the transport of particles.

### 3.4 Conclusions

In this study, we present a computational model for two-dimensional flow through flexible aquatic vegetation. The model was made in four consecutive steps: one-dimensional modelling of flexible vegetation, deriving a principle to represent flexible vegetation by means of rigid rods with changing properties, developing a fast iterative method to determine these properties according to actual hydrodynamic conditions and developing a numerical scheme to do this in two dimensions.

The resulting model compares well to measurements of plant position and flow velocity profiles in meadows of two different seagrass species. The good performance of the model shows that the principle of modelling flow through flexible vegetation by representing it as stiff vegetation with representative properties that change depending on flow conditions, works. The model can be used to study how spatial plant-flow feedbacks depend on plant properties and ambient conditions, which will be done in the following chapter.

The background image is a grayscale photograph of a laboratory experiment. It shows a metal frame with a horizontal bar and a vertical rod. A container, possibly a beaker or a small tank, is suspended from the horizontal bar. The container appears to contain some material, likely the aquatic vegetation mentioned in the text. The overall scene is dimly lit, with the focus on the experimental setup.

## **4 Assessing ecosystem-engineering capacities of aquatic vegetations of contrasting flexibility: a model study**

Based on Dijkstra, J.T. and T.J. Bouma 'Assessing ecosystem-engineering capacities of aquatic vegetations of contrasting flexibility: a model study'; to be submitted

## Abstract

The model developed in the previous chapter was used to assess the ecosystem engineering capacities of three plant species that have a partially overlapping distribution in temperate intertidal areas: the stiff *Spartina anglica*, the short flexible seagrass *Zostera noltii* and the tall flexible seagrass *Zostera marina*. The flow velocity inside the canopy, the canopy flux and the bed shear stress were modelled as proxies for the species' ability to absorb hydrodynamic energy, the supply of nutrients or sediment and the ability to prevent erosion, respectively.

The stiff *Spartina* had a higher canopy flux than both flexible seagrasses, hence a greater ability to trap sediment. This canopy flux was inversely related to spatial density along the entire natural range. For flexible seagrasses, the canopy flux was only related to density in relatively sparse meadows; in denser meadows it remained constant, likely as a consequence of skimming flow. The flexible species were more efficient in reducing bed shear stresses than stiff *Spartina*, hence better at preventing erosion. The length of the leading edge zone, usually less than two metres, could not be related to flow or plant properties. In conclusion, present results show that biomass alone is not a good indicator of ecosystem engineering capacities, as the latter also strongly depends on shoot-stiffness properties and environmental conditions.

**Keywords:** flexible vegetation, rigid vegetation, ecosystem engineering, bed shear stress, canopy flux, two-dimensional modelling, *Zostera noltii*, *Zostera marina*, *Spartina anglica*

## 4.1 Introduction

The objective of this chapter is to assess how the species characteristics flexibility and density affect the biophysical interactions and thereby species ecosystem engineering capacity for a range of water depths and flow velocities. We used the two-dimensional plant-flow model developed in the previous chapter to model the ecosystem engineering by the stiff cordgrass *Spartina anglica* that occurs in the intertidal zone above mean sea level, the small and flexible seagrass *Zostera noltii* that occurs around mean sea level and the longer flexible seagrass *Zostera marina* that occurs below this level.

The ecosystem engineering capacity of these vegetations is evaluated using the following three proxies for habitat modification [Peralta et al., 2008]: i) The velocity inside the canopy, relative to the ambient velocity, as measure of the meadows capacity to reduce hydrodynamic energy and alter currents. ii) The flux through the canopy as an important factor for how much sediment and nutrients can be retained within the meadow and how quickly toxic substances are removed. iii) The bed shear stress as an absolute measure for the erosive potential of the flow, i.e. the plant's ability to protect the bed from erosion.

## 4.2 Methods

### 4.2.1 Parameters used as proxy for ecosystem engineering capacity

We subsequently used the model to evaluate the capacity of three contrasting vegetations to alter their abiotic/physical environment via bio-physical interactions. Similar to Peralta et al. [2008], we evaluate the ecosystem engineering capacities of these vegetations eventually using three hydrodynamic properties as proxies for habitat modification: the reduction of velocity inside the meadow  $U_{in\%red}$ , the relative canopy flux  $q_{in\%}$  and the reduction of the bed shear stress  $\tau_{b\%red}$ . These parameters are a measure for a meadows capacity to alter currents ( $U_{in\%red}$ ), for the flux of water that transports nutrients, sediment or seeds through the canopy ( $q_{in\%}$ ) and for the erosive potential of the flow ( $\tau_{b\%red}$ ), respectively.

The velocity inside the canopy is derived from the canopy flux:

$$U_{in} = \frac{q_{in}}{k_{veg}} \quad (33)$$
$$U_{in\%red} = 100\% \times \frac{(U_{da} - U_{in})}{U_{da}}$$

In which the canopy flux is defined according to:

$$q_{in} = \int_0^{k_{veg}} u(z) dz \equiv \sum_0^{\sigma_{kveg}} q_{\sigma} \quad (34)$$
$$q_{in\%} = 100\% \times \frac{q_{in}}{q_{da}}$$

where  $\sigma_{kveg}$  is the index of the grid cell occupied by the top of the vegetation, counted from the bed and  $q_\sigma$  the flux in a computational layer  $\sigma$ . The reduction of bed shear stress is calculated with respect to a reference bed shear stress  $\tau_{bref}$  of a bare bed in the same hydrodynamic conditions:

$$\tau_{b\%red} = 100\% \times \frac{(\tau_{bref} - \tau_b)}{\tau_{bref}} \quad (35)$$

#### 4.2.2 Dependence of ecosystem engineering capacity on species properties

We modelled three types of contrasting intertidal plant species: *Spartina anglica*, *Zostera noltii* and *Zostera marina* (properties in Table 4.1). We selected these species because they differ in mechanical properties, while their distribution areas partly overlap [cf. Bouma et al., 2005]: the longer flexible *Z. marina* occurs from subtidal to the lower intertidal zone, the shorter flexible *Z. noltii* in the intertidal zone and the stiff *Spartina* in the intertidal zone above mean sea level.

Table 4.1 Properties of artificial plants used for modelling. *Spartina* has a cross-section slightly larger than actual plants of this length to incorporate the additional drag of the leaves, the *Zosteræ* have flat leaves and no shoots. The solidity in the horizontal plane is the product of the width, thickness and number of structures per m<sup>2</sup>, the frontal area is the number of structures multiplied by the width.

	length	width	thickness	spatial density	stems/leaves per plant	structures	elasticity	density	solidity in horizontal plane	frontal area
Species	cm	mm	mm	m <sup>-2</sup>		m <sup>-2</sup>	MPa	kgm <sup>-3</sup>	%	m <sup>-1</sup>
Natural density										
<i>Spartina anglica</i>	25	8.5	5	1500	1	1500	700	1000	6.38	12.75
<i>Zostera noltii</i>	8	1.2	0.15	9815	4	39260	20	950	0.71	47.11
<i>Zostera marina</i>	30	5	0.35	1000	4	4000	20	950	0.70	20.00
Low density										
<i>Spartina anglica</i>	25	8.5	5	50	1	50	700	1000	0.21	0.43
<i>Zostera noltii</i>	8	1.2	0.15	3000	4	12000	20	950	0.22	14.40
<i>Zostera marina</i>	30	5	0.35	300	4	1200	20	950	0.21	6.00

Apart from differences in structure and stiffness (Table 4.1), the three species also differ in spatial density. We studied two densities for all species: the ‘natural’ density (HD) that is representative of field conditions (1500 shoots m<sup>-2</sup> for *Spartina*, 39620 for *Z. noltii* and 4000 m<sup>-2</sup> for *Z. marina*) and a lower ‘comparison’ density (LD; 50, 12000 and 1200 shoots m<sup>-2</sup> respectively) with a similar solidity (0.21%) for all species. We used solidity –defined as the product of width, thickness and number of structures per m<sup>2</sup> of the horizontal plane- rather than the biomass for two reasons: *i*) Solidity directly represents the size of an object as encountered by the flow, whereas biomass also includes properties such as tissue density that do not affect the flow. *ii*)

Biomass also depends on the length of plants, thereby incorporating another possibly complicating parameter.

To study the specific effect of solidity on ecosystem engineering properties, we ran the Dynveg model for a range of plant densities that ranged from extremely sparse to extremely dense: 10-3000 plants per  $\text{m}^2$  for *Spartina*, 100-12000 plants per  $\text{m}^2$  for *Z. noltii* and 10-3000 plants per  $\text{m}^2$  for *Z. marina*. The solidity range of *Z. noltii* is the smallest (0.22-0.71%), the one of *Spartina* the largest (0.21-6.38%).

#### 4.2.3 Dependence of ecosystem engineering capacity on hydrodynamics

In order to cover the full range of depths and flow velocities the plants can be exposed to during a tidal cycle, we first simulated the plant behaviour for each of the mimicked species with the one-dimensional model Dynveg for water depths between 0.25 to 2.5 m and depth averaged velocities between 0.05 to 0.5  $\text{ms}^{-1}$ . Subsequently, we used two-dimensional simulations –similar to a flume experiment– to study the spatial differences in flow and plant position at two water depths of 0.25 and 1.0 m, at depth averaged velocities of 0.05 and 0.3  $\text{ms}^{-1}$ . We chose these settings because these conditions are representative for conditions in the field, where all three species would become submerged regularly depending on the tide and weather conditions.

With these spatial simulations we can focus on the leading edge of the meadow, where the spatial gradients in canopy flux can be large. Here, we define the length of this leading edge zone (LEZ) as the adaptation length of the canopy flux  $q_{in}$ : the grid cell in which  $q_{in}$  does not deviate more than 0.5% from its value in the six surrounding grid cells marks the end of the LEZ.

### 4.3 Results

#### 4.3.1 Effects of hydrodynamic conditions - 1D simulations

Our 1D-Dynveg model simulations showed that in general, the response of vegetation height ( $k_{veg}$ ), velocity in the vegetation ( $U_{in}$ ) and the canopy flux ( $q_{in}$ ) to a change in depth averaged velocity ( $U_{da}$ ; Fig. 4.1) was stronger than to a change in water depth (Fig. 4.2). Clearly, the largest changes in  $k_{veg}$  and  $U_{in}$  occurred at the lower end of the ranges of velocity and water depth. At the upper end of these ranges, the response of  $k_{veg}$ ,  $U_{in}$  and  $q_{in}$  to changes in of velocity or depth was almost linear. The behaviour of  $k_{veg}$ ,  $U_{in}$  and  $q_{in}$  was always very similar for both vegetation densities, but greatly differed between species.

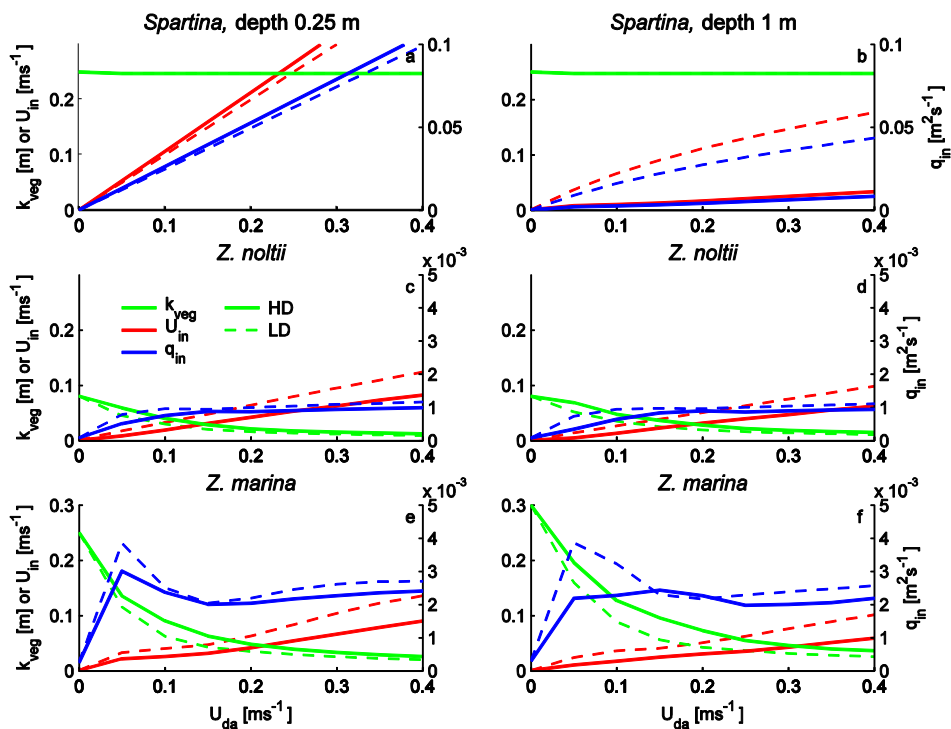


Figure 4.1 The response of vegetation height  $k_{veg}$ , canopy flow velocity  $U_{in}$  and canopy flux  $q_{in}$  to increasing depth averaged velocity at two fixed water depths and. *Spartina* has another scale for  $q_{in}$  (right) than the two seagrass species.

Not surprisingly, for the stiff *Spartina*, the  $k_{veg}$  remained constant irrespective of velocity (Fig. 4.1a & 4.1b) or depth (Fig. 4.2a & 4.2b).  $U_{in}$  and therewith  $q_{in}$  increased practically linearly with increasing  $U_{da}$  (Fig. 4.1a & 4.1b).  $U_{in}$  decreased with depth, which was clearest for the depth range of 0.25-0.5 m (Fig. 4.2a & 4.2b).

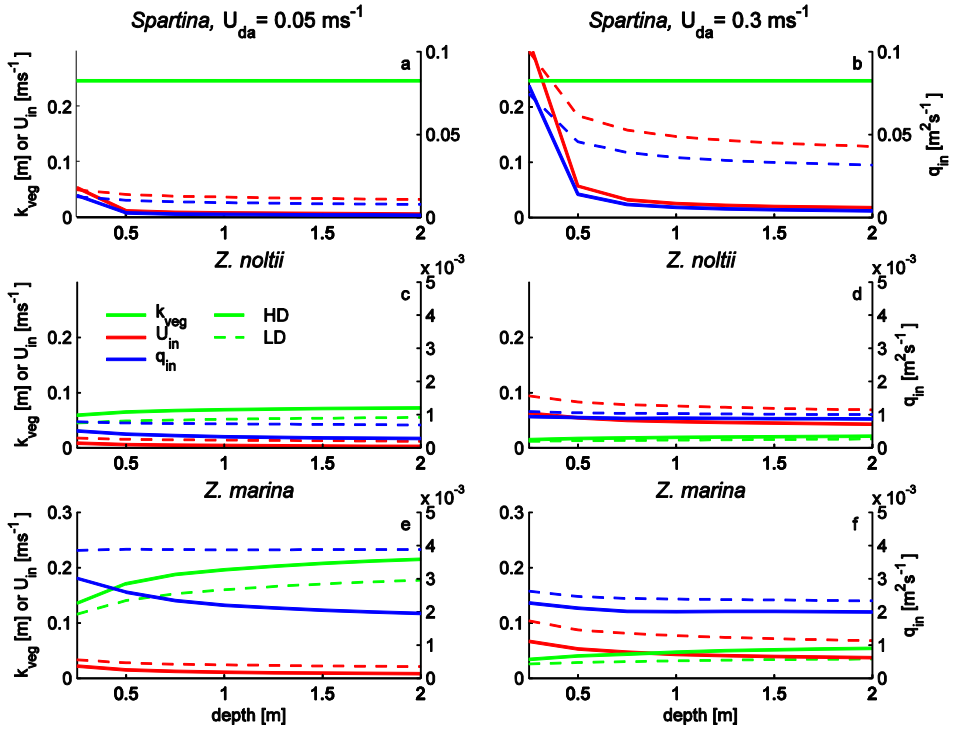


Figure 4.2 The response of vegetation height  $k_{veg}$ , canopy flow velocity  $U_{in}$  and canopy flux  $q_{in}$  to a increasing water depth at two fixed depth averaged velocities. *Spartina* has another scale for  $q_{in}$  (right) than the two seagrass species.

For *Z. noltii*,  $U_{in}$  also responded practically linearly to increasing velocity (Fig. 4.1c & 4.1d) and water depth (Fig. 4.2c & 4.2d), but for *Z. marina* the response of  $U_{in}$  to higher velocities was not completely linear (Fig. 4.1e & 4.1f). The vegetation height ( $k_{veg}$ ) of both flexible species decreased non-linearly with higher velocities (Fig. 4.1c-f), whereas deeper water increased the plant heights only a little (Fig. 4.2c-f). The combined effect of  $k_{veg}$  (decreases with  $U_{da}$ ) and  $U_{in}$  (increases with  $U_{da}$ ) explains why  $q_{in}$  showed a peak at  $0.05 \text{ ms}^{-1}$  for *Z. marina* (Fig. 4.1e & 4.1f). For *Z. noltii*,  $q_{in}$  was almost constant for velocities above  $0.15 \text{ ms}^{-1}$  (Fig. 4.1c & 4.1d) and all depths (Fig. 4.2c & 4.2d), which might be explained by the fact that due to the lower vegetation height,  $k_{veg}$  could not decrease that much with  $U_{da}$ . For *Spartina* and *Z. marina*,  $q_{in}$  decreased as depths increased (Fig. 4.2a & 4.2b, 4.2e & 4.2f), with the exception of the low-density, low velocity *Z. marina* where  $q_{in}$  remained constant at all depths (dashed blue line in Fig. 4.2e).

#### 4.3.2 Effects of plant solidity - 1D simulations

The vegetation height  $k_{veg}$  of the two flexible *Zostera* species increased with solidity (Fig. 4.3d). Nonsurprisingly, for both species,  $k_{veg}$  is highest in low velocity conditions and in deep water. In these conditions, *Z. noltii* was fully upright at a solidity representing the HD vegetation. In contrast, *Z. marina* never reached its maximum height for the set of simulated environmental conditions.

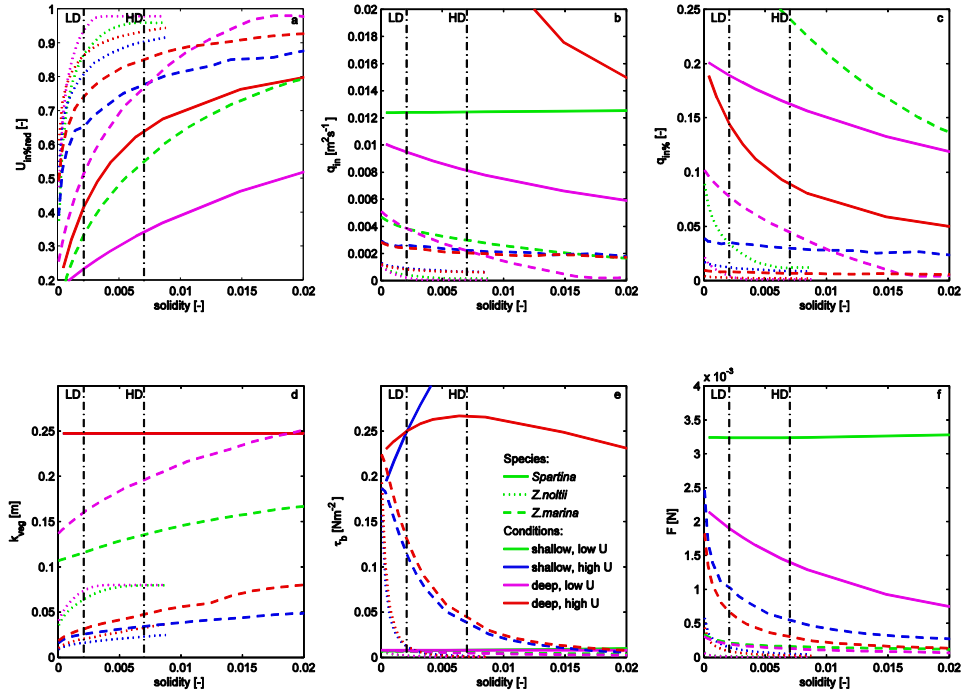


Figure 4.3 Response of ecosystem engineering parameters to increasing vegetation solidity. The vertical dash/dot lines indicate the solidity of the low density (LD) and high density (HD) used in the other simulations. The HD-solidity of *Spartina* (0.06) is outside this figure, just as some results for *Spartina* are outside the plotted range to maintain the readability of the figure. Note that whereas most lines show a similar trend, the line of *Zostera marina* in deep water with a low velocity (pink dashes) crosses other lines, indicating a different response to increasing solidity.

With increasing solidity, the reduction of canopy velocity ( $U_{in\%red}$ ) increased for all three species (Fig. 4.3a), except for *Spartina* at shallow conditions (negative values not shown to enhance clarity of the figure). These negative values for  $U_{in\%red}$  were the result of an increase in canopy velocity at low water depths, when all the water is forced through the non-bending stiff canopy. *Z. noltii* reduced  $U_{in}$  the most, despite having the lowest solidity range. *Spartina* reduced  $U_{in}$  the least. At the highest solidities, all three species reduced  $U_{in}$  by  $\pm 90$  percent. At low solidities, the reduction was largest in deep water with a high velocity (red lines), indicating that these conditions favour skimming flow. At high solidities, the reduction was largest in deep water with a low velocity (pink lines).

Across species, the general response of canopy flux ( $q_{in}$ ; Fig. 4.3b) and relative canopy flux ( $q_{in\%}$ ; Fig. 4.3c) to an increasing solidity was to decrease. This decrease was the clearest at low velocity conditions (green and pink lines), and very small in high velocity conditions (blue and red lines). For *Z. noltii*,  $q_{in}$  was the smallest;  $7 \cdot 10^{-4} \text{ m}^2 \text{ s}^{-1}$  at the high velocity and  $8 \cdot 10^{-5} \text{ m}^2 \text{ s}^{-1}$  at the low velocity, regardless of depth. For *Z. marina*,  $q_{in}$  at the high velocity was remarkably constant along the solidity range and very similar for the two depths ( $2 \cdot 10^{-3} \text{ m}^2 \text{ s}^{-1}$ ). In deep water,  $q_{in}$  at the low velocity decreased to practically nought, whereas in shallow water  $q_{in}$  reached the same value as

for the high velocity. The depth-independence of  $q_{in}$  of the two *Zosterae* was also observed in Figure 4.2c-f.

At the low flow velocity (green and purple lines), the bed shear stress ( $\tau_b$ ) was very low for all three species and for all solidities (max  $8 \cdot 10^{-3} \text{ Nm}^{-2}$ ; Fig. 4.3e). At the high flow velocity (red and blue lines), *Z. noltii* decreased  $\tau_b$  the most: even at the low density,  $\tau_b$  was just  $1.2 \cdot 10^{-2} \text{ Nm}^{-2}$  compared to  $\pm 0.2 \text{ Nm}^{-2}$  of a bare bed (i.e., solidity = 0). The reduction of  $\tau_b$  by denser *Z. marina* was more gradual, whereas denser *Spartina* augmented  $\tau_b$  considerably in shallow water (where the flow is forced to go through the stiff vegetation) and only slightly in deep water at low solidity (around  $6 \cdot 10^{-3} \text{ Nm}^{-2}$ ).

The drag forces imposed on the plants ( $F$ ; Fig. 4.3f) decreased as solidity increased. As expected, the drag forces were lowest for the small flexible *Z. noltii*, and the highest for the stiff *Spartina*.

### 4.3.3 Comparing model predictions of 1D vs. 2D simulations

In two-dimensional simulations, the values of  $k_{veg}$ ,  $U_{inv}$ ,  $q_{in}$  and  $\tau_b$  well inside the meadow (Fig. 4.4) were generally very similar to the values of the one-dimensional Dynveg simulations well inside the vegetation (asterisks and triangles in Fig. 4.4 as derived from Fig. 4.3). This applied to both the high density and the low density (data not shown to enhance readability in Fig. 4.4).

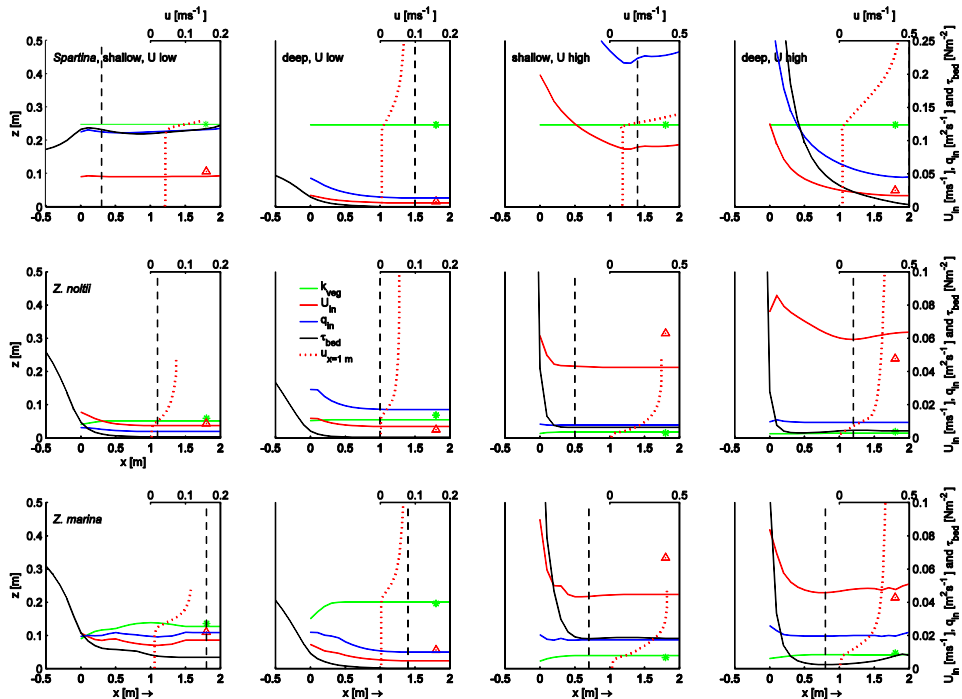


Figure 4.4 Longitudinal cross-sections with  $U_{in}$ ,  $q_{in}$ ,  $\tau_b$  and  $k_{veg}$  for HD vegetation. Flow direction is from left to right; the meadow starts at  $x=0$  m. From top to bottom: *Spartina*, *Zostera noltii* and *Zostera marina*. From left to right:  $h=0.25$  m and  $U_{do}=0.05 \text{ ms}^{-1}$ ,  $h=1.0$  m and  $U_{do}=0.05 \text{ ms}^{-1}$ ,  $h=0.25$  m and  $U_{do}=0.30 \text{ ms}^{-1}$ ,  $h=1.0$  m and  $U_{do}=0.30 \text{ ms}^{-1}$ . Note that not all axes have the same scale. Triangles indicate the value of  $U_{in}$  predicted by Dynveg; asterisks mark  $k_{veg}$ . The vertical dashed lines mark the end of the leading edge zone, while the dotted

vertical line indicates the flow velocity profile at  $x=1$  m.

However, a remarkable difference between 1D and 2D results was observed for *Spartina* in shallow water. Whereas in 1D-simulations all the water was forced through the canopy due to the fixed water level boundary condition, in 2D the flow could pass over the canopy, thereby greatly reducing  $U_{in}$  and  $q_{in}$ . At a low flow velocity this effect was limited, but at a high flow velocity  $U_{in}$  in 2D was reduced from  $0.3 \text{ ms}^{-1}$  to  $0.1 \text{ ms}^{-1}$ .

#### 4.3.4 Spatial patterns generated by 2D simulations

For the non-bending stiff *Spartina*, the vegetation height  $k_{veg}$  was of course constant. However, for both flexible species, the plants at the leading edge of the meadow (left) bent much more than the plants further downstream (Fig. 4.4; green lines).  $k_{veg}$  usually rose to a constant value within the first meter. The difference in  $k_{veg}$  between  $x=0$  m and  $x=1$  m was several centimetres, with  $k_{veg}$  at  $x=0$  varying between 60 and 94% of  $k_{veg}$  at  $x=1$  m. This relative difference was slightly larger in shallow conditions, and substantially larger for *Z. marina* (average 70%) than for *Z. noltii* (average 85%).

The canopy velocity  $U_{in}$  (Fig. 4.4; red lines) demonstrated the opposite behaviour of  $k_{veg}$ : a decrease from the leading edge to a constant value inside the meadow. The distance covered to reach this constant value varied considerably among the species and hydrodynamic conditions, and was generally longer than the distance covered to reach a constant  $k_{veg}$ . The reduction of  $U_{in}$  was largest for *Spartina* in deep, fast flowing water:  $U_{in}$  at  $x=2$  m was only 14% of  $U_{in}$  at  $x=0$  m and still not steady. *Spartina* also showed the longest adaptation lengths, except for shallow, slowly flowing water where the flow was hardly affected. Averaged over all four conditions,  $U_{in}$  at  $x=2$  m was 24% of  $U_{in}$  at  $x=0$  m for *Spartina*, 51% for *Z. marina* and 62% for *Z. noltii*.

The canopy flux  $q_{in}$  (Fig. 4.4; blue lines) followed a pattern very similar to  $U_{in}$ : High at the leading edge, with a lower and steady value further in the canopy. For *Spartina*, with a fixed vegetation height,  $U_{in}$  and  $q_{in}$  are linearly related. For the bended *Zosteraceae*, the stream-wise decrease of  $q_{in}$  was substantially less than the decrease of  $U_{in}$ : in *Z. noltii*,  $q_{in}$  at  $x=2$  m was 76% of  $q_{in}$  at  $x=0$  m, and for *Z. marina* this was 83% averaged over all four conditions. Especially in the high velocity conditions, the canopy flow for both *Zosteraceae* was nearly constant along the meadow.

The bed shear stress (Fig. 4.4; black lines) adapted similarly to  $U_{in}$  and  $q_{in}$ . In high velocity conditions, only the first few centimetres of a *Z. noltii* meadow showed a bed shear stress greater than  $0.1 \text{ Nm}^{-2}$ . In meadows of *Z. marina* this occurred in the first decimetres, whereas in *Spartina* the bed shear stress remained greater than  $0.1 \text{ Nm}^{-2}$  in the first half metre in deep conditions and remained high throughout the meadow in shallow conditions.

The length of the leading edge zone (LEZ) -defined as the distance to the grid cell in which  $q_{in}$  does not deviate more than 0.5% from its value in the six surrounding grid cells- ranged from 0-2 m in all simulations except for *Spartina* in deep water and strong flow, where the leading edge zone was longer. There was no apparent general relation between the lengths of the LEZ on the one hand and vegetation properties like density, length and flexibility or hydrodynamic conditions on the other hand. For the two flexible species, LEZ in most cases was 0.5-1.5 m, whereas for

*Spartina* LEZ varied much more (0.3 →2 m). In shallow water with a low flow velocity, the adaptation of the flow occurred mostly in front of the meadow, hence LEZ was very small.

## 4.4 Discussion

### 4.4.1 Ecosystem engineering capacity: effects of conditions

Present results, as summarized in Table 4.2 and Figure 4.5, clearly showed that the ecosystem engineering capacities of plants, defined as the ability to reduce current velocity inside a canopy ( $U_{in\%red}$ ), the ability to gain resources as nutrient and sediment via the canopy flux ( $q_{in\%}$ ) and the ability to protect the bed from erosion by reducing the bed shear stress ( $\tau_{b\%red}$ ) depend on the hydrodynamic conditions they are subjected to. Changes in these for ecosystem engineering relevant parameters were most distinct at the lower ranges of water depths and flow velocities we assessed, with the response to an increase in velocity being stronger than the response to an increase in depth (Figs. 4.1 and 4.2).

Table 4.2 Deflected plant height, canopy velocity, canopy flux and bed shear stress in the middle of low- (L) and natural- (H) density meadows of *Spartina*, *Zostera noltii* and *Zostera marina* in four flow conditions. S stands for shallow ( $h=0.25$  m) and D for deep ( $h=1$  m); - means a low velocity ( $U_{do}=5$  cms<sup>-1</sup>), + a high velocity ( $U_{do}=30$  cms<sup>-1</sup>). The values in italics indicate a higher bed shear stress than the reference bare-bed value.

Species	density	$k_{veg}$ cm				$U_{in}$ cms <sup>-1</sup>				$q_{in}$ cm <sup>2</sup> s <sup>-1</sup>				$\tau_{bed}$ 10 <sup>-3</sup> Nm <sup>-2</sup>			
		S-	D-	S+	D+	S-	D-	S+	D+	S-	D-	S+	D+	S-	D-	S+	D+
<i>Spartina</i>	H	25.0	25.0	25.0	25.0	4.8	0.6	9.5	1.8	119	14.5	236	45.0	12.2	0.06	32.6	0.44
	L	25.0	25.0	25.0	25.0	5.0	2.8	29.8	15.7	126	69.5	744	392	9.0	3.0	304	102
<i>Z. noltii</i>	H	5.2	5.5	1.8	1.5	0.7	0.7	4.3	6.4	3.7	3.9	7.7	9.3	0.10	0.01	0.60	0.44
	L	5.0	5.7	1.5	1.4	1.4	1.1	6.1	7.3	6.7	6.3	9.0	10.1	0.40	0.10	4.9	2.8
<i>Z. marina</i>	H	12.8	20.1	3.9	4.3	1.7	0.5	4.5	5.2	21.8	10.1	17.6	22.1	0.70	0.03	1.8	0.78
	L	13.8	23.1	3.5	3.9	2.3	1.2	5.7	5.7	31.9	28.6	19.9	21.8	1.8	0.50	4.0	1.9

The differences between deep and shallow conditions are the largest for *Spartina* because the vegetation was fully submerged in deep water ( $k_{veg}/h=0.25$ ; pink and red bars in Fig. 4.5) and almost emergent in shallow water ( $k_{veg}/h\approx 1$ ; green and blue bars). *Leonard & Croft [2006]* found for stiff vegetation similar differences in canopy flux when comparing submerged and emergent conditions. That is, in deep water, the canopy velocity and bed shear stress are reduced more than in shallow water, in which the bed shear stress can even be increased and forces on plants are higher (Fig. 4.3). Consequently, in stiff vegetations, sediment deposition is most likely to occur in deep water, irrespective of ambient flow velocity and plant density, whereas in shallow water erosion may occur and plants are more likely to break at high flow velocities and low plant densities. The deposition rate in deep water will however be limited by the restricted sediment amount supplied by the low canopy flux.

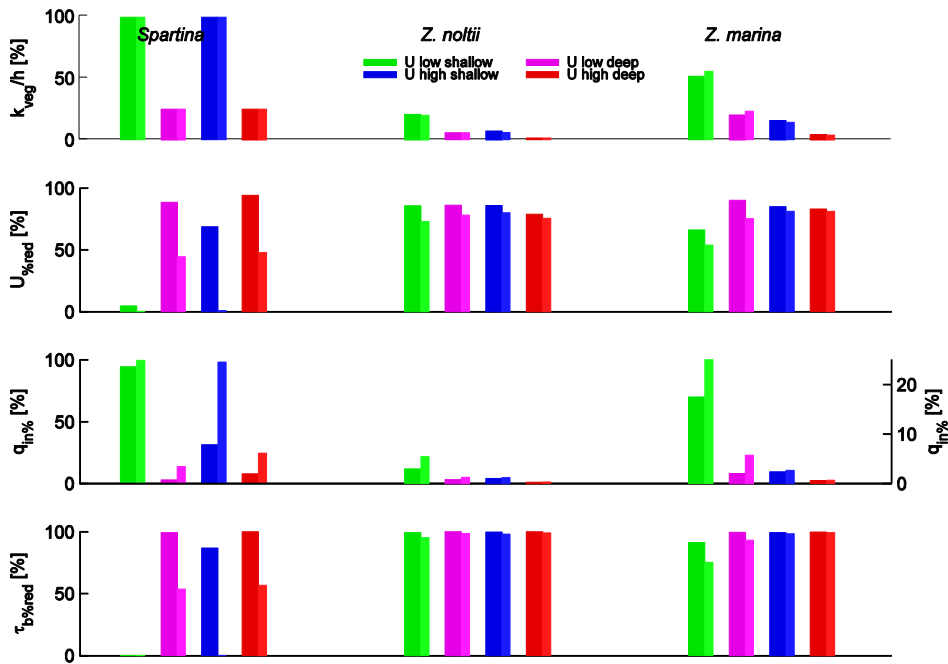


Figure 4.5 Relative vegetation height  $k_{veg}/h$ , reduction of canopy flow velocity  $U_{red}$ , relative canopy flux  $q_{in}$  and reduction of bed shear stress  $\tau_{b:red}$  in the middle of the same meadows of *Spartina*, *Zostera noltii* and *Zostera marina* as displayed in Figure 4.4. Wider, darker coloured bars indicate values at the normal vegetation density; the narrower, lighter bars are for the lower density. Note that the axes for  $q_{in}$  on the right applies to the two flexible species. For *Spartina* in shallow water and low flow velocity,  $\tau_b$  is increased instead of reduced.

For the flexible *Zosterae*, the water depth had less effect on the parameters relevant for ecosystem engineering (Fig. 4.2), because these plants were always submerged ( $k_{veg}/h$  between 0.02 and 0.55). The deeper the water, the higher the vegetation but the lower the flow velocity inside the canopy, resulting in a marginally lower horizontal canopy flux. The water depth might have more effect on the vertical flux through the canopy however, since sufficient depth is an important factor in the occurrence of a possible ‘monami’ according to Ackerman & Okubo [1993], Ghisalberti & Nepf [2002] and Grizzle *et al.* [2006]. Water depth will not affect erosion, since the reduction of the canopy flow velocity and the bed shear stress are similar for all tested depths. Deposition can be affected by water depth: in shallow water, which has the highest relative canopy flux, sediment will deposit rather close to the leading edge, whereas in deep water with a lower relative canopy flux, sediment will deposit further downstream.

The percentage reduction of flow velocity and the reduction of bed shear stress were remarkably similar for both studied flow velocities (Fig. 4.5) in *Zosterae* canopies, regardless of differences in absolute values of bed shear stress and flow velocity (Table 4.2). Hendriks *et al.* [2010] report the same similarity in flow reduction capacity at flow velocities of 0.05 and 0.1  $\text{ms}^{-1}$  for flexible vegetation. This does not apply for the relative canopy flux, which was higher at low flow velocities, indicating a larger capacity to transport nutrients or sediment into the canopy. However, an exchange-increasing ‘monami’ is less likely to occur at low velocities that have little shear between canopy flow and free flow [Ghisalberti & Nepf, 2002; Grizzle *et al.*, 1996].

The ecosystem engineering proxies ( $U_{in\%red}$ ,  $q_{in\%}$  and  $\tau_{b\%red}$ ) of *Spartina* are very similar at both velocities in deep water (Fig. 4.5). In fast flowing shallow water, the drag of the plants caused the water to flow over the meadow instead of through it (Fig. 4.4, upper row), thus hampering a comparison. Notwithstanding the similar percentage reduction of bed shear stress at both velocities, the actual erosion will differ: at  $U_{da}=0.05 \text{ ms}^{-1}$ ,  $\tau_b$  remains well below the critical threshold for erosion of intertidal sediments ( $\tau_{cr}$ ; ranging from 0.11 to 0.18  $\text{Nm}^{-2}$  according to Houwing [1999] and Widdows & Brinsley [2002]), whereas at  $U_{da}=0.3 \text{ ms}^{-1}$ ,  $\tau_b$  exceeds this threshold (0.3  $\text{Nm}^{-2}$ ; Table 4.2), thus inducing erosion.

#### 4.4.2 Ecosystem engineering capacity: effects of plant properties

Besides hydrodynamic conditions, plant properties such as shoot density and flexibility also affect the ecosystem engineering capacities of vegetation meadows, as seen in the, for ecosystem engineering relevant, parameters (Figs. 4.3 and 4.5, Table 4.2). Flexible plants were more effective in reducing canopy flow velocity, bed shear stress and forces on plants at low solidities than the stiff *Spartina*. The canopy flux in the *Zosteræ* meadows decreased with solidity only at low solidities, whereas the canopy flux in *Spartina* was at least twofold higher and related to solidity along the entire studied range. For similar solidities, the small *Z. noltii* paired a smaller canopy flux with more reduction of the flow velocity and bed shear stress than the larger *Z. marina*.

Although it is generally accepted that flow reduction inside the canopy increases with increasing vegetation density [e.g. Ward et al., 1984; Peterson et al., 2004; Leonard & Croft, 2006], some studies [Fonseca & Fisher, 1986; Gambi et al., 1990] did not find an influence of shoot density on flow reduction. Peralta et al. [2008] suggest that shoot density is a good proxy for flow reduction, but only for plants that do not occur in very high densities, i.e. not for *Z. noltii*. Indeed, the ecosystem engineering capacities of *Z. noltii* hardly change above the LD-solidity in Figure 4.3 and the difference between LD and HD in Figure 4.5 is minute. For sufficiently sparse configurations however, the inverse relation between the square root of the vegetation density and the canopy flow velocity found by Peterson et al. [2004] seems to apply.

The large range of solidities in this study also enabled us to explain the contrary findings of both Fonseca & Fisher [1986] and Gambi et al. [1990], who studied intermediate densities (i.e., 485-1000 respectively 400-1200 *Z. marina* shoots  $\text{m}^{-2}$ ; corresponding to solidities between 0.003 and 0.008). At their limited solidity ranges, the reduction of canopy velocity and bed shear stress is not very clear for the four simulated hydrodynamic conditions (Fig. 4.3). The spatial setup of Gambi et al. [1990], where flow around the meadow was also possible, hampers a direct comparison with other measurements. Moreover, in both studies  $\tau_b$  remained well below  $\tau_{cr}$ , not inducing any erosion. Though erosion could have occurred at lower solidities as  $\tau_b$  approaches  $\tau_{cr}$ , Bos et al. [2007] reported sedimentation of mainly fine material in canopies as sparse as 70 shoots  $\text{m}^{-2}$ . This can be the result of a small reduction of  $\tau_b$  (Fig. 4.3e) and a sufficient  $q_{in\%}$  (Fig. 4.3c).

Though only solidity is displayed on the x-axis of Figure 4.3, the plots looked similar whether biomass, shoot density, leaf area or leaf area index were used: lines from different species did not overlap. This confirms that the size and amount of plants alone are not enough to explain all effects on ecosystem engineering parameters; biomechanical properties do also matter [e.g., Peralta et al., 2008; Hendriks et al., 2010; Bouma et al., 2005].

*Z. marina* displayed more complex behaviour than the other two species: The canopy flux showed a remarkable peak at  $U_{do}=0.05 \text{ ms}^{-1}$  (Fig. 4.1e & 4.1f), which is more pronounced for the low density and in shallow water (Fig. 4.5, green bars). This high canopy flux indicates the ability of *Z. marina* to assure the supply of nutrients and dissolved  $\text{CO}_2$  required for photosynthesis also in calm conditions [Koch, 1994]. A rather upright position is a prerequisite for achieving such high canopy flux. An upright position can partly be attained by having a high buoyancy of the plant material. A low vegetation density is however also important for achieving such high canopy flux, as it helps to avoid so-called ‘skimming flow’ – a situation where flow is deflected over the canopy rather than through it- might also play a role. Skimming flow is more likely to occur for dense canopies or high flow velocities, where the energy loss inside the canopy is larger. Worcester [1995] reported similar upright plants and absence of skimming flow in sparse beds of *Z. marina* in low energy conditions.

From the three species studied here, *Z. noltii* seems the most effective in stabilizing the bed because it reduces the bed shear stress more than the others, also at lower densities than its usual occurrence in the field. The low canopy flux of *Z. noltii* however also means that it is not able to filter a substantial amount of particles out of the water column. While *Spartina* might induce erosion at low densities, it does prevent erosion at high densities. Combined with its high canopy flux, *Spartina* could increase deposition substantially. *Z. marina* can be an effective active eco-engineer in calm conditions due to its relatively high canopy flux, while in more dynamic conditions it fulfils a more passive role by decreasing the bed shear stress, though not as strongly as the smaller *Z. noltii*.

Van Katwijk et al. [2010] also observed that the ecosystem engineering capacity of *Z. marina* depends on plant cover as well as external forcing. A direct comparison between our model results and their seemingly contradictory observations in the field –muddification at a dynamic location and no effect at a calm site- is difficult, as they only observed the result of a long period of plant-flow-sediment interactions rather than directly measuring the forcing conditions: At the dynamic site, mud may have settled during calm periods and was subsequently protected from erosion, whereas the supply of sediment on the calm site may have been a limiting factor for sedimentation.

#### 4.4.3 Leading edge effects and other spatial processes

Regardless of the vegetation properties or hydrodynamic conditions treated in this study, the adaptation of the flow velocity and vegetation position generally occurred in the first two meters of a meadow (Fig. 4.4), i.e. within 1-7 times the flow depth. This is well less than the adaptation length of 10-20 water depths often applied as a rule of thumb. For *Spartina*, the adaptation length ranged between 1-10 times the vegetation length, for *Z. noltii* between 10-50 deflected plant heights and for *Z. marina* between 7-15.

The limited length of the leading edge zone (LEZ) implies that, when modelling large areas, the leading edge may be given limited attention, because these two meters are generally only a small part of a meadow [e.g., Fonseca et al., 2002; Leonard & Croft, 2006] and smaller than typical grid cells in most hydrodynamic models of entire estuaries [de Vriend et al., 1993; Lesser et al., 2004]. For small-scale studies into the processes in and around meadows however, grid cell sizes

of the order of decimetres are more appropriate and other types of hydrodynamic models (e.g., Large Eddy Simulation; *Stoesser et al., 2009*) can be applied.

The LEZ found in this study had a similar order of magnitude as in other studies for various vegetation species and conditions, but those also struggled to find quantitative relationships between LEZ, meadow properties and flow conditions: Both *Gambi et al. [1990]* and *Peterson et al. [2004]* explicitly state that no relation between LEZ and flow velocity could be found. *Peterson et al. [2004]* reported that the LEZ is a declining function of meadow density, however being unclear in sparse canopies. *Ghisalberti & Nepf [2002]* describe that the length required to have a fully developed velocity profile was usually roughly ten times the canopy height. The downstream end of the canopy, where turbulent wakes form that extend over greater lengths, was not part of this study despite its relevance [*Folkard, 2005; Fonseca et al., 2007*] for the establishment of other organisms and meadow extension.

For the valuation of ecosystem engineering capacities, the leading edge zone could also be defined as the area where the horizontal canopy flux is larger than the cumulative vertical flux: The further downstream, the more the relatively small vertical fluxes will influence the water quality inside the canopy. The Reynolds-stress, a parameter that indicates the vertical exchange of horizontal momentum, could be used as a measure for the vertical exchange of substances [*cf. Hendriks et al., 2010*]. However, the possible development of a monami [*Ackerman & Okubo, 1993; Grizzle et al., 1996; Ghisalberti & Nepf, 2002; Ghisalberti & Nepf, 2004*] that considerably increases vertical exchange, complicates accurate assessments of cumulative vertical transport.

In the three dimensions of the field, the flow patterns will differ from those in the two dimensions of a flume [*Fonseca & Koehl, 2006*]: Water can pass a meadow also on the sides, which might decrease the canopy flux and bed shear stress inside the meadow, but increase the flow next to the meadow, possibly leading to erosion [*see e.g. Bouma et al., 2009; Vandenbruwaene et al., 2011*]. Moreover, horizontal eddies can also contribute to the transport of substances in and out of the meadow (lateral mixing *cf. Lightbody & Nepf, 2006*). These three-dimensional processes and the flow- and plant properties driving them require further study, in which models like ours can be of great value.

#### **4.4.4 Other processes and other organisms: possible consequences**

Two processes that can also indicate the ecosystem engineering capacities of plants but that were not taken into account in this study are the attenuation of waves and the direct trapping of sediment particles against blades. According to *Hendriks et al. [2008]*, the latter process can form a considerable contribution to the amount of sediment captured by a meadow.

Wave attenuation by vegetation and the consequences for the plants themselves are complicated enough to warrant studies on their own, although no hydrodynamic model currently is able to simulate this with sufficient detail for various types of plants. Waves substantially contribute to mixing in a canopy and impose higher forces on plants and on the bed than steady currents, thus increasing the chances of erosion and the breaking of plants [*e.g., Koch & Gust, 1999; Backhaus & Verduin, 2008; Luhar et al., 2010*].

Other parameters that indicate the ecosystem engineering capacities of plants are turbulence-related: the alteration of profiles of turbulent kinetic energy, turbulence intensity or

Reynolds stress affects the diffusion through the top of the canopy, with consequences for e.g. pollination and sedimentation [Koehl & Alberte, 1988; Ackerman & Okubo, 1993; Ackerman, 1997; Hendriks et al., 2010].

The consequences for other organisms living in and around the studied meadows have not been treated, as these differ widely. Reduction of the flux near the bed by a canopy can be negative for filter-feeders, nevertheless Peterson et al. [1984] report larger *Mercenaria mercenaria* clams inside eelgrass beds. Grizzle et al. [1996] suggest that the formation of a monami benefits mussel settlement. Besides a direct effect of flow on photosynthesis via the transport of nutrients and the thickness of the leaf boundary layer, hydrodynamics also affect the epiphyte cover on leaves [Cornelisen & Thomas, 2006; Schanz et al., 2000; Hughes et al., 2009] and the possible self-shading of the plants [Koehl & Alberte, 1988; Holbrook et al., 1991].

## 4.5 Conclusions

The ecosystem engineering capacities of plants depend on plant properties as well as the hydrodynamic conditions they are subjected to. There is no clear relation between flow or plant properties and the length of the leading edge zone, which usually is less than two metres, or 1-7 times the flow depth. The relation between deflected plant height and adaptation length differs among species: between 1-10 times the vegetation height for *Spartina*, between 10-50 deflected plant heights for *Z. noltii* and between 7-15 for *Z. marina*.

The dependence of ecosystem engineering capacities on flow conditions is more distinct in shallow water and at low flow velocities, and depends more on depth than on velocity. For stiff plants, erosion and breaking of plants are more likely to occur in shallow water due to the higher bed shear stress and forces on plants, whereas deposition is more likely to occur in deep water as a result of a lower canopy flow velocity. For flexible plants, the water depth does not affect erosion because the bed shear stress does not change with depth; the stress acts on the plants rather than the bed.

Stiff plants have a higher canopy flux than flexible plants, hence a higher potential to trap sediment. This canopy flux is inversely related to spatial density along the entire natural range. For flexible plants, the canopy flux is only related to density in relatively sparse meadows; in denser meadows the canopy flux remains constant with increasing density. Flexible plants are more efficient in reducing bed shear stresses than stiff plants, hence better at preventing erosion. The small *Zostera noltii* is a more effective reducer of bed shear stress than the taller *Zostera marina*, which is better at maintaining a sufficient canopy flux. The dependence of ecosystem engineering capacities on plant properties implies that biomass or spatial density alone are not good indicators of ecosystem engineering capacities.

# 5 Effects of a seagrass meadow on flow and sediment transport

*A case study at Baie de l'Écluse, Dinard, France*



## Abstract

Large-scale models for biophysical interactions between vegetation and its environment can be useful tools for management and for fundamental landscape formation studies. However, their validity needs to be assessed by a good comparison with field observations. This contribution is aiming at this.

The Baie de l'Écluse in Dinard, France is a macrotidal bay bordered by a meadow of the seagrass *Zostera marina* at the seaward side. From May 4<sup>th</sup> to 8<sup>th</sup> 2008, measurements on hydrodynamics and sediment dynamics as well as seagrass properties were carried out. Tidal flow dominated over wave action and the water was clear, with little suspended material. Inside the meadow, the near-bed velocity and the turbidity were slightly lower than outside the meadow.

These measurements were used to test a three-dimensional model for flow and sediment transport through flexible vegetation; an extension of Delft3D. In this model, the height and drag coefficients of the plants are extracted from a look-up table created by the plant-flow model Dynveg, using measured biomechanical plant properties. The sediment transport formula handles vegetation effects on sediment pick-up and transport via the effects on hydrodynamics. The observed flow pattern and peaks in sediment transport are simulated well, indicating that the developed model can be applied to water quality studies and environmental impact assessments involving macrophytes, as well as to studies regarding long-term biogeomorphological feedbacks.

**Keywords:** flexible vegetation, sediment transport, field measurements, three-dimensional modelling, biogeomorphology, *Zostera marina*

## 5.1 Introduction

Large-scale models that can simulate the biophysical interactions between vegetation, hydrodynamics and morphology in estuaries, lagoons, lakes and rivers are useful tools for management and conservation of these areas [e.g. Moore, 2004; Zharova et al., 2001], as well as for a more fundamental understanding of how interaction with biota forms the landscape [e.g., Temmerman et al. 2007]. Not only the making of morphodynamic models that deal with flexible aquatic vegetation is cumbersome, as indicated by the fact that just one exists [Chen et al., 2007]: Validation, either with results from laboratory flumes or from the field, seems even more ungainly.

The morphodynamic model to be validated in this chapter is a combination of Delft3D –a tested hydrodynamic and morphological model for rivers and coastal areas [Lesser et al., 2004]- and the plant motion model Dynveg, described and tested in Chapter 2. This combination was validated in Chapter 3, using flume measurements of flow through two types of macrophytes. The process-based nature of both Dynveg and Delft3D implies that up-scaling to the field should be straightforward, contrary to more empirical models. The main concern is the performance of existing sediment transport formulas in the presence of vegetation: fundamental studies of sediment transport through vegetation are limited to López & García [1998], who identified the effects of vegetation on bed shear stress and diffusivity as paramount.

Numerous field studies on sedimentation or resuspension of sediment in seagrass meadows have been undertaken [Bos et al., 2007, Fonseca & Fisher, 1986; Fonseca et al., 2007; Gacia & Duarte, 2001; Gacia et al., 1999; Koch, 1999; Terrados et al., 2000; Vermaat et al., 2000; Ward et al., 1984]. Often, these studies focused on a net result rather than on continuous processes. Or else, the plant properties or physical environment were not measured in sufficient detail to be used in a numerical model.

Laboratory measurements of sediment transport through vegetation are notoriously difficult [López & García, 1998; Baptist, 2005] and therefore scarce: The transport of coarse bed material, i.e. sand, inside a vegetation meadow only occurs in rather dynamic flow conditions [Lefebvre et al., 2010], which are difficult to reproduce in laboratory settings. The transport of fine suspended material is also difficult to reproduce: the low fall velocity of these particles causes adaptation lags of several meters. Annular flumes [e.g., Widdows & Brinsley, 2002] overcome this adaptation length problem, but generate disadvantageous secondary currents. Long, tilted flumes with sediment recirculation systems are required to do thorough experiments. Even then, only a small range of conditions can be studied.

Performing a new field experiment on sediment transport in and around a seagrass meadow provides a large-scale test case for a three-dimensional morphodynamic model and solves many of these problems, albeit being less controllable.

This chapter describes a validation case for flow and sediment transport in and around a seagrass meadow in a tidal embayment. First, the location, seagrass occurrence, instrumental set-up and conditions during the measurements are described. Second, the results of the measurements on flow and sediment transport are analysed. Third, a computational model is set up and compared to these results. The chapter concludes with a discussion of possible applications.

## 5.2 Materials and Methods

### 5.2.1 Location choice and description

The Baie de l'Écluse ( $48^{\circ}38'16''\text{N}$ ,  $2^{\circ}03'13''\text{W}$ ; Fig. 5.1) in Dinard, France was considered to be a suitable area for this field experiment. This bay is roughly half a kilometre wide and has a sandy beach of similar length, which becomes entirely covered with water during flood. Dinard is situated about one kilometre west of St. Malo, across the Rance estuary that accommodates a tidal power plant three kilometres inland. The Baie de l'Écluse was considered suitable because of the presence of a large seagrass (*Zostera marina*; eelgrass) meadow (Fig. 5.2; red area), soft sediments, a sheltered orientation and easy access. Furthermore, this area is macrotidal, which enables working without divers during low tide, as well as measurements over a large range of depths and tidal flow dominating over wave action. The experiments took place between May 4<sup>th</sup> and 8<sup>th</sup> 2008, a time with large spring tides, sufficient eelgrass, usually fair weather and not too many tourists.

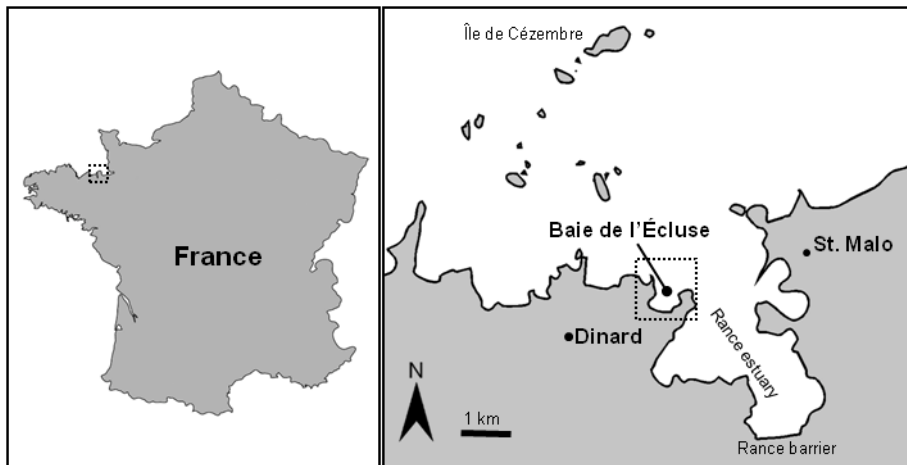


Figure 5.1. Location of the 'Baie de l'Écluse', Dinard, France.

### 5.2.2 Instrument set-up

Measurement frames were positioned at two positions (numbers 2 and 4 in Fig. 5.2) in order to gather information about vertical differences in a vegetated respectively bare area with similar depths. The instrument measurement volumes were situated at 10.5 and 100 cm from the bed. At both levels, the frames were equipped with an EMF (Valeport 802), an OBS (Seapoint), a pressure sensor (GE Druck PTX 1830) and a water sample bottle. The instruments were connected to two data loggers (Campbell Scientific CRX10) and batteries in watertight casings placed several tens of meters away from the frames to avoid disturbance. All equipment was marked by buoys to avoid accidents with bathers and surfers. Additionally, the flow pattern near the entrance of the bay was assessed using floaters.

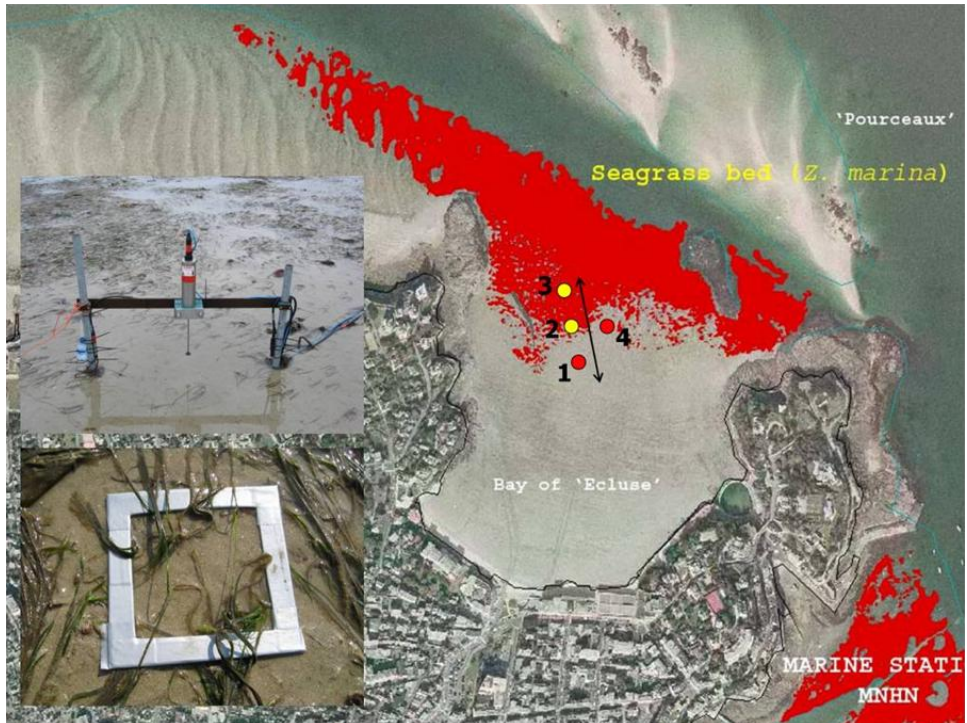


Figure 5.2. Positions of instruments (numbered dots) and location of seagrass meadows (hatched). The arrow indicates the prevalent flow direction near the instruments. (image MNHN) Upper inset: set-up of instrument frames. Lower inset: seagrass coverage measurement frame.

Data were gathered at a frequency of 4 Hz in intervals of 15 minutes. Each of these intervals started with a system check, followed by three minutes in which an average and standard deviation are determined per parameter, concluded by eight minutes sampling of raw (4 Hz) data. Because this 4 Hz data is spiky and difficult to interpret, averages over 30 seconds as well as 15 minutes were determined. These are that are easier to visualise and filter out short-term fluctuations due to turbulence.

The original experimental design also comprised four measurement positions about 50 m apart (Fig. 5.2) to study spatial differences in flow velocity and sediment transport near the bed: Three in the prevalent flow direction, respectively 1) outside, 2) near the edge and 3) well inside a seagrass meadow, and 4) one next to this meadow. Unfortunately, the measurements performed in this four-position set-up were inadequate due to malfunctioning electronics and therefore not used.

### 5.2.3 Environmental conditions

The bed level in the bay and its surroundings was measured by means of a jetski equipped with RTK-DGPS and a single-beam echo sounder, as an addition to the less detailed and less recent map of the Service Hydrographique et Océanographique de la Marine (SHOM). The SHOM also provided 10-minute water level data from their tidal gauge at St. Malo. The weather for the duration of the fieldwork was experienced to be fairly calm with little wind. Data acquired through

Weather Underground [[www.wunderground.com](http://www.wunderground.com)] supported these observations. The numerous small islands and shallow areas in front of the bay protect it from large waves: during the measurements waves were estimated mostly smaller than 5 cm, with the exception of short periods with ship-induced waves around 40 cm.

The Musée National d'Histoire Naturelle (MNHN) provided a map of eelgrass occurrence (Fig. 5.2). The coverage of the field was also assessed by RTK-DGPS and by counting the number of leaves in a randomly thrown 10 by 10 cm frame. Besides spatial density, the dimensions and buoyancy of 41 seagrass plants were determined throughout the field: leaf length 27.8 ( $\pm 8.6$ ) cm, width 4.8 ( $\pm 1.1$ ) mm, thickness 0.35 ( $\pm 0.04$ ) mm. The volumetric density was determined at 970 ( $\pm 49$ ) kgm<sup>-3</sup> by adding plants to a known mass and volume of water and measuring the increase in both. The elasticity modulus was not measured, but estimated at 20·10<sup>6</sup> Nm<sup>-2</sup> (as in Chapter 3). The plants in the deeper parts were somewhat larger than the plants in shallower areas. The plants had small sheaths (<2 cm) and usually 5 leaves.

Sediment samples were taken at six locations in the lower intertidal. After drying, the grain size was analysed with a Malvern Mastersizer at the Netherlands Institute for Ecological Research (NIOO). The sediment composition was similar at all locations, with a median grain size D<sub>50</sub> of 0.167 ( $\pm 0.014$ ) mm, D<sub>90</sub> = 0.331 ( $\pm 0.046$ ) mm and 26 ( $\pm 5$ ) % fines.

#### 5.2.4 Model description

The Delft3D modelling package (Version 3.54.23.00; Lesser *et al.*, [2004]) is used to simulate the flow and sediment transport in and around the Baie de l'Écluse during one tidal period. This model has been applied in numerous studies of coastal and estuarine environments, thereby incorporating the effect of biota on flow [Temmerman *et al.*, 2005, Borsje *et al.*, 2008] if necessary. The sediment transport formulations are described in Appendix B and in more detail in Van Rijn [1993]. These formulations are suitable for sand as well as silt. Teeter *et al.* [2001] recommend using multiple grain size fractions and allowing simultaneous erosion and deposition to correctly simulate the amount of suspended matter. The need to correctly represent the effect of vegetation on the flow velocity profile requires three-dimensional modelling instead of a depth averaged 2DH model. Waves are not taken into account in this study because in this area tidal processes dominated over wave processes during the period of interest.

#### 5.2.5 The model grid

Delft3D uses a staggered curvilinear grid, with velocity points defined at the mid-points of grid cell sides, depth points at the cell centre and water level points at the cell corners. The presence and properties of vegetation are defined at the cell centre and cannot vary within a cell. Consequently, the spatial variation in plant properties is also a factor in determining the required grid cell size. A previous study [Dijkstra and Bouma, *subm. and Chapter 3-4*] has shown that the adaptation length of the flow at the leading edge of a meadow is often less than two metres. Given the size of the study area it is not feasible to choose a grid cell size small enough to resolve this flow adaptation exactly, neither is this necessary since this study aims at studying the large-scale effects of meadows.

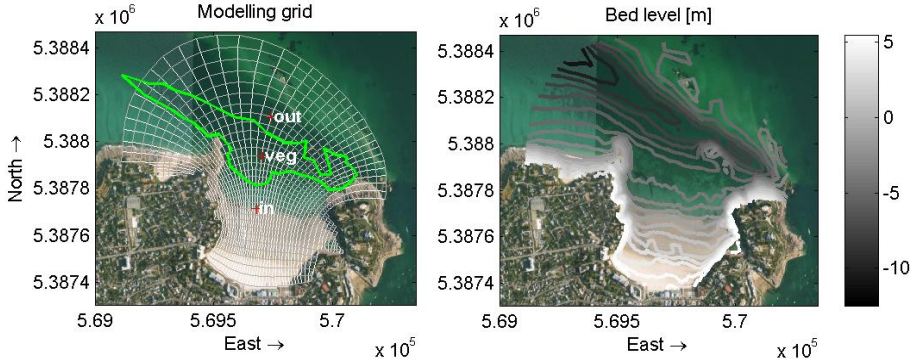


Figure 5.3. (left) The computational grid with the extent of the seagrass field and the location of the observation points used for Figs. 6.2, 6.3 and 6.7. (right) Depth contours as measured using a jetski in and near the Baie de l'Écluse (reference level: IGN 69). Images: GoogleEarth.

The grid cell dimension in east-west direction is limited by the distance between the measurement locations; since this  $\pm 25$  m requires several grid cells, the minimum cell width is 6 m. The cell length in north-south direction cannot be more than twice the size in the other direction for numerical reasons and needs to be able to represent bed level gradients well. Cells farther from the measurement points are bigger to save calculation time by reducing the number of grid points. For the vertical  $\sigma$ -grid, twenty cells were chosen. The time step was set at 0.6 s to ensure stability also during drying and flooding. Test runs with a finer horizontal and vertical grid and a corresponding smaller time step did not show substantially different flow patterns; coarser grids and larger time steps did. Therefore, the 32 by 50 cell grid (Fig. 5.3) was used for all simulations. On this grid, we defined a bathymetry and seagrass cover based on our own measurements and the data from MNHM and SHOM described in Section 5.2.3.

### 5.2.6 Model boundaries, bed roughness and eddy viscosity

On the landward sides of the bay, the high walls and rocks surrounding the bay form a natural border of the grid. The seaward border of the grid is chosen as far away as possible while still covered by our own detailed bathymetry data, which in the northeast part stretches to the 'Pourceaux' sandbank. At this seaward border, the model is driven by a water level boundary condition for hydrodynamics and a given sediment concentration for sediment transport. The nearby SHOM tidal gauge at St. Malo provided local water level data. Since the tidal wave propagates from west to east, it was necessary to apply a phase difference between the east side and the west side of the model boundary. Based on the water depth and corresponding propagation velocity, this phase difference was calculated to be in the order of one minute.

The bed roughness for the sandy areas is expressed as a roughness height  $z_o$ , based on the sediment size. For the small rocky areas at the grid borders  $z_o$  was estimated equal to the size of the boulders, i.e. 30 cm. To avoid the use of the horizontal eddy viscosity as an additional tuning parameter, the Horizontal Large Eddy Simulation (HLES) option was used in conjunction with a background value of  $1 \text{ m}^2 \text{ s}^{-1}$ .

### 5.2.7 Vegetation modelling

The presence of seagrass was taken into account by applying the vegetation functionality of Delft3D: Vegetation is represented as porous medium with a number of rods per area that have a thickness and drag coefficient that may vary along their length. The effect of this vegetation on flow is incorporated in the momentum equation:

$$\rho_0 \frac{\partial u(z)}{\partial t} + \frac{\partial p}{\partial x} = \frac{\rho_w}{1 - A_p(z)} \frac{\partial}{\partial z} \left( (1 - A_p(z)) (\nu + \nu_T(z)) \frac{\partial u(z)}{\partial z} \right) - \frac{F(z)}{1 - A_p(z)} \quad (36)$$

in which  $\rho_w$  is the fluid density ( $\text{kgm}^{-3}$ ),  $\partial p / \partial x$  the horizontal pressure gradient ( $\text{kgm}^{-2}\text{s}^{-2}$ ),  $\nu$  the kinematic viscosity ( $\text{m}^2\text{s}^{-1}$ ),  $\nu_T$  the eddy viscosity ( $\text{m}^2\text{s}^{-1}$  defined by a  $k$ - $\epsilon$  turbulence model, and  $A_p$  (-) the solidity of the vegetation across a horizontal plane, i.e. the cross-sectional area  $b(z) \times d(z)$  ( $\text{m}^2$ ) of a leaf times the number of leaves ( $n$ ) per  $\text{m}^2$ . Because we consider a horizontal plane, the thickness  $d$  depends on the angle of the leaf.  $F(z)$  is the resistance imposed on the flow:

$$F(z) = \frac{1}{2} \rho_w C_D a(z) u(z) |u(z)| \quad (37)$$

where  $C_D$  is the drag coefficient (-) and  $a(z) = d(z)n(z)$  ( $\text{m}^{-1}$ ) is the solid area projected on the vertical plane perpendicular to the flow, per unit depth and per unit width. The effect of vegetation on turbulence production and dissipation is also included by means of additional terms in the  $k$ - $\epsilon$  model as explained in *Dijkstra & Uittenbogaard [2010]*.

The flexibility of the plants was taken into account by varying the height, drag coefficient and porosity of the plants over time, in accordance with the actual flow conditions. These representative plant properties are read from a pre-defined look-up table every five minutes of the Delft3D simulation. After these five minutes, the representative properties are fed back into Delft3D and a subsequent simulation starts with slightly adapted vegetation. The flow will adapt too and after five minutes the next update occurs. This method has been described and tested in Chapter 3 and is computationally more efficient than including fully dynamic vegetation, while giving similar results in slowly varying flow.

The look-up table was generated by running Dynveg (a 1DV model for flow through flexible vegetation; Chapter 2) specifically for *Zostera marina*. The properties of *Z. marina* are: length 28 cm, width 4.8 mm, thickness 0.35 mm, elasticity modulus 20 MPa and specific density  $970 \text{ kgm}^{-3}$ . Values in this table cover a depth range of 0.1 to 2 m, a flow velocity range of 0 to  $0.5 \text{ ms}^{-1}$  and spatial densities between 10 and 10,000 plants per  $\text{m}^2$ . Including higher velocities or larger depths in this table was not necessary because the representative plant properties would remain practically the same.

### 5.2.8 Model calibration

The limited amount of data did not allow a calibration and subsequent validation study. Therefore the model was calibrated only; sediment parameters were calibrated after the hydrodynamics compared satisfactory with measured values.

First, observed water levels, flow velocities and flow directions were first used to calibrate the phase difference at the seaward boundary, which had a major effect on the flow pattern in

the bay and second to calibrate the bed roughness, which mainly affected the velocity amplitude. A phase difference of 1 minute (range 0, 0.5, 1, 1.5, 2 minutes) gave the most realistic flow directions when compared to observations with floaters. A larger phase difference created a circulation pattern inside the bay, whereas the absence of a phase difference created a predominantly north-south directed flow pattern. Moreover, the theoretically derived phase difference, based on the distance and the celerity of a tidal wave, is of similar order. A  $z_o$  of 3 mm (range 0.5, 1, 2, 3, 5 mm) for the sandy areas provided the best comparison with measured flow magnitudes, despite being considerably higher than the often used theoretical  $3 \cdot D_{90}$  [Van Rijn, 1993].

Second, the sediment transport model was calibrated by varying the fall velocity ( $w_s$ ) and the critical shear stress for erosion ( $\tau_{cr,e}$ ) of the fine sediment fraction. The fall velocity  $w_s$  ( $0.55 \text{ mm s}^{-1}$ ) was chosen such that the sediment concentration decreased at a similar rate as in the observations, whereas  $\tau_{cr,e}$  ( $0.05 \text{ Nm}^{-2}$ ) was set to give a similar pick-up of sediment.

### 5.3 Results

The sediment concentrations are expressed in V (Volts) instead of  $\text{gl}^{-1}$  because of problems with the electronics that caused an offset: these data are coherent, but the actual values are uncertain and therefore only used in a qualitative sense. The positive  $u$ -direction is defined from north to south as this was the main flow direction during flood; positive  $v$  is from west to east.  $U$  is the flow vector with subscripts indicating the position, i.e.  $U_{2b}$  means the velocity at location 2 near the bed.

#### 5.3.1 Flow measurements

The flow sequence during both tidal periods was very similar for all four positions, apart from some peaks probably due to shipping or wind-induced bursts (Fig. 5.4): About 1.5 hours after low water slack, the lower instruments became submerged;  $U_b$  was around  $2 \text{ cm s}^{-1}$ . Three quarters later, the higher instruments were also underwater, which was directly followed by a peak in velocity where  $U_b$  reached over  $10 \text{ cm s}^{-1}$ . Then,  $U_b$  was around  $2 \text{ cm s}^{-1}$  again until getting close to zero at the high water slack at  $t = 5.75 \text{ h}$ . Velocities near the bed were rather constant during ebb; at the vegetated position 2 they were slightly higher than during flood, whereas at the bare position 4 they were lower (Table 5.1). At the higher positions, the velocity tended to increase before the instruments fell dry again at  $t = 11.25 \text{ h}$ . The velocities at 1 m were always 2-4 times higher than near the bed; the flow directions were mostly similar. The ebb period lasted longer than the flood period. The hydropower plant in the Rance barrier is normally switched on about three hours after slack [Pigeard, 1999]; its effect on the flow near l'Écluse is unknown.

Table 5.1 Flow velocities  $U$  ( $\text{cm s}^{-1}$ ) and sediment concentrations SC (mV) averaged per flood (f) and ebb (e) period. \*Indicates an exceptionally high value, probably caused by an object in the measurement volume. \*\*Values seem unrealistically high.

position	Uf1	Uf2	Ue1	Ue2	Scf1	Scf2	SCe1	SCe2
2 bed	2.9	3.3	3.7	3.5	59.8**	43.3**	39.7**	60.7**
2 1m	11.5	7.6	9.9	7.0	13.5	8.3	2.7	5.5
4 bed	5.3	5.9	3.3	2.7	206.5*	16.7	16.1	27.1
4 1m	10.0	11.2	7.9	7.9	12.8	12.3	2.9	0.7

### 5.3.2 Sediment concentration

At both the vegetated and the bare position, the sediment concentration  $SC$  (V) peaked when the water reached the instruments (Fig. 5.4). Similar peaks occurred just before the instruments fell dry, which was slightly more pronounced at the bare positions. The concentration during flood was higher than during ebb (Table 5.1). The decrease in concentration occurred slowly rather than dropping suddenly during slack. Near the bed,  $SC$  was clearly higher than at 1 m. At position 4 near the bed, the readings at the beginning of the first flood period exceeded the usual range by far, which could indicate the passing of large objects through the measurement volume.

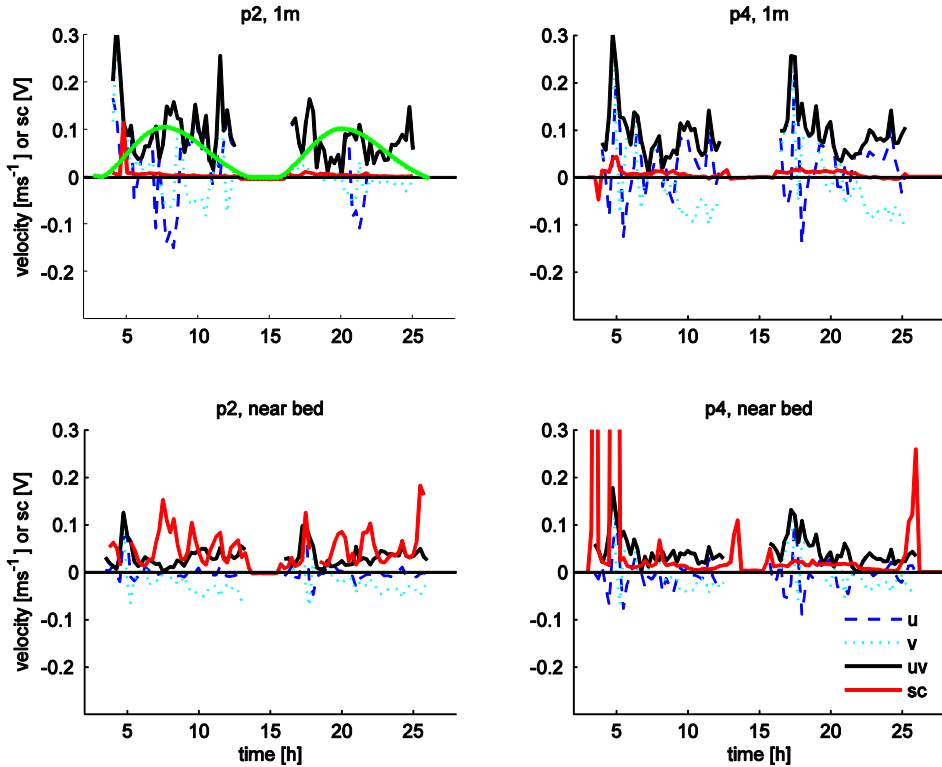


Figure 5.4. Data per sensor, averaged over 15 minutes: Velocity, water depth and sediment concentration. Time  $t=0$  corresponds to low water slack at May 7, 14:00 CET.

The raw 4 Hz data (not shown) from the lower sensor at position 2 displayed highly variable values over the entire measurement period. The lack of a relation between local transport conditions ( $u|u|$ ) and  $SC$  for position 2bed in Figure 5.5a in conjunction with high readings that did not occur in nearby instruments could be a sign of an object, possibly seagrass leaves or macroalgae, in the measurement volume. For the other positions, the correspondence between  $u|u|$  and  $SC$  was also basically absent, indicating that the advection of suspended sediment dominated the local pick-up of bed load material, consequently indicating that the sediment was fine enough to remain suspended in calm conditions. Despite the lack of actual sediment concentrations, visual observations of very clear water were a sign of low concentrations.

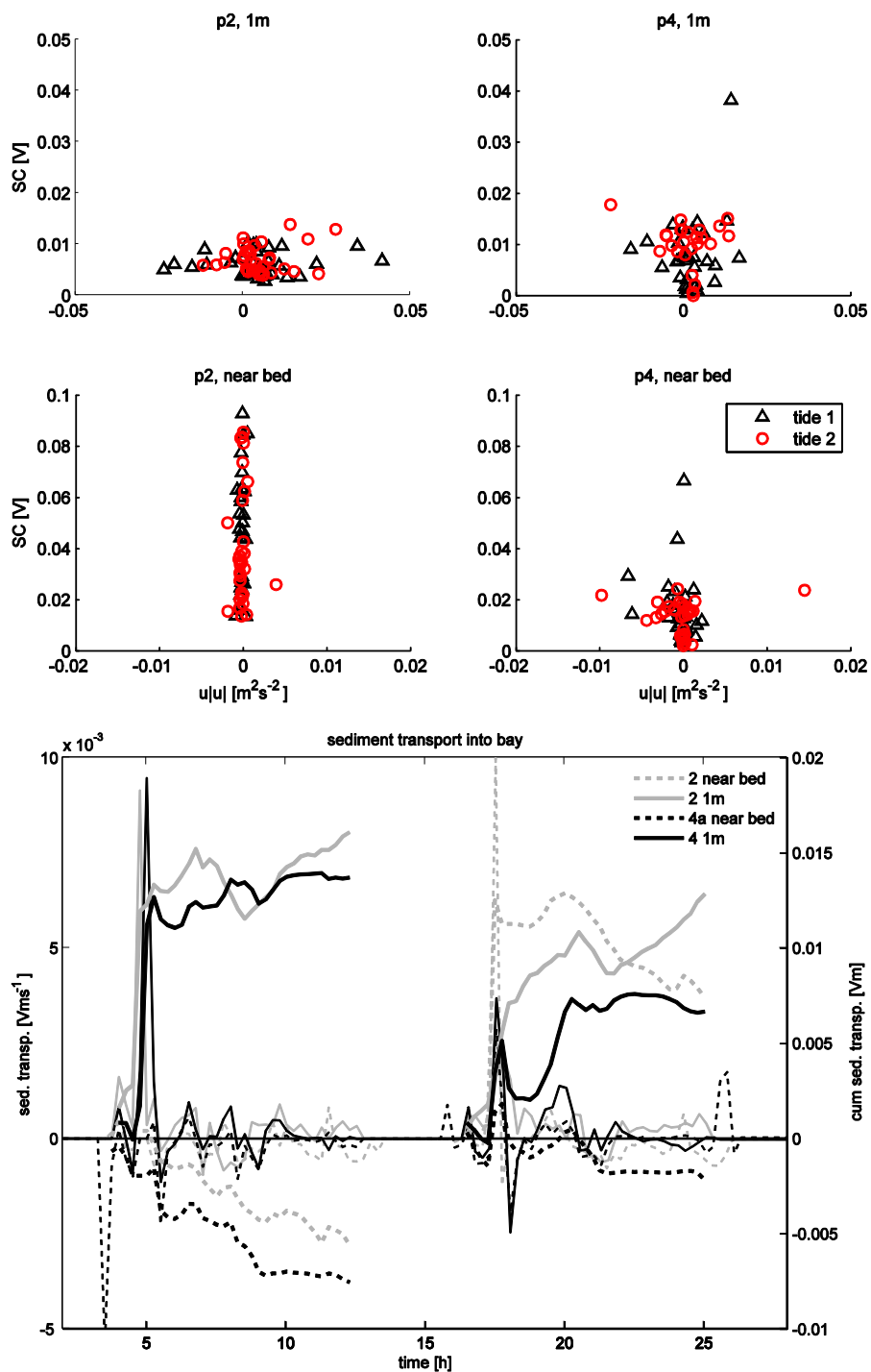


Figure 5.5 a) (upper) Relation between local shear stress ( $u|u|$ ) and sediment concentration for the four measurement positions. b) (lower) Cumulative (thick lines) and instantaneous (thin lines) sediment transport over two tides.

### 5.3.3 Sediment transport

The sediment transport into the bay (Fig. 5.5b) -calculated as  $u \cdot SC$ - varied more between the tides than the flow velocities, although a comparison was hampered by some extreme values of the OBS's near the bed. For all positions, the sediment transport varied around zero during the majority of the tidal cycle. The concentration peaks at the start of a flood period had a strong effect on the residual transport direction of sediment (Fig. 5.5b): If these peaks are taken into account when determining the cumulative transport, the resulting transport direction was into the bay (as in Table 5.1); in correspondence with the tidal asymmetry. If the peaks would be disregarded as erroneous however, the resulting transport direction might have been outward.

### 5.3.4 Model calibration and validation

The model reproduced the observed water level well (Fig. 5.6). The flow velocities were also well reproduced after calibration, though the measured differences between the four positions were much larger than the differences in model results. Despite some divergence in actual values –especially at position 4- the flow magnitude was very similar, as was the sequence: A peak at the beginning of the flood period, then lower velocities until a peak just after the turning of the tide, followed by a period of lower velocities at the end of the ebb that were slightly higher than those during the second half of the flood.

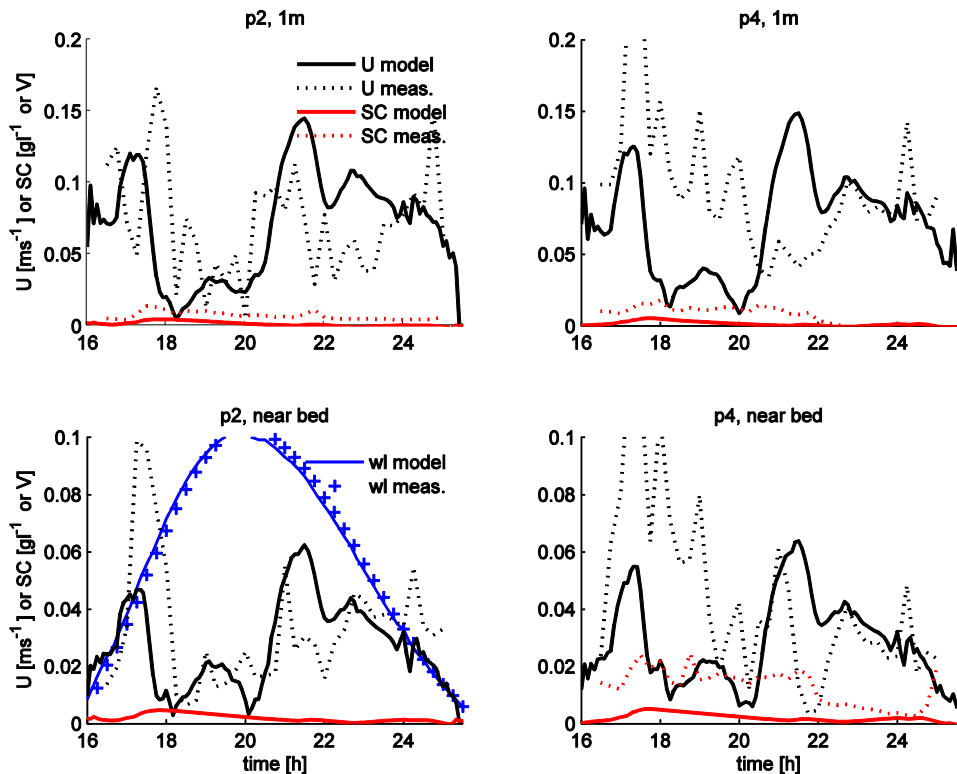


Figure 5.6 Comparison between measurements and model results for the 2<sup>nd</sup> tide. Note that the measured sediment concentration has the unit V, whereas the modelled concentration is in  $gr^{-1}$ .

The sediment concentration was difficult to compare because the measured value was not in real grams per litre. Clearly, the real concentration varied more rapidly than the modelled one, which might be due to an irregular along-shore transport or waves. Nevertheless, the sequence in sediment concentration was similar to the measured cycle: The highest concentration occurred in the beginning of the flood, roughly coinciding with the peak in flow velocity. Then, the concentration slowly decreased, with a small peak just after the peak in ebb velocity. The concentration during ebb was lower than during flood and the concentration near the bed was higher than at 1 m above the bed. Furthermore, the bed forms just west of the bay on the aerial image (Figs. 5.2 and 5.3) indicated a very dynamic area, which was affirmed by the high flow velocities and sedimentation/erosion rates calculated by the model.

### 5.3.5 Model results: sedimentation and erosion

According to the model, most widespread accretion –about 0.5 mm- occurred at the entrance of the bay, inside the polygon that indicates the meadow borders (Fig. 6.4; RV, next chapter). Less accretion –about 0.3 mm- occurred at the edge of the main channel and sand flat to the North-West. The sedimentation on the beach further inside the bay was minimal. Very locally –the scale of a single grid cell- the sedimentation amounted to 2 mm, for example in the dynamic and shallow areas east and west of the bay, as well as near the rocky outcrop directly west of the bay. These are also the areas where most erosion took place: 0.2 mm west of the bay and on the bank north of bay, vs. 2 mm east of the bay. The latter is near the model boundary and in a hydraulically complicated area due to the Rance barrier-outflow, thus possibly not realistic. Sedimentation and residual transports are treated more elaborately in the next chapter.

## 5.4 Discussion

### 5.4.1 Observations

The observed flow velocities in the bay were fairly low: a peak of  $30 \text{ cm s}^{-1}$  during flood and an average of around  $10 \text{ cm s}^{-1}$  one meter above the bed (Fig. 5.4). Given the geometry of the bay – more a sheltered beach with a limited volume than a tidal lagoon- such low velocities could be expected.

The low flow velocities, hence the low bed shear stresses and transport capacity, corresponded to the observed clear water and low backscatter or sediment concentrations. The highest backscatter was observed by the lower sensors in shallow water, especially at the bare position. Though this high turbidity seems contrary to observations of seagrass decreasing suspended particular matter concentrations in shallow water more than in deep water [Ward *et al.*, 1984] it is probably due to a small amount of foul water affected by waves. Moreover, the backscatter was lower in the water that passed through the meadow.

The lack of a relation between local hydrodynamics and sediment concentration means that the advection of suspended sediment was larger than the bed load transport. Under more dynamic conditions, i.e. with substantial waves, the bed shear stress and bed load transport will be higher; a requirement for considerable morphologic changes.

These findings differed little between the two locations, with the exception of the definitely lower near-bed velocity inside the seagrass meadow during flood (pos. 2 in Table 5.1). This lower velocity was likely the result of flow attenuation by the plants because the velocities above the vegetation at both locations were similar for the first tide. The flow directions at the two locations differed among both tides (Fig. 5.4).

#### 5.4.2 Model calibration and validation

The model was able to reproduce the observed hydrodynamics rather well, as Figure 5.6 illustrates. The essential developments during a tidal period are replicated, both with respect to magnitude as to direction. The field measurements showed more variability, probably as a result of passing ships, waves or wind driven currents or the operation of the Rance barrier; all these phenomena were not represented in the model.

The performance of the model with respect to sediment transport (Fig. 5.6) is more difficult to assess: The main trends are reproduced after calibration, but some phenomena seem to be missing in the model. If there would be a chance to perform a similar experiment, some changes would reduce the many uncertainties encountered in the present data and contribute to firmer conclusions: *i)* Measurements should cover an entire spring-neap cycle, which also enables a preliminary assessment of data and allows for possible repairs. *ii)* A ship-mounted ADCP could provide better spatial information regarding flow and possibly sediment transport if supported by samples of suspended sediment, especially near the boundaries of the model area. *iii)* The use of LISST (Laser In-Situ Scattering and Transmissometry) instruments that sample both particle concentration and particle size would give a better idea of sediment movement than possible with an OBS.

*Van Rijn's [1993; Appendix B]* transport formulations do account for waves, but Delft3D does not deal with wave damping by flexible vegetation. As the waves during the measurements were negligible for most of the time, the decision was made not to include waves rather than do so haphazardly. Overall, the model in this study seems to satisfy the three principles for an adequate numerical model stated by *Teeter et al. [2001]*: *i)* incorporation of relevant processes and geometry to represent the vertical turbulence structure and general circulation pattern, *ii)* provide a stable solution within reasonable time, with *iii)* a sufficient accuracy. Using a three-dimensional model and vegetation elements rather than a tuned bed roughness coefficient is essential to meet these criteria.

#### 5.4.3 Sediment transport formulations

Contrary to the large amount of empirical investigations of sediment transport in vegetation meadows (see *Madsen et al. 2001* for an overview), very few studies have fundamentally assessed sediment transport formulations in the presence of vegetation [*López & García, 1998; Teeter et al., 2001*]. *López & García [1998]* found two effects of vegetation: the concentration of suspended sediment in vegetated areas can be slightly higher than above a bare bed due to a higher diffusivity, and the reduced bed shear stress limits resuspension.

The sediment transport formulations used in this study cope with the effect of vegetation to a large extent (see Appendix B for formulas): Erosion and deposition of cohesive sediment (based on the well-known Partheniades-Krone formulations; *Partheniades, 1965*) are governed by the

bed shear stress, which is reduced by the modelled vegetation. The concentration and the transport of suspended sediment are determined by the flow velocities and the diffusivity due to turbulence, which are also affected by the modelled vegetation, except for a possible physical blocking by leaves.

The effect of vegetation on bed load transport is incorporated less clearly: this transport formulation is based on an effective depth averaged velocity that is reconstructed from the velocity in the bottom layer assuming a logarithmic profile. As such, in the presence of plants the mobility of the sediment is lower than in case of a bare bed where the near-bed velocity is higher. Two processes not included in this model are the trapping of particles against leaves [Hendriks *et al.*, 2008, 2010] and the erosion caused by small-scale flow intensification around the stems of the plants [Koch, 1999; Nepf & Koch, 1999; Bouma *et al.*, 2009]. While not all processes are fully incorporated, the behaviour of the sediment transport in this study is simulated well, which would not be the case if the presence of vegetation would be modelled as a higher bed roughness.

#### 5.4.4 Model applicability

Though the model described in this paper was applied to a relatively small area and for a short period only, it can be applied at the same large spatial and temporal scales as the general Delft3 version. As such, this model is a useful tool to study long-term biogeomorphological developments. Studies on smaller scales [e.g. Peralta *et al.*, 2008; Luhar *et al.*, 2008; Morris *et al.*, 2008; Chapter 2] are also possible, though models that provide more detailed turbulence information like those of Stoesser *et al.* [2009] can have their benefits.

Studies into the development of intertidal flats [Temmerman *et al.*, 2007] and salt marshes [D'Alpaos *et al.*, 2006] can be extended with flexible vegetation. Likewise, field-based studies that assess the effect of biomechanical plant properties on landscape formation, such as by Fonseca *et al.* [2007], can be combined with model results to provide additional insights.

Due to the ability to simulate sediment transport and the sediment-related turbidity, the model can also be used to perform environmental impact- or suitability analyses [like e.g. Zimmerman *et al.*, 1991; Best *et al.*, 2001] where the amount of light available for photosynthesis is paramount. Here, taking biogeomorphological feedbacks into account that possibly enhance habitat suitability means a more realistic analysis. Combinations with water quality models are also possible, thus providing studies on nutrient uptake by macrophytes [e.g. Zharova *et al.*, 2001] or seed dispersal [e.g. Erftemeijer *et al.*, 2008] with a more realistic flow field. Moreover, such combinations could provide a process-based foundation for studies on alternative stable states such as those of Van der Heijde *et al.* [2007], thus enabling modelling studies of why eelgrass disappeared from the Wadden Sea and struggles to return [Den Hartog & Polderman, 1975; Van Katwijk *et al.*, 2009].

Most of the examples mentioned above consider coasts and estuaries but the model is equally applicable to rivers and lakes. In waters where the vegetation occupies only a small part of the water column, considering the vegetation position constant in time is computationally more efficient without compromising the results. The inclusion of a process description for particle trapping [cf. Hendriks *et al.*, 2008, 2010] would be useful and is a feasible improvement. Incorporating plants with a complex morphology or with strongly heterogenic properties within a meadow involves more effort. Modelling wave attenuation by flexible vegetation and its effect on

bed shear stress and sediment re-suspension requires additional research. A first step however might be the application of a recently developed version of the SWAN (Simulating Waves Near Shore) model that incorporates wave damping by stiff plants [Suzuki *et al.*, 2011].

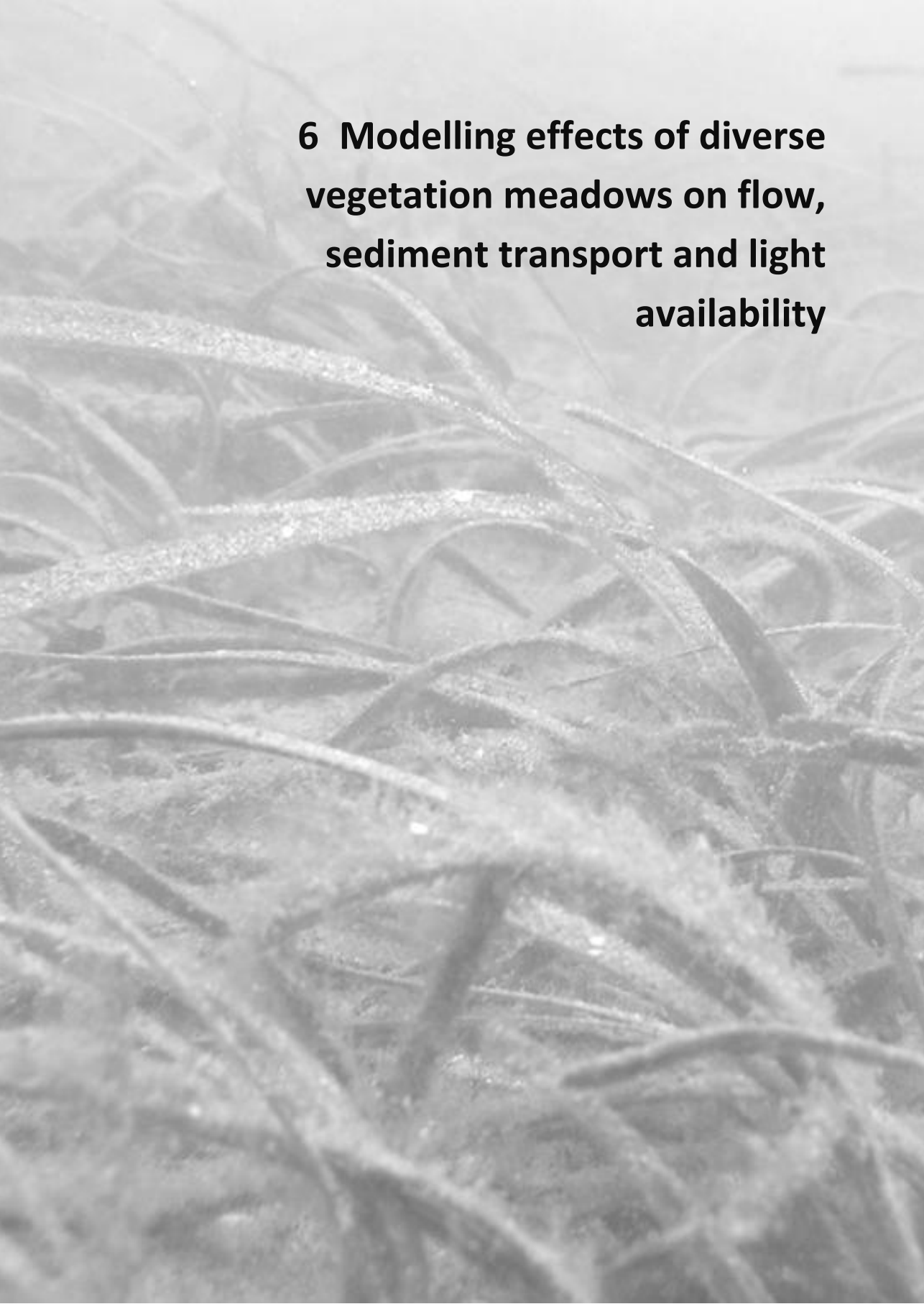
## 5.5 Conclusions

The field measurements showed that the conditions in the bay were fairly calm: tidal flow dominated wave action. The average velocity one metre above the bed was  $10 \text{ cm s}^{-1}$ , hence only the peak of  $30 \text{ cm s}^{-1}$  during flood exceeded the pick-up velocity for sandy sediment. Consequently, the water was very clear and the transported sediment was mainly fine suspended material. Both the flow velocity and the sediment concentration differed slightly between the measurement location inside the seagrass meadow and the adjacent station on the bare beach: the near-bed velocities were lower inside the meadow, and the sediment concentration was higher outside the meadow.

The three-dimensional numerical model was able to reproduce the main features of the observations, indicating that the processes of vegetation bending and sediment transport through vegetated areas are incorporated correctly. The existing sediment transport formula used [van Rijn, 1993] deals with vegetation effects on sediment pick-up and transport via the effects on hydrodynamics. Physical filtering by blades and flow intensification around shoots are not taken into account. The model is a useful tool to study biophysical interactions in this and other areas. Extensions to water quality models can easily be made. Modelling wave attenuation and its effect on sediment transport would substantially expand the applicability of the model.

## Acknowledgements

The author would like to thank the Netherlands Institute for Ecological Research-Centre for Estuarine and Marine Ecology (NIOO-CEME) for the use of equipment, Jérôme Fournier and Laurent Godet of the Musée National d'Histoire Naturelle for their hospitality, Walter Jacobs, Matthieu de Schipper and Sierd de Vries for help in the field and the Netherlands Organisation for Scientific Research (NWO) for funding by grant 014.27.014.

An underwater photograph showing a dense meadow of seagrass. The seagrass blades are long, narrow, and arching, with a textured, slightly fuzzy appearance. They are growing from a sandy or silty seabed. The lighting is somewhat dim, creating a soft, ethereal atmosphere. The text is overlaid on the upper right portion of the image.

## **6 Modelling effects of diverse vegetation meadows on flow, sediment transport and light availability**

## Abstract

To understand how different species of aquatic plants can affect coastal and estuarine morphology and water quality, we used a numerical model developed to simulate three-dimensional flow and sediment transport in areas with flexible vegetation. The results obtained with the model described in the previous chapter show the following: At the entrance of a macrotidal bay, sparse flexible vegetation such as *Zostera marina* (eelgrass) can be more efficient in trapping sediment inside the bay than denser or stiffer vegetation. In these conditions, where the vegetation only occupies a small part of the water column, plants mainly prevent erosion rather than increase deposition and they have more effect on bed-load transport than on the transport of suspended sediment. The presence of macrophytes increased the light availability over a tidal cycle up to 7% with respect to a bare bed. The effects of the relatively open eelgrass meadow on the bed shear stress and light availability were less strong than that of a denser meadow or a meadow of stiff vegetation of equal density. The influence of macrophytes is more pronounced in shallower areas where plants occupy a larger part of the water column.

**Keywords:** *Zostera marina*, flexible vegetation, sediment transport, light availability, modelling, biogeomorphology

## 6.1 Introduction

Whereas the previous chapters have described and discussed the step-by-step development and testing of models for flow and sediment transport through flexible vegetation, this chapter deals with the final objective of this thesis: Studying the interaction of flexible plants and their environment by means of a validated model. This study is a quantitative illustration of how macrophytes affect physical environmental variables that are important for their development and could be seen as a step towards a fully interactive model for plant growth. The latter however would require a thorough incorporation of plant growth processes, which is beyond the scope of this study.

Apart from chemical and biological conditions [Koch, 2001; van der Heide *et al.*, 2009], the development of seagrasses is determined by the forces on plants [Boller *et al.*, 2007], by the morphological changes of the surrounding seabed [Duarte *et al.*, 1997; Cabaço & Santos, 2007] but mostly by the amount of light available for photosynthetic growth [Duarte, 1991; Short & Wylie-Echeverria, 1996; Greve & Krause-Jensen, 2005; van der Heide *et al.*, 2009]. Turbidity reduction is regarded as probably the most important positive feedback mechanism in seagrass systems [De Boer, 2007].

In this chapter, we assess the effect of vegetation on these physical conditions by comparing the near bed velocity -as a proxy for the bed shear stress-, the sediment transport and the light availability near the bed. The model applied here was developed in Chapter 5 and concerns the same eelgrass meadow in Baie de l'Écluse, along with three other scenarios of vegetation cover intended for comparison: a bare bed, a very dense eelgrass meadow and a meadow of stiff vegetation. For these scenarios, we evaluate the effect of the vegetation type on flow velocity and sediment transport patterns as well as the light climate over one tidal period. We conclude with a discussion of possible applications.

## 6.2 Materials and Methods

### 6.2.1 Modelling scenarios

The purpose of this study is to assess the capacity of different vegetation meadows to alter sediment transport and –as a consequence– light availability. Therefore, we used four scenarios: *i*) The reference situation with realistic vegetation (RV; equal to the calibrated simulation in the previous chapter), *ii*) a scenario with a bare bed, i.e. no vegetation (NV), *iii*) a scenario with high-density vegetation (DV) and *iv*) a scenario with stiff vegetation (SV), which may serve as an example for a restoration effort with artificial vegetation. Many more scenarios are possible, e.g., longer plants, larger or smaller coverage, but these four cover the most basic configurations.

All scenarios are evaluated over one tidal period and have the same settings for hydrodynamic and sediment transport parameters; only the vegetation differs. For RV, the plants are the same as in the previous chapter: flexible and eelgrass-like, with a uniform density of 1800 leaves  $\text{m}^{-2}$  or 360 plants  $\text{m}^{-2}$ . In DV, the density of the same plants is almost tripled to 1000 plants or 5000 leaves  $\text{m}^{-2}$ ; a more common density later in the growing season. The plants in SV have the same density as in RV but have a fixed height of 30 cm and a constant drag coefficient of 1.

Three monitoring points -outside the bay, in the meadow and further inside the bay (Fig. 5.3 in previous chapter)- are used to observe time series. Two monitoring cross-sections –one roughly at the seaside of the meadow, the other at the landward side (Fig. 6.6) are used to calculate residual transports over one tidal period.

### 6.2.2 Light availability

Plants can affect the amount of sediment in the water column and consequently the amount of light that reaches the bed available for photosynthesis. The amount of light reaching the bed  $I_b$ , relative to the surface irradiation  $I_s$ , is related to the depth  $z$  (m) and the light attenuation coefficient  $K$  ( $\text{m}^{-1}$ ), according to the Lambert-Beer equation:

$$I_b = I_s e^{-Kz} \quad (38)$$

Where  $K$  is a combination of a background value  $K_0$  representing attenuation by e.g. phytoplankton and dissolved organic matter, as well as  $K_f$  and  $K_c$  ( $\text{m}^{-1}/\text{gm}^{-3}$ ) that respectively represent the attenuation by fine and coarse sediments as a function of their concentration ( $c_f$  and  $c_c$ ;  $\text{gm}^{-3}$ ):

$$K = K_0 + K_f c_f + K_c c_c \quad (39)$$

Because the light attenuation was not measured in situ, coefficients are based on literature [Colijn, 1982; Lund-Hansen, 2004; Van Duin et al., 2001; Zimmerman et al., 1991]:  $K_0=0.1 \text{ m}^{-1}$  and  $K_f=50 \text{ m}^{-1}/\text{gm}^{-3}$ . As small particles attenuate more light than coarse particles [Baker & Lavelle, 1984],  $K_c=10 \text{ m}^{-1}/\text{gm}^{-3}$  was chosen.

## 6.3 Results

### 6.3.1 Spatial flow patterns

The maximum depth averaged flow velocity  $U_{da,max}$  during one tide was very similar for all four scenarios, as Figure 6.1a shows. The highest flow velocities ( $0.7$  to  $0.8 \text{ ms}^{-1}$ ) occurred near the channel, in West-East direction. Velocities were especially high near the rocky outcrop just west of the bay entrance and at the sill to the east. On the sand bank directly north of the bay  $U_{da,max}$  was lower, around  $0.4 \text{ ms}^{-1}$ .  $U_{da,max}$  inside the vegetated area ranged roughly between  $0.25$  to  $0.6 \text{ ms}^{-1}$ , mainly depending on depth.

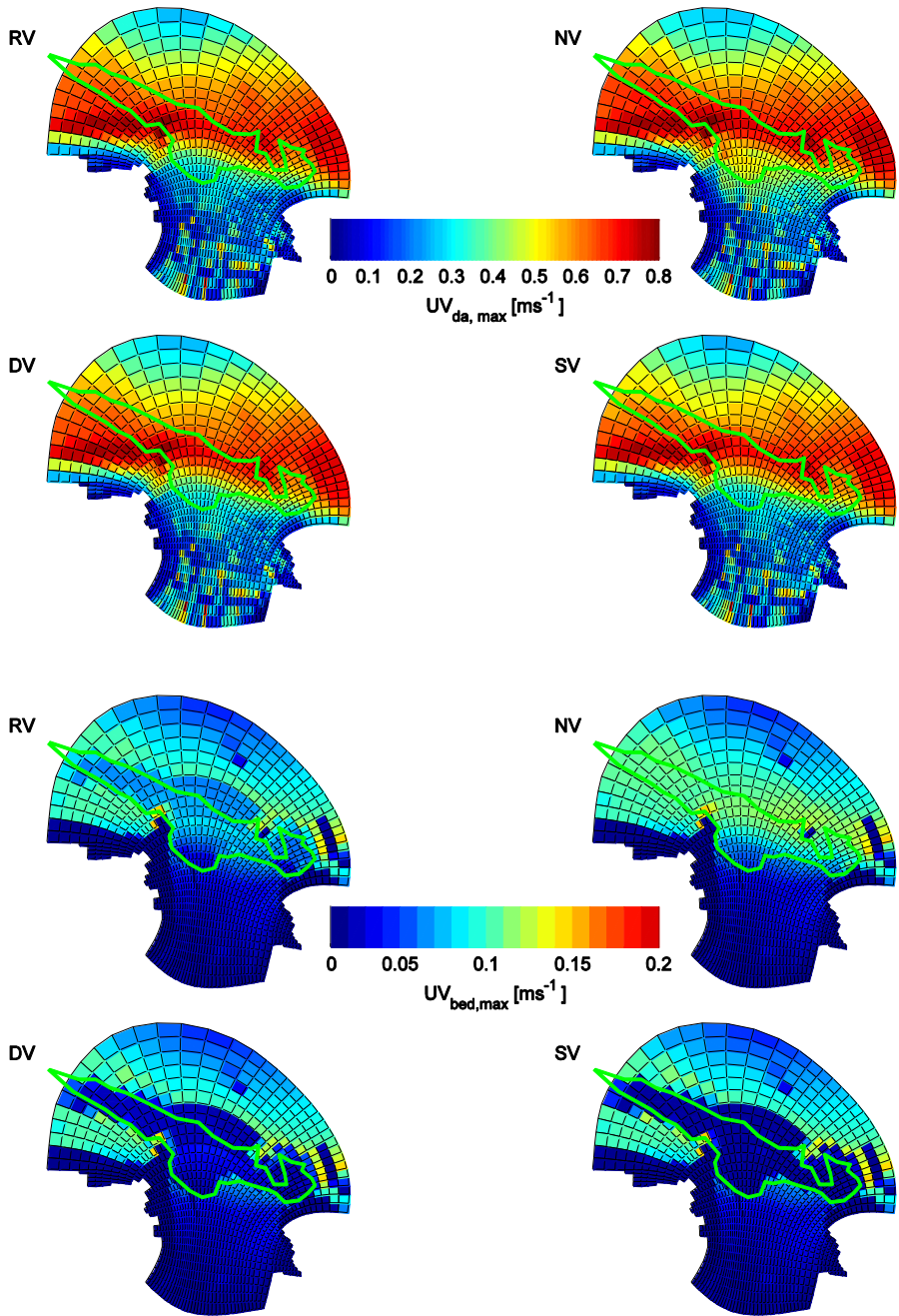


Figure 6.1 a) (upper) Depth averaged flow velocity (maximum during one tide) for all four scenarios, plotted on the computational grid. The green polygon indicates the outline of the seagrass meadow. b) (lower) Flow velocity near the bed (maximum during one tide) for all four scenarios.

Inside the bay some cells showed a high flow velocity, but this seems to be a numerical artefact associated with drying and flooding rather than a realistic result. For this same reason, the maximum flow velocity near the bed ( $U_{bed,max}$ ) during one tide is plotted in Figure 6.1b as an indicator for the bed shear stress, rather than the bed shear stress itself.

Though  $U_{da,max}$  differed little between the scenarios, the difference in  $U_{bed,max}$  was considerable: In the scenarios with the dense and the stiff vegetation,  $U_{bed,max}$  was practically zero inside the vegetation, whereas in the scenario without vegetation it was around  $0.1 \text{ ms}^{-1}$  in the same area. In the RV-scenario  $U_{bed,max}$  was slightly above  $0.05 \text{ ms}^{-1}$ . The presence of the meadow affected  $U_{bed,max}$  also outside the vegetated area, especially just north of the meadow.

### 6.3.2 Flow and transport time-series

The time-series of  $U_{da}$ ,  $U_{bed}$  and sediment concentrations at locations seaward of the meadow, inside the meadow and inside the bay in Figure 6.2 showed very similar values for all four scenarios. Especially DV and SV were similar. The largest differences between the scenarios were observed for  $U_{bed}$  and the concentration of sand. Most differences were observed inside and seaward of the meadow; the values inside the bay were practically the same among the scenarios.

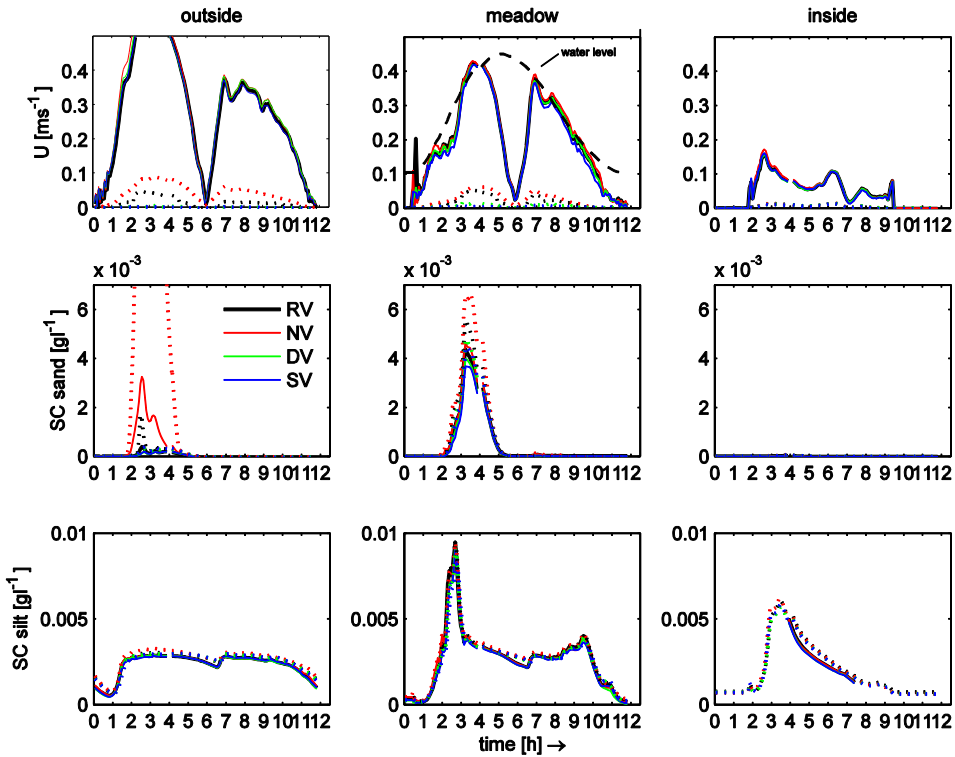


Figure 6.2 Comparison of the time-series of the four scenarios, at positions outside the bay, in the vegetated area and further inside the bay (for locations: see Fig. 5.3). Continuous lines are 1 m above the bed; dotted lines 10 cm from the bed.  $t_0$  corresponds to  $t=16 \text{ h}$  in Figs. 5.4-5.6. The water level is not absolute; shown for reference only.

During flood  $U_{da,out}$  gradually increased to over  $0.5 \text{ ms}^{-1}$ , then gradually decreased to zero at  $t=6 \text{ h}$ . During ebb,  $U_{da,out}$  increased rapidly to  $0.3\text{-}0.4 \text{ ms}^{-1}$  to vary between these values for three hours, followed by a continuous decrease towards the end of the tidal period.  $U_{da,out}$  was marginally higher for NV than for the other scenarios, but only during flood.  $U_{da,md}$  peaked when the meadow became flooded. Until  $t=3 \text{ h}$ ,  $U_{da,md}$  irregularly rose to  $0.2 \text{ ms}^{-1}$ , after which it rapidly rose to  $0.4 \text{ ms}^{-1}$  at  $t=4 \text{ h}$  and decreased at the same rate to almost zero at  $t=6 \text{ h}$ . During ebb,  $U_{da,md}$  rose rapidly to nearly  $0.4 \text{ ms}^{-1}$  at  $t=7 \text{ h}$ , after which it intermittently decreased. The differences between the scenarios were the largest during this last phase. Inside the bay,  $U_{da,in}$  was much smaller than at the more seaward locations, with a maximum of  $0.15 \text{ ms}^{-1}$  during flood.  $U_{da,in}$  never dropped to zero.

$U_{bed}$  had a similar development to  $U_{da}$  at all locations, but with much smaller values and larger differences between the scenarios. For the observation point outside the bay, the maximum value for  $U_{bed}$  was  $0.1 \text{ ms}^{-1}$  for NV,  $0.06 \text{ ms}^{-1}$  for RV and almost zero for DV and SV. Inside the meadow the maximum of NV was  $0.05 \text{ ms}^{-1}$ , that of RV slightly lower and that of DV and SV near zero. Inside the bay, all near-bed velocities were marginal in all scenarios.

The concentration of sand peaked during flood ( $t=2$  until  $t=5 \text{ h}$ ), coinciding with high velocities. Despite similar velocity magnitudes, no transport occurred during ebb. Near-bed values were higher and differed more between the scenarios than the depth-averaged ones, which is best seen outside the meadow. All concentrations were low;  $6 \text{ mg l}^{-1}$  was hardly exceeded. The concentrations in NV were the highest, followed by RV, SV and then DV. Remarkably, concentrations inside the meadow were higher than outside. Also, the near-bed concentrations here were much closer to the depth-averaged ones. No sand transport occurred at the location inside the bay.

The silt concentration did not markedly differ between the four scenarios. Outside the bay, the concentration was almost constantly equal to the  $3 \text{ mg l}^{-1}$  applied at the model boundaries; it only dropped during slack periods. Inside the meadow a peak of  $10 \text{ mg l}^{-1}$  occurred during flood and a smaller peak of  $4.5 \text{ mg l}^{-1}$  during ebb at  $t=10 \text{ h}$ . Inside the bay, the silt concentration peaked at  $6 \text{ mg l}^{-1}$  just after the flood reached this area, followed by an exponential decrease. The similarity between the depth-averaged and near-bed values at all locations indicates a constant concentration over the depth.

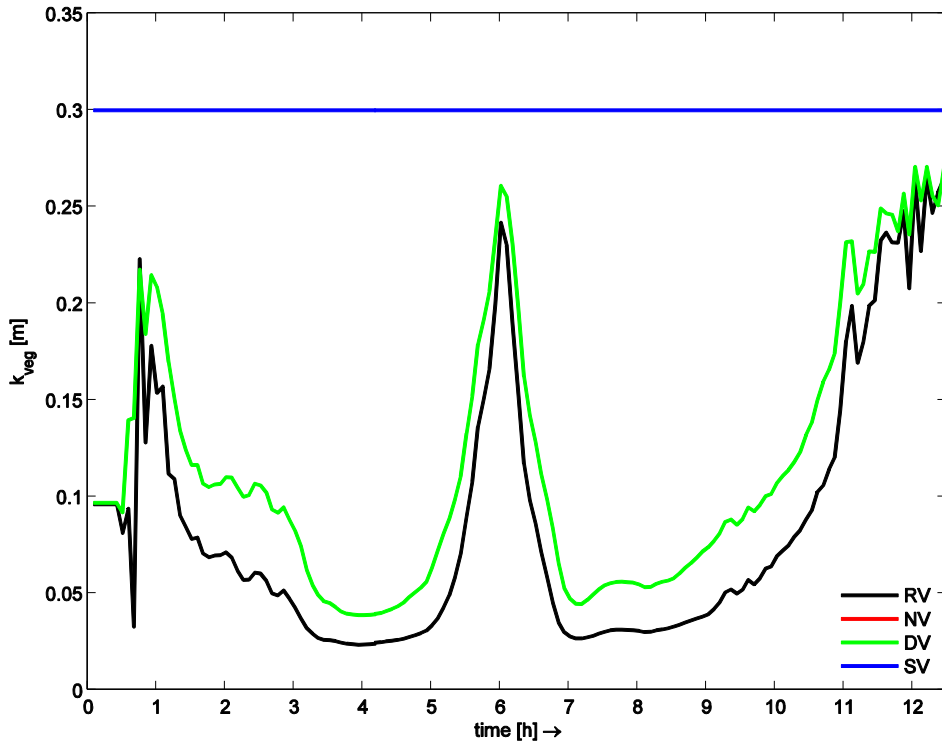


Figure 6.3 The vegetation height (at position 'veg' in Fig. 5.3) in time.

The height of flexible vegetation mirrored the magnitude of the flow velocity (Fig. 6.3). For a dense meadow (DV), the vegetation height was slightly higher than for a sparse meadow (RV). Both lines showed jumps of several centimetres at the onset of flood and at the end of the ebb period, possibly indicating numerical difficulties in shallow water when the depth changes rapidly.

### 6.3.3 Sedimentation and residual sediment transport

The sedimentation/erosion pattern in NV clearly differed from the other scenarios: part of the area inside the polygon eroded more than 0.5 mm, whereas in the simulations with vegetation this area accreted slightly (Fig. 6.4). In NV, the accretion was a bit higher in the shallower zone inside the polygon. In the scenarios with vegetation, sedimentation also occurred directly north of the meadow. Around the rocky area at the east, which is surrounded by vegetation, most sedimentation/erosion occurred for RV and NV.

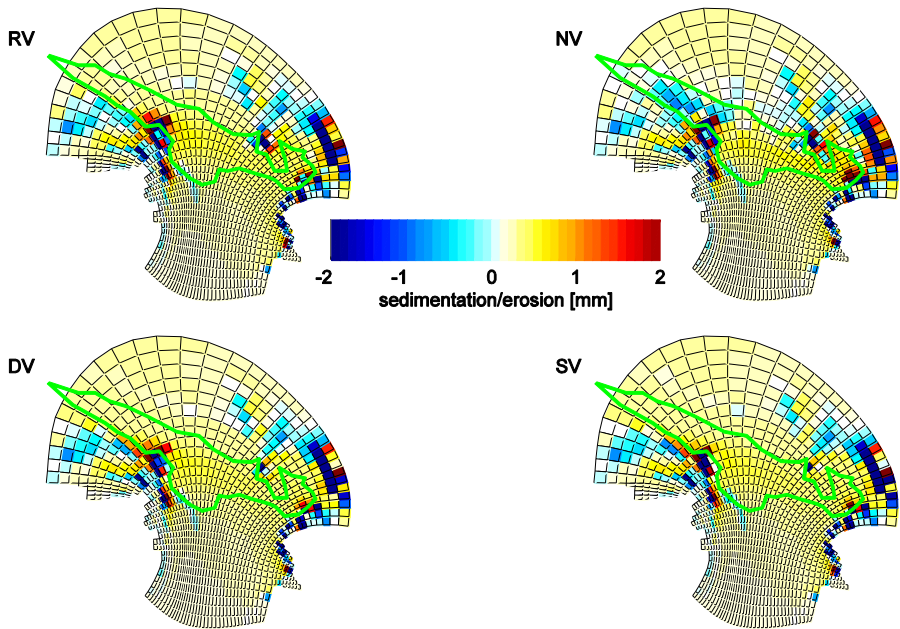


Figure 6.4 Sedimentation and erosion for all four scenarios after one tidal period.

The bars in Figure 6.5 show how much sediment passes through two cross-sections: one just outside the bay at the seaward side of the meadow (A-A'') and one inside the bay on the sandy beach (B-B''). The sediment transport inside the bay was negligible. The transport through A-A'' showed the same magnitudes for all scenarios; only the quantities differed. During flood, both silt and sand were transported into the bay through the two sections on the left and to a lesser extend conveyed outward through the two sections on the right. The import exceeded the export. During ebb, hardly any sand moved in or out. Silt was transported inward through the eastern sections and outward in the sections to the west. Import and export were nearly equal.

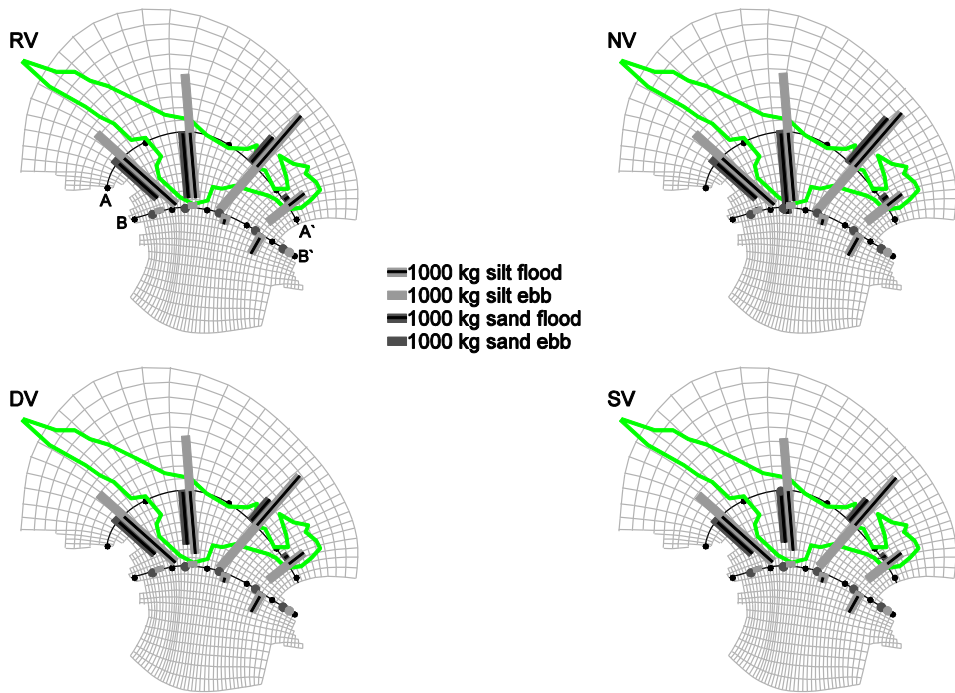


Figure 6.5 Residual sediment transports per fraction over one tidal period.

The presence of vegetation affected the transport of sand more than it affected the transport of silt (Fig. 6.6): In NV  $1.40 \cdot 10^4$  kg of sand passed A-A'', of which  $5.05 \cdot 10^3$  kg (36 %) remained in the bay. In RV this was  $1.08 \cdot 10^4$  kg resp.  $5.61 \cdot 10^3$  kg (52 %), whereas for the scenarios DV and SV the total transports were  $9.36 \cdot 10^3$  resp.  $8.97 \cdot 10^3$  kg of which  $4.95 \cdot 10^3$  and  $4.64 \cdot 10^3$  kg (both 52 %) was left.

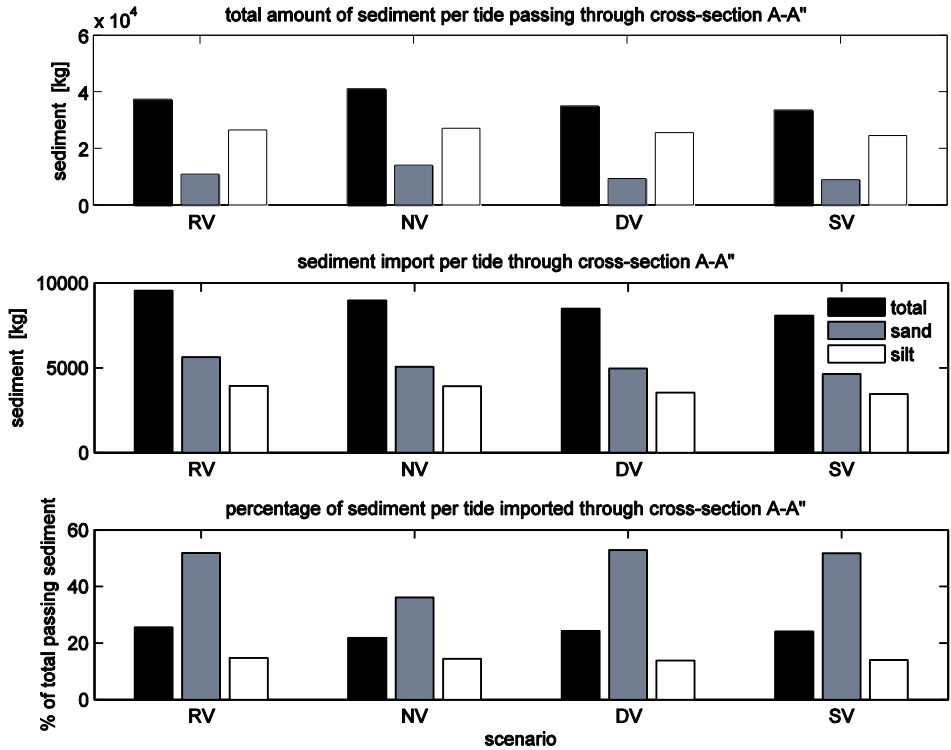


Figure 6.6 Sediment import and total amount of sediment passing through cross section AA' per tide, for all four scenarios.

The total amount of silt conveyed in NV was  $2.71 \cdot 10^4$  kg, in RV  $2.65 \cdot 10^4$  kg, in DV  $2.56 \cdot 10^4$  kg and in SV  $2.46 \cdot 10^4$  kg. The import of silt was, respectively,  $3.91 \cdot 10^3$ ,  $3.93 \cdot 10^3$ ,  $3.54 \cdot 10^3$  and  $3.44 \cdot 10^3$  kg; all between 14-15%. Hence, the relative imports of all scenarios with vegetation were similar, but the absolute import of sediment in RV was higher due to the fact that more sediment was conveyed in this scenario. The most sediment was conveyed in the situation without vegetation, both in and out of the bay.

### 6.3.4 Light availability

The light availability during a tidal period differed only marginally between the four scenarios (Fig. 6.7): The background attenuation ( $K_0$ ) in combination with the water depth was the main cause of light attenuation and therefore the same for all scenarios. The silt concentration, the second cause of attenuation, was also similar along the four scenarios (Fig. 6.2) on these three locations. Despite a lesser attenuation coefficient for sand than for silt, the concentration of sand differed more, resulting in a lower light availability at  $t=3-4$  h for NV that coincided with a peak in sand transport in Figure 6.2.

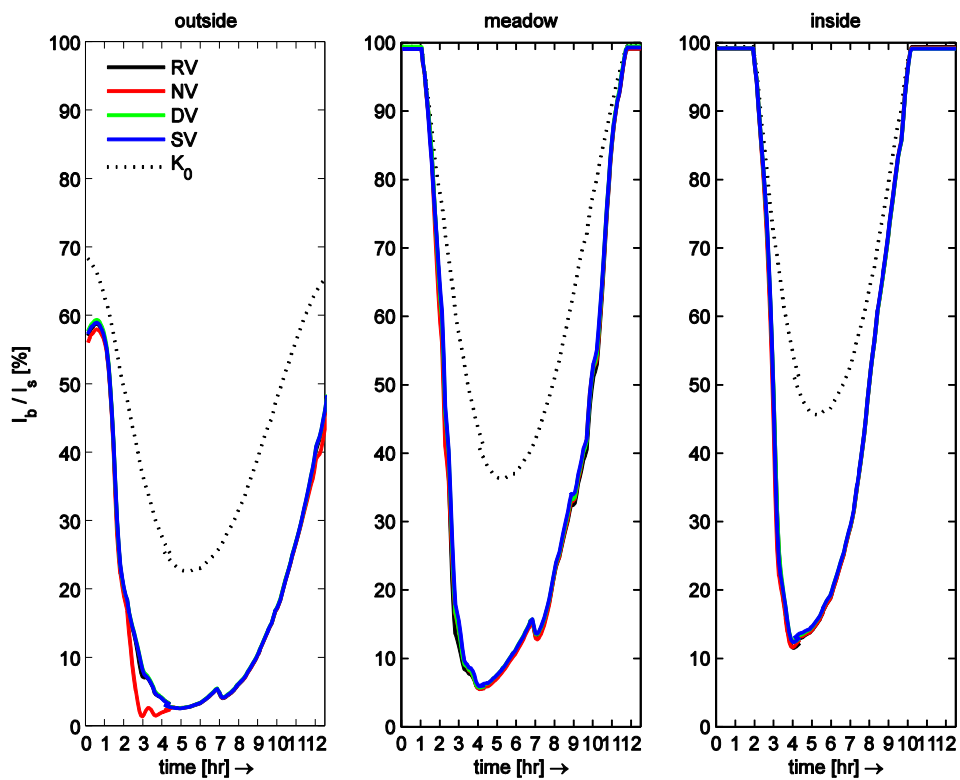


Figure 6.7 Irradiance reaching the bed at three locations, for all scenarios and for background light attenuation ( $K_0$ ; dotted line) only.

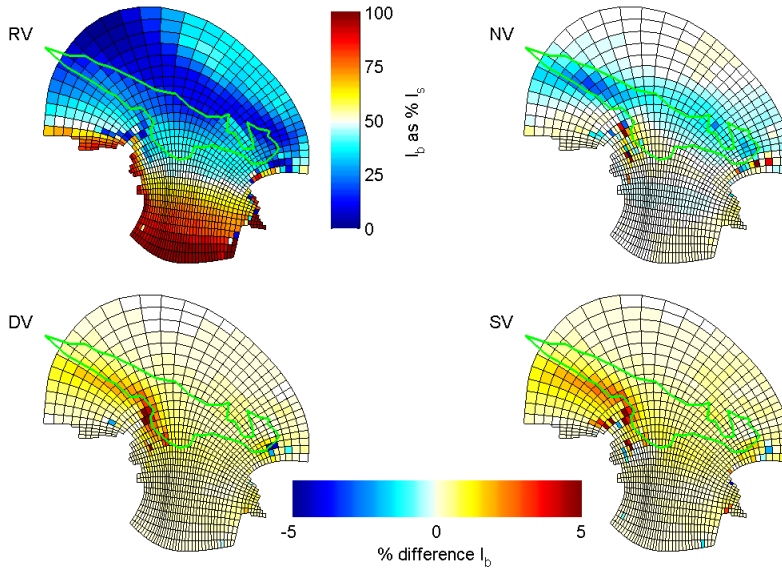


Figure 6.8 Percentage of surface irradiance reaching the bed, averaged over a tidal period. Upper left, vertical colorbar: for realistic vegetation (RV). Other figures, horizontal colorbar: difference with scenario RV.

The spatial representation of the average irradiance reaching the bed ( $I_{bed}$ ; Fig. 6.8) also indicated that water depth was the main cause of attenuation; the plot follows the contours of the bathymetry (Fig. 5.3). In the scenario for real vegetation (RV),  $I_{bed}$  inside the eelgrass meadow was between 20 and 35% of the surface irradiance. In the scenario without vegetation (NV), up to 4% less light was available in the meadow area where erosion occurred (Fig. 6.2) and up to 2% less outside this area. For the scenarios with dense (DV) or stiff (SV) vegetation, the light availability increased slightly throughout the bay, but most clearly (3%) at the west border of the meadow, where deposition took place (Fig. 6.2).

## 6.4 Discussion

### 6.4.1 Effects of vegetation on flow and sediment transport

When comparing the scenario without vegetation (NV) to the scenarios with vegetation (RV, DV, SV), it is clear that the presence of plants affected the maximum velocity near the bed but not the depth averaged velocity. Likewise, the transport of sand, which primarily occurs near the bed, was more affected by the presence of vegetation than the transport of fines, which are suspended throughout the water column and hardly affected in deep water (Figs. 6.2 and 6.8; López & García, 1998).

The presence of seagrass-like vegetation (RV) increased the deposition in the vegetated area slightly, but more importantly prevented the substantial erosion that occurred in the absence of plants. Hence, the seagrass is more effective in preventing erosion than in reducing sediment transport, which is not surprising given the fact that it only occupies a small part of the water column for most of a tidal period. *Ward et al. [1984]* and *Gruber & Kemp [2010]* reported lower suspended particular matter (SPM) concentrations as a result of wave attenuation by macrophytes, hence less resuspension, in shallow water. They also noted that this mechanism was less effective at elevated water levels, when SPM is conveyed from elsewhere over the canopy. *Terrados & Duarte [2000]* and *Gacia et al. [1999]* observed that particle resuspension was lower inside a meadow of *Posidonia oceanica* than on the nearby bed, at similar depths as in our study.

The depth averaged velocities in the scenarios with dense and stiff vegetation were similar to that in the real vegetation. However, the near-bed velocities -i.e. the bed shear stress- in these two scenarios (DV and SV) were much lower than in RV (Fig. 6.1). The near bed velocity is not directly related to vegetation height or density: SV and RV have the same density and DV and RV a similar vegetation height (Fig. 6.4), but the near bed velocity differs considerably.

As a consequence of the low bed shear stress, the transport of especially sand was lower in DV and SV (Fig. 6.2). As a result, the real vegetation allowed for the largest import of sediment into the bay, as most sand entered the bay during flood that was not transported outwards during ebb (Fig. 6.5). DV and SV displayed higher sedimentation rates though, especially in the north western part of the meadow, capturing the sediment before it enters the bay. Similar to the higher sedimentation rate in DV when compared to RV, *Gacia et al. [1999]* found a correlation between vegetation density (expressed as leaf area index) and the amount of trapped particles for a single species. However, not only the density matters, also the shape and flexibility of the plant affect the amount of sedimentation as the comparison between RV and SV, which have the same density, shows in correspondence to *Hendriks et al. [2008]* and *Bouma et al. [2009]*.

The sedimentation and erosion rates found in this study are modest, which is good for the survival of the plants [*Cabaço & Santos, 2007*] and therefore a good sign of the performance of the model: if the model would have predicted excessive erosion or sedimentation, the plants would not survive –whereas they do in reality. Moreover, the simulated sedimentation rates in the meadow have the same order of magnitude as those measured by *Gacia et al. [1999]*; 5-36  $\text{gm}^{-2}\text{d}^{-1}$ .

The magnitude and location of sedimentation can differ considerably under more dynamic conditions: Sedimentation is a function of sediment availability and opportunities for deposition; waves considerably increase the pick-up and therefore availability of sediment over a bare bed, but the interaction between waves, vegetation and sediment is not quantified yet. An exact comparison to values of flow velocity reduction or sedimentation rates found by others is difficult, as the circumstances (wave regime, tidal range, sediment composition, meadow characteristics) or the time scale of their measurements substantially differ.

#### 6.4.2 Effects of vegetation on light availability

Because the two most important parameters affecting light availability –water depth and the concentration of fine suspended material- differed little among the scenarios, the light availability at the bed differed only slightly too (Fig. 6.8). In the studied area, known for its clear water, the

effect of the water depth on the light attenuation is stronger than that of the sediment concentration. Nevertheless, the 3-7% variation between the scenarios can be crucial for the condition of the plants, notably in harsh environments. For shallower meadows, with more turbid water, the feedback between plant presence and sediment concentration or light availability is likely stronger. A relation between the water depth/vegetation height-ratio and the strength of the feedback is hard to derive, as this also depends on the plant- and sediment properties

Despite light availability often being the paramount factor determining the depth distribution of seagrasses [Duarte, 1991; Short & Wylie-Echeverria, 1996; Greve & Krause-Jensen, 2005; van der Heide et al., 2009], different parameterizations of a threshold for light availability exist: A minimum duration for irradiance-saturated photosynthesis [e.g. Dennison & Alberte, 1985; Zimmerman et al., 1991] which requires the measurement of photosynthetic quantum fluxes and tissue respiration, or -simpler- a percentage of the surface irradiance [Ochieng et al. 2009, overview in Lee et al., 2007], which varies with latitude. Simple approaches are useful in for instance habitat suitability studies where long timescales are implied, but for studies of the importance of events such as storms or nearby engineering works, shorter timescales are needed. The model structure has no problem with such timescales, due to the fast hydrodynamic processes it was developed for, but scaling the short-term photosynthetic needs of individual plants to the long-term development of meadows remains a challenge [Sand-Jensen et al., 2007].

We realise that our light attenuation model could be more refined. Nevertheless, the model incorporates the most important processes and more detail is not required for the purpose of comparing the effects of different vegetation types on the light climate. Besides, the contour of the actual meadow and the contour of the simulated minimum light availability (Fig. 6.8) of 11-29% of surface irradiance in the review of Lee et al. [2007] correspond very well. As *Z. marina* can tolerate currents up to 12-150  $\text{cm s}^{-1}$  [Fonseca et al., 1983], the flow velocity is not a limiting factor for seagrass occurrence in deeper parts of the bay (Fig. 6.1). Nutrients are unlikely to be a limiting factor; hence the light availability must be the limiting factor, thus seems properly calculated.

### 6.4.3 Possible applications

The study in this chapter is performed using the model of the eelgrass meadow in Baie de l'Écluse developed in the previous chapter, but the principles are applicable to areas all over the world. To our knowledge, this is the first model that simulates the vertical flow structure, sediment transport and the associated light climate in the presence of flexible vegetation on a landscape scale.

The model can be used to study long-term landscape formation in the presence of flexible vegetation, similar to the studies of e.g., D'Alpaos et al. [2006], Temmerman et al. [2007] and Vandenbruwaene et al. [2011] for stiff vegetation. Moreover, because the model can be straightforwardly combined with the DelWAQ water quality model, it could be used for environmental impact assessments where macrophytes are involved [Erftemeijer & Robin Lewis III, 2006] and process-based spatially explicit studies of stable states in rivers, lakes and estuaries [van Nes et al., 2003; van der Heide et al., 2007; Carr et al., 2010]. The model might help to clarify why eelgrass disappeared from the Dutch Wadden Sea in the 1930's and has struggled to return so far, or facilitate calculations of minimum meadow sizes and densities in case of restoration efforts [van Katwijk et al., 2009].

The applicability of this and similar models would benefit from studies that *i)* quantify the interaction between waves and flexible vegetation, *ii)* adapt existing sediment transport formula to the presence of vegetation and *iii)* quantify the development of plants in relation to physical parameters. The latter has been subject of numerous studies, but mainly on fairly large spatial or temporal scales; detailed models like these offer the possibility to study smaller scales with more temporal detail.

## **6.5 Conclusions**

The effects of a macrophyte meadow on flow, sediment transport and the amount of light available for photosynthesis depend on the properties of the plants. As a consequence of the large depth in the study area in comparison to the canopy height, the influence on the depth averaged flow velocity pattern and magnitude is nil. The velocity near the bed is considerably lowered by the plants however, as are the bed shear stress and the sediment transport. As a result, the light availability over a tidal cycle can increase up to 7% in comparison to a bare bed. The effect of a relatively open meadow of flexible vegetation is less strong than that of a dense meadow of the same vegetation or a meadow of stiff vegetation of equal density. In this particular situation, the relatively open meadow allows for the largest net transport of sand into the bay: this meadow blocks less sediment outside the bay than the other meadow types, whereas more is fixated inside than in the situation without vegetation. The effects are likely more pronounced in shallower areas where plants occupy a larger part of the water column.

The agreement between model results and field observations gives confidence in the applicability of this model. Due to its generic nature, the model can also be applied to other areas, to study for example biogeomorphological process such as landscape formation or as a tool in water quality and environmental impact assessment studies.

## 7 Synthesis



Aquatic vegetation has an important role in estuaries and rivers by acting as bed stabilizer, filter, food source and nursing area. Unfortunately, macrophyte populations worldwide are threatened by anthropogenic pressure and climate change. Protection and restoration efforts often have limited success. Likely, these will benefit from more insight into the biophysical feedbacks between vegetation condition and development, currents, waves and sediment transport. Such insights can come from experimental research in laboratory flumes or in the field, but physical experiments are practically limited by flume dimensions or unknown processes in the field. Therefore, a widely applicable computational model that simulates these biophysical interactions would be of great benefit to practical management-related studies as well as scientific studies regarding the effects of plant- and environmental properties on these feedbacks. Because most aquatic plants are flexible, the modelling of plant bending in flow is crucial. This final chapter integrates the most important findings related to model development and plant-flow interactions, and provides recommendations for further advancement.

## **7.1 Model development**

The primary aim of this thesis was to develop a generically applicable numerical model for the interaction of flexible aquatic plants and their physical environment. Starting at the scale of a single plant, the validity of the model has been successfully extended to the scale of an estuary.

### **7.1.1 Small-scale modelling: individual plants**

'Dynveg', a numerical model for the dynamic interaction between very flexible vegetation and flow was created by combining a novel plant bending model based on a Lagrangian force balance with an existing 1DV  $k-\epsilon$  turbulence model suitable to low Reynolds-number flows.

Very flexible plants can assume a position almost parallel to the flow direction. Therefore, it is necessary to incorporate friction too, rather than just the drag perpendicular to a leaf. Measurements on strips of eelgrass-like proportions provided the actual values for drag- and friction coefficients, and showed that the cross-flow principle of *Hoerner [1965]* can be applied.

The effect of multiple plants on hydrodynamics is incorporated by assuming that all plants in a meadow do the same, and by defining two turbulence length scales: One for internally generated turbulence, related to the wakes behind individual stems, and one for larger eddies created in the shear layer above, penetrating the canopy depending on the space between the stems.

This model was validated using observations of positions of various types of flexible plastic strips and of the forces they are subjected to along a range of flow velocities, as well as using hydrodynamic measurements. The model simulates the forces on plants, the flow velocity profile and the turbulence characteristics well. Theoretically, Dynveg has the ability to simulate the interaction between waves and plants too, but this has not been tested.

Dynveg is based on biomechanical properties of plants like length, width, thickness, but also on the volumetric density and the elasticity modulus. This is a great advantage because these properties are measurable and in that sense contribute to Dynveg's generic applicability. The disadvantage however, is that measuring these properties correctly is not straightforward, whereas the model is sensitive to just these parameters.

Simulations that incorporate flexible vegetation give far more realistic flow patterns than those based on rigid vegetation or an adjusted bed roughness coefficient, but are computationally intensive.

### **7.1.2 Two-dimensional modelling: plants in laboratory flumes**

In order to model spatial processes in and around meadows of flexible vegetations, the detailed Dynveg model was combined with the large-scale hydrodynamic model Delft3D and compared to flume experiments.

The leading principle for this integration is the conditional similarity between flow characteristics in flexible vegetation and those in stiff vegetation: If the stiff vegetation has *i)* the same height as the deflected vegetation, *ii)* its plant volume redistributed over the vertical accordingly and *iii)* a drag coefficient that is representative of the streamlined shape, the flow is practically analogous for a range of plant properties and hydrodynamic conditions (Chapter 3).

Dynveg can be used to create a 'look-up' table for these representative plant properties along a range of expected depths and flow velocities. This table serves as input for the rigid vegetation module of Delft3D. In an iterative procedure, Delft3D searches the table for representative plant properties given the water depth and the velocity inside the canopy, calculates a corresponding flow pattern and searches the table again. Spatial and temporal averaging is required for a stable solution.

This modelling approach was validated by comparing model results with flume experiments on two seagrass species, showing good agreement for canopy height, flow velocity profile and flow adaptation length.

The good performance of the two-dimensional model shows that the principle of modelling flow through flexible vegetation by representing it as stiff vegetation with representative properties that change depending on flow conditions, works in stationary or slowly varying flow. The model cannot be used for rapidly varying flow, e.g. a monami, as the model does not resolve flow structures.

### **7.1.3 Three-dimensional modelling: a natural meadow**

To enable application to natural meadows, the two-dimensional plant-flow model was extended to three dimensions, following the same principles. A field measurement campaign in a macrotidal bay bordered by an eelgrass meadow provided validation data: Time-series of flow velocity and sediment dynamics inside this meadow and over a bare adjacent area.

The three-dimensional numerical model was able to reproduce the main features of the observations, indicating that the processes of vegetation bending in non-stationary flow and sediment transport through vegetated areas are incorporated correctly.

The existing sediment transport formula used [*van Rijn, 1993*] deals with vegetation effects on sediment pick-up and transport via the effects of plants on hydrodynamics, i.e. flow velocity, bed shear stress and diffusivity. Physical filtering by blades and flow intensification directly around shoots are not taken into account.

The three-dimensional model can be applied to water quality studies and environmental impact assessments involving macrophytes, as well as to studies regarding long-term biogeomorphological feedbacks.

## **7.2 Bio-physical feedbacks**

The second objective of this thesis was to use the developed models as a tool to learn more about biophysical interactions in different situations.

### **7.2.1 Individual plants and small meadows**

The developed two-dimensional model was used to assess the ecosystem engineering capacities of three plant species that have a partially overlapping distribution in temperate intertidal areas: the stiff *Spartina anglica*, the short flexible seagrass *Zostera noltii* and the tall flexible seagrass *Zostera marina*. The flow velocity inside the canopy, the canopy flux and the bed shear stress are used as proxies for the species' ability to absorb hydrodynamic energy, to ensure the supply of nutrients or sediment and to prevent erosion, respectively.

Stiff plants have a higher canopy flux than flexible plants, hence a higher potential to trap sediment. This canopy flux is inversely related to spatial density along the entire natural range. For flexible plants, the canopy flux is only related to density in relatively sparse meadows; in denser meadows the canopy flux remains constant with increasing density.

Flexible plants are more efficient in reducing bed shear stresses than stiff plants, hence better at preventing erosion. The small *Zostera noltii* is a more effective reducer of bed shear stress than the taller *Zostera marina*, which is better at maintaining a sufficient canopy flux.

For very thin plants, buoyancy is the most important determinant of position in given flow conditions. For intermediately flexible plants, the structural rigidity is the most influential parameter, whereas for (nearly) stiff plants, the spatial density is dominant. The flow velocity has more effect on the plant position than the depth, except for conditions in which the depths is close to the canopy height.

The dependence of ecosystem engineering capacities on conditions is more distinct in shallow water and at low flow velocities, and depends more on depth than on velocity. For stiff plants, erosion and breaking of plants are more likely to occur in shallow water due to the higher bed shear stress and forces on plants, whereas deposition is more likely to occur in deep water as a result of a lower canopy flow velocity. For flexible plants, the water depth does not affect erosion because the bed shear stress is so strongly reduced that it does not change with depth; the stress acts on the plants rather than the bed.

A species' eco-engineering capacity depends on the plants spatial density, its size, its structural rigidity and its buoyancy, but also on environmental conditions. Therefore, biomass, leaf area index or other lumped parameters that neglect structural properties cannot be good generic indicators of ecosystem engineering capacities. However, they may work fine within well-defined conditions.

The length of the leading edge zone, i.e. the length required for adaptation of the flow velocity profile is usually less than two metres, or 1-7 times the water depth. This is smaller than

the universally accepted adaptation length of 10-20 water depths over a bare bed. This length is related to flow as well as plant properties, but this relationship could not be quantified.

### 7.2.2 Large meadows and their surroundings

The developed three-dimensional model was used to study the effects of different types of macrophytes on (residual) sediment transport and light availability under the same conditions. The effects of the real, relatively sparse eelgrass meadow were compared to that of a meadow with the same spatial density of stiff plants, a dense eelgrass meadow and a bare bed.

In deep water, sparse flexible vegetation can be more efficient in trapping sediment inside a bay than denser or stiff vegetation: When vegetation only occupies a small part of the water column, plants mainly prevent erosion rather than increase deposition and they have more effect on bed-load transport than on the transport of suspended sediment. Stiff and denser plants affect the bed-load more than sparse flexible vegetation, in this case blocking the sediment transport into the bay, which leads to sedimentation on the outside instead of the inside.

The presence of dense or stiff macrophytes increased the light availability at the bed averaged over a tidal cycle up to 7% with respect to a bare bed. The increase of light availability was less pronounced for the relatively open eelgrass meadow: up to 3%.

Though the differences in sediment transport and light availability between the four vegetation scenarios seem small –only a few percent- the consequences on long timescales can be considerable.

The effects of a macrophyte meadow on near-bed flow, sediment transport and the amount of light available for photosynthesis depend on the properties of the plants and on the sediment properties. The influence of vegetation is in all probability more pronounced in shallower areas where plants occupy a larger part of the water column.

## 7.3 Recommendations

### 7.3.1 Model development and application

To increase the applicability of both Dynveg and the large-scale model, several improvements regarding modelling are recommended:

1. Incorporate wave attenuation by flexible vegetation: Wave attenuation is not only relevant for safety purposes, but also for sediment transport and the corresponding turbidity, hence for the development of the plants. Some formulations for wave damping by stiff vegetation are available [e.g., Kobayashi *et al.*, 1993; Suzuki, 2011], but the dynamics of the plants are a strong determinant of energy loss [Verduin & Backhaus, 2000]. Moreover, waves can induce currents that provide an important flux through the canopy [Luhar *et al.*, 2010].
2. Incorporate more complicated plant morphologies: Most seagrasses have a simple shape, but most macro-algae (e.g., kelp) and freshwater macrophytes have more intricate shapes with branches, stipes, leaves or air bladders that all affect the flow pattern, plant position and forces on the plant.

3. Increase the user-friendliness of the large-scale model: While to some extent it might be instructive that a complicated model forces the user to think about the assumptions behind the model and to be careful with parameterisations, a model always needs to be transparent to allow the verification of results and be simple to use in order to be accepted by many.
4. Improve the numerical stability of vegetation position in the large-scale model: Some combinations of flow- and plant properties caused numerical instabilities in the canopy height, leading to unrealistic fluctuations. Likely, specific attention to the implementation of a more advanced numerical scheme could solve this.
5. Develop sediment transport formulations that explicitly account for the presence of vegetation: Whereas the currently applied formulation does account for the most important effects of the presence of vegetation via the hydrodynamics, two processes are missing: filtering or particle trapping by blades [cf. Hendriks *et al.*, 2008, 2010] and locally increased bed shear stress in the flow acceleration zone close to the stems. The incorporation of these processes seems feasible, but performing the experiments required for validation is probably more challenging.

Regarding the use of this model, it is stressed that applying an advanced model is not always necessary and strongly depends on the purpose of the study; sometimes the challenge of finding appropriate parameterisations is just relocated instead of solved because incorporating more processes also requires more input.

### 7.3.2 Ecological aspects

Models that describe bio-physical feedbacks become more common and more powerful tools to provide answers to questions related to the management of ecologically valuable areas as well as to the clarification of bio-physical interactions. To fully exploit these benefits, it is recommended to:

6. Study plant development processes on a spatial and temporal scale that matches hydrodynamic models: With these models, it is possible to simulate both short-term (i.e., one tidal period) and long-term (i.e., several years) developments. This requires quantitative insights however, in how plants develop and respond to environmental changes over these timescales: What is the maximum force, bed shear stress or erosion rate plants tolerate? How long can a plant survive in limited light conditions, high concentrations of toxic substances or on a desiccated tidal flat? How do biomechanical properties change over time, depending on ambient conditions?
7. Pay more attention to the measurement of biomechanical properties: Without good registration of plant- and meadow properties such as spatial density, buoyancy, elasticity modulus and dimensions, a reproduction of field results or a study on the effect of the same species in other non-tested conditions with a model that does not include these properties, is impossible.
8. Use models like the one in this thesis to study eco-engineering capacities: Whereas experiments in the field and in the laboratory usually offer information for a limited range of conditions, process-based models can be applied along larger ranges of plant properties or environmental conditions.



## References

- Abdelrhman, M. A. (2003), Effect of eelgrass *Zostera marina* canopies on flow and transport, Marine Ecology Progress Series, 248, 67-38.
- Abdelrhman, M. A. (2007) Modeling coupling between eelgrass *Zostera marina* and water flow. Marine Ecology Progress Series 338:81-96
- Ackerman, J. D., and A. Okubo (1993), Reduced mixing in a marine macrophyte canopy, Functional Ecology, 7, 305-309.
- Ackerman, J. D. (1997), Submarine pollination in the marine angiosperm *Zostera marina* (Zosteraceae). I. The influence of floral morphology on fluid flow, American Journal of Botany, 84(8), 1099.
- Amos, C. L., A. Bergamasco, G. Umgiesser, S. Cappucci, D. Cloutier, L. DeNat, M. Flindt, M. Bonardi, and S. Cristante (2004), The stability of tidal flats in Venice Lagoon--the results of in-situ measurements using two benthic, annular flumes, Journal of Marine Systems, 51(1-4), 211-241.
- Backhaus, J. O., and J. J. Verduin (2008), Simulating the interaction of seagrasses with their ambient flow, Estuarine, Coastal and Shelf Science, 80(4), 563-572.
- Baker, E. T., and J. W. Lavelle (1984), The Effect of Particle Size on the Light Attenuation Coefficient of Natural Suspensions, J. Geophys. Res., 89(C5), 8197-8203.
- Baptist, M. J. (2005) Modelling floodplain biogeomorphology. Ph.D. thesis, Delft University of Technology
- Baptist, M. J., V. Babovic, J. R. Uthurburu, M. Keijzer, R. E. Uittenbogaard, A. Mynett, and A. Verwey (2007), On inducing equations for vegetation resistance, Journal of Hydraulic Research, 45(4), 435-450.
- Barbier, E. B., E. W. Koch, B. R. Silliman, S. D. Hacker, E. Wolanski, J. Primavera, E. F. Granek, S. Polasky, S. Aswani, L. A. Cramer, D. M. Stoms, C. J. Kennedy, D. Bael, C. V. Kappel, G. M. E. Perillo, and D. J. Reed (2008), Coastal Ecosystem-Based Management with Nonlinear Ecological Functions and Values, Science, 319(5861), 321-323.
- Best, E. P. H., C. P. Buzzelli, S. M. Bartell, R. L. Wetzel, W. A. Boyd, R. D. Doyle, and K. R. Campbell (2001), Modeling submersed macrophyte growth in relation to underwater light climate: modeling approaches and application potential, Hydrobiologia, 444(1-3), 43-70.
- Bocci, M., G. Coffaro, and G. Bendoricchio (1997), Modelling biomass and nutrient dynamics in eelgrass (*Zostera marina* L.): applications to the Lagoon of Venice (Italy) and Oresund (Denmark), Ecological Modelling, 102(1), 67-80.
- Boller, M. L., and E. Carrington (2007), Interspecific comparison of hydrodynamic performance and structural properties among intertidal macroalgae, The Journal of Experimental Biology, 210, 1874-1884.
- Borsje, B. W., M. B. de Vries, S. J. M. H. Hulscher, and G. J. de Boer (2008), Modeling large-scale cohesive sediment transport affected by small-scale biological activity, Estuarine, Coastal and Shelf Science, 78(3), 468-480.
- Bos, A. R., T. J. Bouma, G. L. J. de Kort, and M. M. van Katwijk (2007), Ecosystem engineering by annual intertidal seagrass beds: Sediment accretion and modification, Estuarine, Coastal and Shelf Science, 74(1-2), 344-348.
- Bouma, T. J., M. B. De Vries, E. Low, G. Peralta, I. C. Tanczos, J. Van de Koppel, and P. M. J. Herman (2005), Trade-offs related to ecosystem-engineering: a case study on stiffness of emerging macrophytes, Ecology, 86(6), 2187-2199.
- Bouma, T. J., M. Friedrichs, P. Klaassen, B. K. van Wesenbeeck, F. G. Brun, S. Temmerman, M. M. van Katwijk, G. Graf, and P. M. J. Herman (2009), Effects of shoot stiffness, shoot size and

- current velocity on scouring sediment from around seedlings and propagules, *Marine Ecology-Progress Series*, 388, 293-297.
- Brugem, W. P., B. J. Boersma, and R. E. Uittenbogaard (2006), The influence of wall permeability on turbulent channel flow, *Journal of Fluid Mechanics*, 562, 35-72.
- Brun, F. G., I. Hernández, J. J. Vergara, P. G., and J. L. Pérez-Lloréns (2002), Assessing the toxicity of ammonium pulses in the survival and growth of *Zostera noltii* Hornem., *Marine Ecology Progress Series*, 225, 177-187.
- Cabaço, S., and R. Santos (2007), Effects of burial and erosion on the seagrass *Zostera noltii*, *Journal of Experimental Marine Biology and Ecology*, 340(2), 204-212.
- Carollo, F. G., V. Ferro, and D. Termini (2005), Flow Resistance Law in Channels with Flexible Submerged Vegetation, *Journal of Hydraulic Engineering*, 131(7), 554-564.
- Carr, J., P. D'Odorico, K. McGlathery, and P. Wiberg (2010), Stability and bistability of seagrass ecosystems in shallow coastal lagoons: Role of feedbacks with sediment resuspension and light attenuation, *Journal of Geophysical Research*, 115, G03011.
- Chen, S. N., L. P. Sanford, E. W. Koch, F. Shi, and E. W. North (2007), A nearshore model to investigate the effects of seagrass bed geometry on wave attenuation and suspended sediment transport, *Estuaries and Coasts*, 30(2), 296-310.
- Christiansen, C., H. Christoffersen, J. Dalsgaard, and P. Nørnberg (1981), Coastal and near-shore changes correlated with die-back in eel-grass (*Zostera marina*, L.), *Sedimentary Geology*, 28(3), 163-173.
- Colijn, F. (1982), Light absorption in the waters of the Ems-Dollard estuary and its consequences for the growth of phytoplankton and microphytobenthos, *Netherlands Journal of Sea Research*, 15(2), 196-216.
- Cornelisen, C. D., and F. I. M. Thomas (2006), Water flow enhances ammonium and nitrate uptake in a seagrass community, *Marine Ecology Progress Series*, 312, 1-13.
- Costanza, R., R. d'Arge, R. de Groot, S. Farber, M. Grasso, B. Hannon, K. Limburg, S. Naeem, R. V. O'Neill, J. Paruelo, R. G. Raskin, P. Sutton, and M. van den Belt (1997), The value of the world's ecosystem services and natural capital, *Nature*, 387(6630), 253-260.
- D'Alpaos, A., S. Lanzoni, S. M. Mudd, and S. Fagherazzi (2006), Modeling the influence of hydroperiod and vegetation on the cross-sectional formation of tidal channels, *Estuarine, Coastal and Shelf Science*, 69(3-4), 311-324.
- de Boer, W. (2007), Seagrass-sediment interactions, positive feedbacks and critical thresholds for occurrence: a review, *Hydrobiologia*, 591(1), 5-24.
- Den Hartog, C., and P. J. G. Polderman (1975), Changes in the seagrass populations of the Dutch Wadden Sea, *Aquatic Botany*, 1, 141-147.
- Dennison, W. C., and R. S. Alberte (1985), Role of daily light period in the depth distribution of *Zostera marina* (eelgrass), *Marine Ecology Progress Series*, 25, 51-61.
- de Vriend, H. J., M. Capobianco, T. Chesher, H. E. de Swart, B. Latteux, and M. J. F. Stive (1993), Approaches to long-term modelling of coastal morphology: a review, *Journal of Coastal Engineering*, 23, 225-269.
- Dijkstra, J. T., and R. E. Uittenbogaard (2010), Modeling the interaction between flow and highly flexible aquatic vegetation, *Water Resour. Res.*, 46(12), W12547.
- Duarte, C. M. (1991), Seagrass depth limits, *Aquatic Botany*, 40(4), 363-377.
- Duarte, C. M., J. Terrados, N. S. R. Agawin, M. D. Fortes, S. Bach, and W. J. Kenworthy (1997), Response of a mixed Philippine seagrass meadow to experimental burial, *Marine Ecology Progress Series*, 147, 285-294.
- Erftemeijer, P. L. A., and R. R. Robin Lewis III (2006), Environmental impacts of dredging on seagrasses: A review, *Marine Pollution Bulletin*, 9(6).

- Erftemeijer, P. L. A., J. K. L. van Beek, C. A. Ochieng, Z. Jager, and H. J. Los (2008), Eelgrass seed dispersal via floating generative shoots in the Dutch Wadden Sea: a model approach, *Marine Ecology-Progress Series*, 358, 115-124.
- Finnigan, J. (2000), Turbulence in Plant Canopies, *Annual Review of Fluid Mechanics*, 32(1), 519-571.
- Folkard, A. M. (2005), Hydrodynamics of model *Posidonia oceanica* patches in shallow water, *Limnology and oceanography*, 50(5), 1592-1600.
- Fonseca, M. S., and J. A. Cahalan (1992), A preliminary evaluation of wave attenuation by four species of seagrass, *Estuarine, Coastal and Shelf Science*, 35, 565-576.
- Fonseca, M. S., and J. S. Fisher (1986), A comparison of canopy friction and sediment movement between four species of seagrass with reference to their ecology and restoration, *Marine Ecology Progress Series*, 29, 15-22.
- Fonseca, M. S., J. S. Fisher, J. C. Zieman, and G. W. Thayer (1982), Influence of the seagrass, *Zostera marina* L., on current flow, *Estuarine, Coastal and Shelf Science*, 15, 351-364.
- Fonseca, M. S., and M. A. R. Koehl (2006), Flow in seagrass canopies: The influence of patch width, *Estuarine, Coastal and Shelf Science*, 67(1-2), 1-9.
- Fonseca, M. S., M. A. R. Koehl, and B. S. Kopp (2007), Biomechanical factors contributing to self-organization in seagrass landscapes, *Journal of Experimental Marine Biology and Ecology*, 340(2), 227-246.
- Fonseca, M. S., P. E. Whitfield, N. M. Kelly, and S. S. Bell (2002), Modeling seagrass landscape pattern and associated ecological attributes, *Ecological Applications*, 12(1), 218-237.
- Fonseca, M. S., J. C. Zieman, G. W. Thayer, and J. S. Fisher (1983), The role of current velocity in structuring eelgrass (*Zostera marina* L.) meadows, *Estuarine, Coastal and Shelf Science*, 17(4), 367-380.
- Gacia, E., and C. M. Duarte (2001), Sediment Retention by a Mediterranean *Posidonia oceanica* Meadow: The Balance between Deposition and Resuspension, *Estuarine, Coastal and Shelf Science*, 52, 505-514.
- Gacia, E., T. C. Granata, and C. M. Duarte (1999), An approach to measurement of particle flux and sediment retention within seagrass (*Posidonia oceanica*) meadows, *Aquatic Botany*, 65(1-4), 255-268.
- Gambi, M. C., A. R. M. Nowell, and P. A. Jumars (1990), Flume observations on flow dynamics in *Zostera marina* (eelgrass) beds, *Marine Ecology Progress Series*, 61, 159-169.
- Garcia, C. M., M. I. Cantero, Y. Nino, and M. H. Garcia (2005), Turbulence measurements with acoustic Doppler velocimeters, *Journal of Hydraulic Engineering-Asce*, 131(12), 1062-1073.
- Gaylord, B., and M. Denny (1997), Flow and flexibility. I. Effects Of size, shape and stiffness in determining wave forces on the stipitate kelps *Eisenia arborea* and *Pterygophora californica*, *Journal of Experimental Biology*, 200(24), 3141-3164.
- Gere, J. M., and S. P. Timoshenko (1999), *Mechanics of materials*, Stanley Thornton, Cheltenham.
- Ghisalberti, M., and H. M. Nepf (2002), Mixing layers and coherent structures in vegetated aquatic flows, *Journal of Geophysical Research*, 107, 3/1-3/11.
- Ghisalberti, M., and H. M. Nepf (2004), The limited growth of vegetated shear layers, *Water Resources Research*, 40.
- Giesen, W. B. J. T., M. M. van Katwijk, and C. Den Hartog (1990), Temperature, salinity, insolation and wasting disease of eelgrass (*Zostera marina* L.) in the Dutch Wadden Sea in the 1930's, *Netherlands Journal of Sea Research*, 25(3), 395-404.
- Godet, L., J. Fournier, M. M. van Katwijk, F. Olivier, P. Le Mao, and C. Retiere (2008), Before and after wasting disease in common eelgrass *Zostera marina* along the French Atlantic coasts: a general overview and first accurate mapping, *Diseases of Aquatic Organisms*, 79(3), 249-255.

- Goldberg, U., and D. Apsley (1997), A wall-distance-free low Re  $k - \epsilon$  turbulence model, *Computer Methods in Applied Mechanics and Engineering*, 145(3-4), 227-238.
- Green, E. P., and F. T. Short (Eds.) (2003), *World atlas of seagrasses*, 298 pp., California University Press, Berkeley.
- Greve, T. M., and D. Krause-Jensen (2005), Predictive modelling of eelgrass (*Zostera marina*) depth limits, *Marine Biology*, 146(5), 849-858.
- Grizzle, R. E., F. T. Short, C. R. Newell, H. Hoven, and L. Kindblom (1996), Hydrodynamically induced synchronous waving of seagrasses: 'monami' and its possible effects on larval mussel settlement, *Journal of Experimental Marine Biology and Ecology*, 206(1-2), 165-177.
- Gruber, R. K., and W. M. Kemp (2010), Feedback effects in a coastal canopy-forming submersed plant bed, *Limnology and oceanography*, 55(6), 2285-2298.
- Hemminga, M. A., and C. M. Duarte (2000), *Seagrass Ecology*, Cambridge University Press.
- Hendriks, I., T. Bouma, E. Morris, and C. Duarte (2010), Effects of seagrasses and algae of the *Caulerpa* family on hydrodynamics and particle-trapping rates, *Marine Biology*, 157(3), 473-481.
- Hendriks, I. E., T. Sintes, T. J. Bouma, and C. M. Duarte (2008), Experimental assessment and modeling evaluation of seagrass (*P. oceanica*) on flow and particle trapping, *Marine Ecology Progress Series*.
- Hoerner, S. F. (1965), *Fluid-dynamic drag*, Hoerner Fluid Dynamics, Vancouver.
- Holbrook, N. M., M. W. Denny, and M. A. R. Koehl (1991), Intertidal "trees": consequences of aggregation on the mechanical and photosynthetic properties of sea palms *Postelsia palmaeformis* Ruprecht. , *Experimental Marine Biology and Ecology*, 146, 39-67.
- Houwing, E. J. (1999), Determination of the Critical Erosion Threshold of Cohesive Sediments on Intertidal Mudflats Along the Dutch Wadden Sea Coast, *Estuarine, Coastal and Shelf Science*, 49(4), 545-555.
- Hughes, A. R., S. L. Williams, C. M. Duarte, K. L. Heck, and M. Waycott (2009), Associations of concern: declining seagrasses and threatened dependent species, *Frontiers in Ecology and the Environment*, 7(5), 242-246.
- Ikeda, S., T. Yamada, and Y. Toda (2001), Numerical study on turbulent flow and honami in and above flexible plant canopy, *International Journal of Heat and Fluid Flow*, 22, 252-258.
- Järvelä, J. (2002), Flow resistance of flexible and stiff vegetation: a flume study with natural plants, *Journal of Hydrology*, 269(1-2), 44-54.
- Järvelä, J. (2005), Effect of submerged flexible vegetation on flow structure and resistance, *Journal of Hydrology*, 307(1-4), 233-241.
- Jones, C. G., J. H. Lawton, and M. Shachak (1994), Organisms as ecosystem engineers, *Oikos*, 69, 373-386.
- Klaassen, G. J., and J. J. van Zwaard (1974), Roughness Coefficient of Vegetated Flood Plains, *Journal of the Hydraulics Division*, 12.
- Kobayashi, N., A. W. Raichle, and T. Asano (1993), Wave attenuation by vegetation, *Journal of Waterway, Port, Coastal, and Ocean Engineering*, 119(1), 30-48.
- Koch, E. W. (1994), Hydrodynamics, diffusion-boundary layers and photosynthesis of the seagrasses *Thalassia testudinum* and *Cymodocea nodosa*, *Marine Biology (Historical Archive)*, 118(4), 767-776.
- Koch, E. W. (1999), Sediment resuspension in a shallow *Thalassia testudinum banks ex König* bed, *Aquatic Botany*, 65(1-4), 269-280.
- Koch, E.W. (2001), Beyond light: Physical, geological, and geochemical parameters as possible submersed aquatic vegetation habitat requirements, *Estuaries and Coasts*, 24(1), 1-17.

- Koch, E. W., and G. Gust (1999), Water flow in tide- and wave dominated beds of the seagrass *Thalassia testudinum*, Marine Ecology Progress Series, 184, 63-72.
- Koch, E. W., and S. Beer (1996), Tides, light and the distribution of *Zostera marina* in Long Island Sound, USA, Aquatic Botany, 53(1-2), 97-107.
- Koehl, M. A. R., and R. S. Alberte (1988), Flow, flapping, and photosynthesis of *Nereocystis luetkeana*: A functional comparison of undulate and flat blade morphologies., Marine Biology, 99, 435-444.
- Kouwen, N., and R.-M. Li (1980), Biomechanics of vegetative channel linings, Journal of the Hydraulics Division, 106(6), 1085-1106.
- Kouwen, N., and T. E. Unny (1970), Flow Retardance in Vegetated Channels, Journal of Irrigation and Drainage Engineering, 95, 329-342.
- Kouwen, N., and T. E. Unny (1973), Flexible roughness in open channels, Journal of the Hydraulics Division, 99, 713-728.
- Kutija, V., and H. T. M. Hong (1996), A numerical model for assessing the additional resistance to flow introduced by flexible vegetation, Journal of Hydraulic Research, 34(1), 99-114.
- Lauder, B. E., and D. B. Spalding (1974), The numerical computation of turbulent flows, Computer Methods in Applied Mechanics and Engineering, 3, 269-289.
- Lee, K.-S., S. R. Park, and Y. K. Kim (2007), Effects of irradiance, temperature, and nutrients on growth dynamics of seagrasses: A review, Journal of Experimental Marine Biology and Ecology, 350, 144-175.
- Lefebvre, A., C. E. L. Thompson, and C. L. Amos (2010), Influence of *Zostera marina* canopies on unidirectional flow, hydraulic roughness and sediment movement, Continental Shelf Research, 30(16), 1783-1794.
- Leonard, L. A., and A. L. Croft (2006), The effect of standing biomass on flow velocity and turbulence in *Spartina alterniflora* canopies, Estuarine, Coastal and Shelf Science, 69(3-4), 325-336.
- Lesser, G. R., J. A. Roelvink, J. A. T. M. van Kester, and G. S. Stelling (2004), Development and validation of a three-dimensional morphological model, Coastal Engineering, 51(8-9), 883-915.
- Lightbody, A. F., and H. M. Nepf (2006), Prediction of velocity profiles and longitudinal dispersion in salt marsh vegetation, Limnology and oceanography, 51(1), 218-228.
- López, F., and M. García (1998), Open-channel flow trough simulated vegetation: Suspended sediment transport modeling, Water Resources Research, 34(9), 2341-2352.
- López, F., and M. H. García (2001), Mean Flow and Turbulence Structure of Open-Channel Flow Through Non-Emergent Vegetation, Journal of Coastal Engineering, 127, 392-402.
- Luhar, M., S. Coutu, E. Infantes, S. Fox, and H. Nepf (2010), Wave-induced velocities inside a model seagrass bed, J. Geophys. Res., 115(C12), C12005.
- Luhar, M., J. Rominger, and H. Nepf (2008), Interaction between flow, transport and vegetation spatial structure, Environmental Fluid Mechanics.
- Lund-Hansen, L. C. (2004), Diffuse attenuation coefficients  $K_d(\text{PAR})$  at the estuarine North Sea-Baltic Sea transition: time-series, partitioning, absorption, and scattering, Estuarine, Coastal and Shelf Science, 61(2), 251-259.
- Madsen, J. D., P. A. Chambers, W. F. James, E. W. Koch, and D. F. Westlake (2001), The interaction between water movement, sediment dynamics and submersed macrophytes, Hydrobiologia, 444(1-3), 71-84.
- Maltese, A., E. Cox, A. M. Folkard, G. Ciraolo, G. La Loggia, and G. Lombardo (2007), Laboratory measurements of flow and turbulence in discontinuous distributions of ligulate seagrass, Journal of Hydraulic Engineering, 133(7), 750-760.

- Möller, I., T. Spencer, J. R. French, D. J. Leggett, and Dixon M. (1999), Wave Transformation Over Salt Marshes: A Field and Numerical Modelling Study from North Norfolk, England, *Estuarine, Coastal and Shelf Science*, 49(3), 411-426.
- Moore, K. A. (2004), Influence of seagrasses on water quality in shallow regions of the lower Chesapeake Bay, *Journal of Coastal Research*, 62, 162-178.
- Morison, J. R., M. P. O'Brien, J. W. Johnson, and S. A. Schaaf (1950), The force exerted by surface waves on piles, *Petroleum Transactions*, 189, 149-154.
- Morris, E. P., G. Peralta, F. G. Brun, L. van Duren, T. J. Bouma, and J. L. Perez-Llorens (2008), Interaction between hydrodynamics and seagrass canopy structure: Spatially explicit effects on ammonium uptake rates, *Limnology and Oceanography*, 53(4), 1531-1539.
- Neary, V. S. (2003), Numerical Solution of Fully Developed Flow with Vegetative Resistance, *Journal of Engineering Mechanics*, 129(5), 558-563.
- Nepf, H. M. (1999), Drag, turbulence, and diffusion in flow through emergent vegetation, *Water Resources Research*, 35(2), 479-489.
- Nepf, H. M., and E. W. Koch (1999), Vertical secondary flows in submerged plant-like arrays, *Limnology and oceanography*, 44(4), 1072-1080.
- Nepf, H. M., and E. R. Vivoni (2000), Flow structure in depth-limited, vegetated flow, *Journal of Geophysical Research*, 105(C12), 28,547-528,557.
- Neumeier, U., and P. Ciavola (2004), Flow resistance and associated sedimentary processes in a *Spartina maritima* salt-marsh, *Journal of Coastal Research*, 20(2), 435-447.
- Neumeier, U. (2007), Velocity and turbulence variations at the edge of saltmarshes, *Continental Shelf Research*, 27(8), 1046-1059.
- Nikora, V. I., and D. G. Goring (1998), ADV measurements of turbulence: Can we improve their interpretation?, *Journal of Hydraulic Engineering-Asce*, 124(6), 630-634.
- Nikora, V. I., and P. M. Rowinski (2008), Rough-bed flows in geophysical, environmental, and engineering systems: Double-Averaging Approach and its applications - Preface, *Acta Geophysica*, 56(3), 529-533.
- Ochieng, C. A., F. T. Short, and D. I. Walker (2009), Photosynthetic and morphological responses of eelgrass (*Zostera marina* L.) to a gradient of light conditions, *Journal of Experimental Marine Biology and Ecology*, 382(2), 117-124.
- Olesen, B., N. Marba, C. M. Duarte, R. S. Savelle, and M. D. Fortes (2004), Recolonization dynamics in a mixed seagrass meadow: The role of clonal versus sexual processes, *Estuaries*, 27(5), 770-780.
- Orth, R. J., T. J. B. Carruthers, W. C. Dennison, C. M. Duarte, J. W. Fourqurean, K. L. Heck, A. R. Hughes, G. A. Kendrick, W. J. Kenworthy, S. Olyarnik, F. T. Short, M. Waycott, and S. L. Williams (2006a), A Global Crisis for Seagrass Ecosystems, *BioScience*, 56(12), 987-996.
- Orth, R. J., M. Luckenbach, and K. A. Moore (1994), Seed dispersal in a marine macrophyte: implications for colonization and restoration, *Ecology*, 75(7), 1927-1939.
- Orth, R. J., M. L. Luckenbach, S. R. Marion, K. A. Moore, and D. J. Wilcox (2006b), Seagrass recovery in the Delmarva Coastal Bays, USA, *Aquatic Botany*, 84(1), 26-36.
- Partheniades, E. (1965), Erosion and deposition of cohesive soils, *Journal of the Hydraulic Division*, 91(HY1).
- Patterson, M. R., M. C. Harwell, L. M. Orth, and R. J. Orth (2001), Biomechanical properties of the reproductive shoots of eelgrass, *Aquatic Botany*, 69(1), 27-40.
- Pedersen, O., T. Binzer, and J. Borum (2004), Sulphide intrusion in eelgrass (*Zostera marina* L.), *Plant, Cell & Environment*, 27(5), 595-602.

- Peralta, G., L. A. van Duren, E. P. Morris, and T. J. Bouma (2008), Consequences of shoot density and stiffness for ecosystem engineering by benthic macrophytes in flow dominated areas: a hydrodynamic flume study, *Marine Ecology Progress Series*, 368, 103-115.
- Peterson, C. H., R. A. Luettich Jr, F. Micheli, and G. A. Skilleter (2004), Attenuation of water flow inside seagrass canopies of differing structure, *Marine Ecology Progress Series*, 268, 81-92.
- Peterson, C. H., H. C. Summerson, and P. B. Duncan (1984), The influence of seagrass cover on population structure and individual growth rate of a suspension-feeding bivalve, *Mercenaria mercenaria*, *Journal of Marine Research*, 42(1), 123-138.
- Pigeard, A. (1999), L'Usine marémotrice de la Rance, 45 pp, EIVL, Blois.
- Poggi, D., and G. G. Katul (2008), Micro- and macro-dispersive fluxes in canopy flows, *Acta Geophysica*, 56(3), 778-799.
- Poggi, D., G. G. Katul, and J. D. Albertson (2004), Momentum Transfer and Turbulent Kinetic Energy Budgets within a Dense Model Canopy, *Boundary-Layer Meteorology*, 111(3), 589-614.
- Raupach, M. R. (1992), Drag and drag partition on rough surfaces, *Boundary-Layer Meteorology*, 60(4), 375-395.
- Sand-Jensen, K. (2008), Drag forces on common plant species in temperate streams: consequences of morphology, velocity and biomass, *Hydrobiologia*, 610(1), 307-319.
- Sand-Jensen, K., T. Binzer, and A. L. Middelboe (2007), Scaling of photosynthetic production of aquatic macrophytes - a review, *Oikos*, 116(2), 280-294.
- Schanz, A., P. Polte, H. Asmus, and R. Asmus (2000), Currents and turbulence as a top-down regulator in intertidal seagrass communities, *Biologica Marina Mediterranea*.
- Schanz, A. A., H. (2003), Impact of hydrodynamics on development and morphology of intertidal seagrasses in the Wadden Sea, *Marine Ecology Progress Series*, 261, 123-134.
- Schutten, J., and A. J. Davy (2000), Predicting the hydraulic forces on submerged macrophytes from current velocity, biomass and morphology, *Oecologia*, 123, 445-452.
- Sfriso, A., and A. Marcomini (1997), Macrophyte production in a shallow coastal lagoon. Part I: Coupling with chemico-physical parameters and nutrient concentrations in waters, *Marine Environmental Research*, 44(4), 351-375.
- Shimizu, Y., and T. Tsujimoto (1994), Numerical analysis of turbulent open-channel flow over a vegetation layer using a *k-e* turbulence model, *Journal of Hydrosience and Hydraulic Engineering*, 11(2), 57-67.
- Short, F. T., and S. Wyllie-Echeverria (1996), Natural and human-induced disturbance of seagrasses, *Environmental Conservation*, 23(1), 17-27.
- Stephan, U., and D. Gutknecht (2002), Hydraulic resistance of submerged flexible vegetation, *Journal of Hydrology*, 269(1-2), 27-43.
- Stoesser, T., G. P. Salvador, W. Rodi, and P. Diplas (2009), Large Eddy Simulation of Turbulent Flow Through Submerged Vegetation, *Transport in Porous Media*, 78(3), 347-365.
- Sukhodolov, A., and T. Sukhodolova (2006), Evolution of mixing layers in turbulent flow over submersed vegetation: Field experiments and measurement study, paper presented at River Flow 2006, Taylor & Francis Group, London, Lisbon.
- Suzuki, T. (2011), Wave dissipation over vegetation fields, Ph.D. thesis thesis, 176 pp, Delft University of Technology, Delft.
- Suzuki, T., M. Zijlema, B. Burger, M. Meijer and S. Narayanan (2011). Wave dissipation by vegetation with layer schematization in SWAN. *Coastal Engineering*.
- Tamaki, H., M. Tokuoka, W. Nishijima, T. Terawaki, and M. Okada (2002), Deterioration of eelgrass, *Zostera marina* L., meadows by water pollution in Seto Inland Sea, Japan, *Marine Pollution Bulletin*, 44(11), 1253-1258.

- Teeter, A. M., B. H. Johnson, C. Berger, G. Stelling, N. W. Scheffner, M. H. Garcia, and T. M. Parchure (2001), Hydrodynamic and sediment transport modeling with emphasis on shallow-water, vegetated areas (lakes, reservoirs, estuaries and lagoons), *Hydrobiologia*, 444(1-3), 1-23.
- Temmerman, S., T. J. Bouma, G. Govers, Z. B. Wang, M. B. de Vries, and P. M. J. Herman (2005), Impact of vegetation on flow routing and sedimentation patterns: Three-dimensional modeling for a tidal marsh, *Journal of Geophysical Research*, 110.
- Temmerman, S., T. J. Bouma, J. Van de Koppel, D. Van der Wal, M. B. De Vries, and P. M. J. Herman (2007), Vegetation causes channel erosion in a tidal landscape, *Geology*, 35(7), 631-634.
- Terrados, J., and C. M. Duarte (2000), Experimental evidence of reduced particle resuspension within a seagrass (*Posidonia oceanica* L.) meadow, *Journal of Experimental Marine Biology and Ecology*, 243(1), 45-53.
- Uittenbogaard, R. E. (2003), Modelling turbulence in vegetated aquatic flows, paper presented at Riparian Forest Vegetated Channels Workshop, Trento (Italy).
- Uittenbogaard, R., and G. Klopman (2001), Numerical simulation of wave-current driven sediment transport, paper presented at 4th International Conference on Coastal Dynamics, Amer Soc Civil Engineers, Lund, Sweden, Jun 11-15.
- Van Duin, E. H. S., G. Blom, F. J. Los, R. Maffione, R. Zimmerman, C. F. Cerco, M. Dortch, and E. P. H. Best (2001), Modeling underwater light climate in relation to sedimentation, resuspension, water quality and autotrophic growth, *Hydrobiologia*, 444(1-3), 25-42.
- Vandenbruwaene, W., S. Temmerman, T. J. Bouma, P. C. Klaassen, M. B. de Vries, D. P. Callaghan, P. van Steeg, F. Dekker, L. A. van Duren, E. Martini, T. Balke, G. Biermans, J. Schoelynck, and P. Meire (2011), Flow interaction with dynamic vegetation patches: Implications for biogeomorphic evolution of a tidal landscape, *J. Geophys. Res.*, 116(F1), F01008.
- van der Heide, T. (2009) Stressors and feedbacks in temperate seagrass ecosystems. Ph.D. thesis, Radboud University
- van der Heide, T., E. T. H. M. Peeters, D. C. R. Hermus, M. M. van Katwijk, J. G. M. Roelofs, and A. J. P. Smolders (2009), Predicting habitat suitability in temperate seagrass ecosystems, *Limnology & Oceanography*, 54(6), 2018-2024.
- van der Heide, T., E. H. van Nes, G. W. Geerling, A. J. P. Smolders, T. J. Bouma, and M. M. van Katwijk (2007), Positive feedbacks in seagrass ecosystems: Implications for success in conservation and restoration, *Ecosystems*, 10(8), 1311-1322.
- van Katwijk, M. M., A. R. Bos, D. C. R. Hermus, and W. Suykerbuyk (2010), Sediment modification by seagrass beds: Muddification and sandification induced by plant cover and environmental conditions, *Estuarine, Coastal and Shelf Science*, 89(2), 175-181.
- van Katwijk, M. M., A. R. Bos, V. N. de Jonge, L. S. A. M. Hanssen, D. C. R. Hermus, and D. J. de Jong (2009), Guidelines for seagrass restoration: Importance of habitat selection and donor population, spreading of risks, and ecosystem engineering effects, *Marine Pollution Bulletin*, 58(2), 179-188.
- van Katwijk, M. M., and D. C. R. Hermus (2000), Effects of water dynamics on *Zostera marina*: Transplantation experiments in the intertidal Dutch Wadden Sea, *Marine Ecology-Progress Series*, 208, 107-118.
- van Nes, E. H., M. Scheffer, M. S. van den Berg, and H. Coops (2003), Charisma: a spatial explicit simulation model of submerged macrophytes, *Ecological Modelling*, 159, 103-116.
- van Rijn, L. C. (1993), Principles of sediment transport in rivers, estuaries and coastal seas, Aqua Publications, Amsterdam.
- Velasco, D., A. Bateman, and V. Medina (2008), A new integrated, hydro-mechanical model applied to flexible vegetation in riverbeds, *Journal of Hydraulic Research*, 46(5), 579-597.

- Verduin, J. J., and J. O. Backhaus (2000), Dynamics of Plant-Flow Interactions for the Seagrass *Amphibolis antarctica*: Field Observations and Model Simulations, *Estuarine, Coastal and Shelf Science*, 50(2), 185-204.
- Vermaat, J. E., N. S. R. Agawin, M. D. Fortes, J. S. Uri, C. M. Duarte, N. Marba, S. Enriquez, and W. van Vierssen (1997), The capacity of seagrasses to survive increased turbidity and siltation: The significance of growth form and light use, *Ambio*, 26(8), 499-504.
- Vermaat, J. E., L. Santamaria, and P. J. Roos (2000), Water flow across and sediment trapping in submerged macrophyte beds of contrasting growth form, *Archiv Fur Hydrobiologie*, 148(4), 549-562.
- Vermaat, J. E., and F. C. A. Verhagen (1996), Seasonal variation in the intertidal seagrass *Zostera noltii* Hornem: Coupling demographic and physiological patterns, *Aquatic Botany*, 52(4), 259-281.
- Vogel, S. (1981), *Life in moving fluids*, 352 pp., Willard Grant Press, Boston.
- Ward, L. G., W. M. Kemp, and W. R. Boynton (1984), The influence of waves and seagrass communities on suspended particles in an estuarine embayment, *Marine Geology*, 59, 85-103.
- Waycott, M., C. M. Duarte, T. J. B. Carruthers, R. J. Orth, W. C. Dennison, S. Olyarnik, A. Calladine, J. W. Fourqurean, K. L. Heck, A. R. Hughes, G. A. Kendrick, W. J. Kenworthy, F. T. Short, and S. L. Williams (2009), Accelerating loss of seagrasses across the globe threatens coastal ecosystems, *Proceedings of the National Academy of Sciences*, 106(30), 12377-12381.
- Widdows, J., and M. Brinsley (2002), Impact of biotic and abiotic processes on sediment dynamics and the consequences to the structure and functioning of the intertidal zone, *Journal of Sea Research*, 48(2), 143-156.
- Wilson, C. A. M. E., T. Stoesser, P. D. Bates, and A. B. Pinzen (2003), Open Channel Flow through Different Forms of Submerged Flexible Vegetation, *Journal of Hydraulic Engineering*, 129(11), 847-853.
- Worcester, S. E. (1995), Effects of eelgrass beds on advection and turbulent mixing in low current and low shoot density environments, *Marine Ecology Progress Series*, 126, 223-232.
- Wu, F.-C., H. W. Shen, and Y.-J. Chou (1999), Variation of Roughness Coefficients for Unsubmerged and Submerged Vegetation, *Journal of Hydraulic Engineering*, 125(9), 934-942.
- Zharova, N., A. Sfriso, A. Voinov, and B. Pavoni (2001), A simulation model for the annual fluctuation of *Zostera marina* biomass in the Venice lagoon, *Aquatic Botany*, 70(2), 135-150.
- Zimmerman, R. C., J. L. Reguzzoni, and R. S. Alberte (1995), Eelgrass (*Zostera-Marina* L) Transplants in San-Francisco Bay - Role of Light Availability on Metabolism, Growth and Survival, *Aquatic Botany*, 51(1-2), 67-86.
- Zimmerman, R. C., J. L. Reguzzoni, S. Wyllie-Echeverria, M. Josselyn, and R. S. Alberte (1991), Assessment of Environmental Suitability for Growth of *Zostera-Marina* L (Eelgrass) in San-Francisco Bay, *Aquatic Botany*, 39(3-4), 353-366.
- <http://www.wunderground.com/history/airport/LFRD/2008/5/10/WeeklyHistory.html>



## Appendix A Dynveg-Delft3D coupling verification

To study the sensitivity of the two-dimensional model for different numerical and hydraulic parameters, a number of simulations were made with a standard set of parameters. These resembled normal conditions in a long straight flume ( $h=0.4$  m,  $U=0.1$  ms<sup>-1</sup>), using a 6 m long meadow of *Zostera marina*-like vegetation. We used 30 cm tall, 5 mm wide and 0.35 mm thick plants, with a density ( $\rho_v$ ) of 950 kgm<sup>-3</sup>, elasticity ( $E$ ) of  $20 \cdot 10^6$  Nm<sup>-2</sup> and 1000 individuals per m<sup>2</sup>. Standard numerical settings were: 20 classes,  $\theta=0.5$  ( $\theta$  indicates the amount of information from the previous time step used in the current time step on a scale of 0-1; 0 means none, 1 means fully copied). The standard initial position of the vegetation was half the leaf length. The normal simulation time was two minutes; with an information exchange time step  $dt$  of 0.1 min (6 s, i.e. 20 iterations). The horizontal grid cell size was 10 cm; the vertical grid consisted of 40 layers with a thickness related to the water depth.

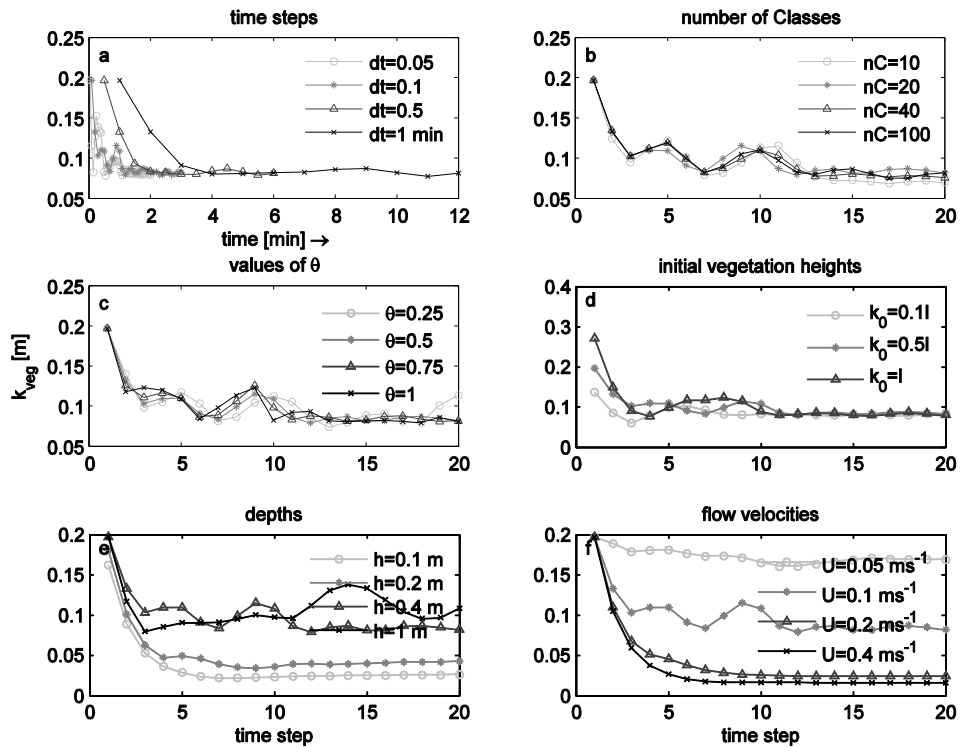


Figure A.1 Sensitivity of predicted vegetation height, for four numerical settings and two environmental conditions: The height of a plant in the middle of the meadow ( $x=9$  m) during the simulations.

The development in time in Figure A.1a shows that the time step did not influence the final result, but only how fast this result was reached. For small communication time steps ( $dt=0.05$  and  $0.1$  s), the model reached a stationary situation within 2 minutes, but this required a lot of time-consuming communication between Matlab and Delft3D. Larger time steps meant equilibrium was reached after about 4 iterations, but required more calculation time for hydrodynamics. Consequently, larger communication time steps are useful for longer calculations.

The other three numerical settings, i.e. the number of classes (Fig. A.1b), the values of  $\theta$  (Fig. A.1c) and the initial vegetation height (Fig A.1d) did not matter for the final result, nor did they determine how rapidly the simulation converged.

The graphs of the physical parameters (Fig. A.1e,f) basically show the expected: In shallower water, the vegetation bent more because there was less space for flow rerouting, i.e. more water was forced through the meadow. Similarly, when flow velocities were low, plants were more upright than at high velocities. In deeper water ( $h=1$  m) there was more room for the plants to move, which they did. This movement may also have to do with the larger thickness of the computational layers at this larger depth: If a plant moves from one layer to the other,  $U_{in}$  (and therewith  $k_{veg}$ ) changes more when the layers are thick.

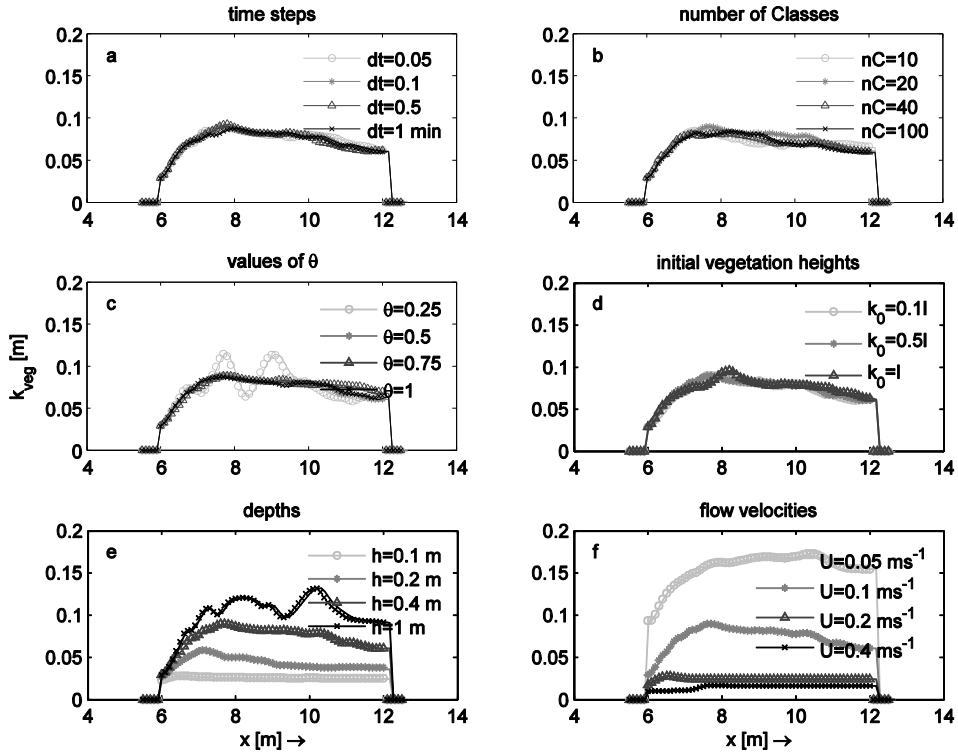


Figure A.2 Sensitivity of predicted vegetation height, for four numerical settings and two environmental conditions: The height of plants along the meadow at the final timestep (flow from left to right)

The spatial pattern at the end of the simulations (Fig. A.2) clearly showed more plant bending at the leading edge of the meadow, as well as a more or less constant height downstream. Also, the fact that all solutions were very similar for the four numerical parameters (Fig. A.2a-d), except for the not-to-be-used  $\theta=0.25$ , gives confidence.

For the physical parameters (Fig. A.2e,f) the results also seemed trustworthy, with the exception of  $h=1$  m due to reasons mentioned before. However, as the depth is larger, the exact position of the vegetation is less important because the difference in  $k_{veg}$  is only a small percentage of the water column. At high flow velocities or shallow depths, the vegetation

assumed the same position all along the meadow. This might be natural, but it could be because these conditions are on the limit of the model's capabilities.



## Appendix B Sediment transport and vegetation

In Delft3D FLOW version 3.54.23.00, the Online Morphology addition uses the TRANSPOR1993 formulations for sediment transport, based on the principles of *Van Rijn [1993]* that distinguish bed load and suspended load transports. These formulations deal with both currents and waves, but only the current-related part is discussed here.

### Suspended transport

Three-dimensional current-related transport of suspended sediment  $q_s$  ( $\text{kgm}^{-1}\text{s}^{-1}$ ) is calculated by multiplication of the velocity and concentration profiles:

$$q_s = \rho_s \int_{z_a}^h c(z)U(z)dz \quad (\text{B1})$$

Where  $z$  is the vertical coordinate,  $z_a$  the reference height (m),  $h$  the water level (m),  $\rho_s$  the density of sediment ( $\text{kgm}^{-3}$ ),  $c$  the sediment concentration per fraction ( $\text{kgm}^{-3}$ ) and  $U$  the flow velocity.

The concentration profile is obtained by solving the advection-diffusion (mass-balance) equation per fraction

$$\frac{\partial c}{\partial t} + \frac{\partial uc}{\partial x} + \frac{\partial vc}{\partial y} + \frac{\partial (w - w_s)c}{\partial z} - \frac{\partial}{\partial x} \left( \epsilon_x \frac{\partial c}{\partial x} \right) - \frac{\partial}{\partial y} \left( \epsilon_y \frac{\partial c}{\partial y} \right) - \frac{\partial}{\partial z} \left( \epsilon_z \frac{\partial c}{\partial z} \right) = 0 \quad (\text{B2})$$

Where  $u$ ,  $v$  and  $w$  are the flow velocity components ( $\text{ms}^{-1}$ ),  $w_s$  is the (hindered) sediment settling velocity ( $\text{ms}^{-1}$ ) and  $\epsilon_x$ ,  $\epsilon_y$  and  $\epsilon_z$  are the eddy diffusivity in horizontal and vertical directions ( $\text{m}^2\text{s}^{-1}$ ). The diffusivities are an addition of (1) molecular viscosity, (2) horizontal subgrid mixing calculated by a Horizontal Large Eddy Simulation (HLES) model and (3) three-dimensional turbulence calculated by a  $k$ - $\epsilon$  model for flow through vegetation [*Dijkstra & Uittenbogaard, 2010*]. Hence, vegetation affects advection and diffusion of suspended sediment via the flow velocities  $u$ ,  $v$  and  $w$  and via the diffusivities  $\epsilon_x$ ,  $\epsilon_y$  and  $\epsilon_z$  in Equation B2.

The exchange of each sediment fraction with the bed is governed by the boundary condition

$$-w_s c - \epsilon_z \frac{\partial c}{\partial z} = D - E \quad (\text{B3})$$

$D$  is the rate of deposition,  $E$  the rate of erosion. The formulations for these rates strongly differ for cohesive and non-cohesive sediment.

For cohesive sediments, these fluxes are calculated with the Partheniades-Krone formulations [*Partheniades, 1965*]:

$$\begin{aligned} E &= MS(\tau_{cw}, \tau_{cr,e}) \\ D &= w_s c_b S(\tau_{cw}, \tau_{cr,d}) \end{aligned} \quad (\text{B4})$$

Where  $M$  is a user-defined erosion parameter ( $\text{kgm}^{-2}\text{s}^{-1}$ ),  $\tau_{cw}$  the bed shear stress from currents and waves ( $\text{Nm}^{-2}$ ),  $\tau_{cr,e}$  and  $\tau_{cr,d}$  user-defined critical bed shear stress for erosion resp. deposition and  $c_b$  ( $\text{kgm}^{-3}$ ) the average sediment concentration in the computational layer closest to the bed.  $S$  is a step-function:

$$\begin{aligned}
 S(\tau_{cw}, \tau_{cr,e}) &= \left( \frac{\tau_{cw}}{\tau_{cr,e}} - 1 \right) \text{ if } \tau_{cw} > \tau_{cr,e}, \\
 &= 0 \quad \text{if } \tau_{cw} \leq \tau_{cr,e}. \\
 S(\tau_{cw}, \tau_{cr,d}) &= \left( 1 - \frac{\tau_{cw}}{\tau_{cr,d}} \right) \text{ if } \tau_{cw} < \tau_{cr,d}, \\
 &= 0 \quad \text{if } \tau_{cw} \geq \tau_{cr,d}.
 \end{aligned} \tag{B5}$$

Hence, vegetation affects the fluxes of deposition and erosion through the actual bed shear stress  $\tau_{cw}$ .

For non-cohesive sediments, the settling velocity of a sediment fraction is computed following the method of *Van Rijn [1993]*, depending on the representative diameter  $d_r$ :

$$\begin{aligned}
 w_s &= \frac{\Delta g d_r^2}{18\nu} \quad \text{for } 65 \mu\text{m} < d_r \leq 100 \mu\text{m} \\
 w_s &= \frac{10\nu}{d_r} \left[ \left( 1 + \frac{\Delta g d_r^3}{\nu^2} \right)^{0.5} - 1 \right] \text{ for } 100 \mu\text{m} < d_r \leq 1000 \mu\text{m} \\
 w_s &= 1.1(\Delta g d_r)^{0.5} \quad \text{for } 1000 \mu\text{m} < d_r \\
 \Delta &= \frac{\rho_s}{\rho_w} - 1
 \end{aligned} \tag{B6}$$

Where  $g$  is the gravitational constant,  $\nu$  the kinematic viscosity of water ( $\text{m}^2\text{s}^{-1}$ ) and  $\rho_w$  the density of water ( $\text{kgm}^{-3}$ ).

The vertical sediment mixing coefficient  $\varepsilon_s$  is directly related to the fluid mixing coefficient  $\varepsilon_z$  calculated by the  $k$ - $\varepsilon$  model:

$$\begin{aligned}
 \varepsilon_s &= \beta \varepsilon_z \\
 \beta &= 1 + 2 \left( \frac{w_s}{u_{*,c}} \right)^2
 \end{aligned} \tag{B7}$$

## Bed load transport

The bed load transport in the presence of both currents and waves  $q_b$  reads:

$$q_b = 0.006 \rho_s D_{50} w_s M^{0.5} M_e^{0.7} \quad (B8)$$

In which  $D_{50}$  is the median grain size (m),  $M$  the sediment mobility number and  $M_e$  the excess sediment mobility number, defined as

$$M = \frac{v_{eff}^2}{\Delta D_{50}} \quad (B9)$$

$$M_e = \frac{(v_{eff} - v_{cr})^2}{\Delta D_{50}}$$

wherein  $v_{cr}$  ( $\text{ms}^{-1}$ ) is a critical depth averaged velocity for the initiation of motion based on the Shields curve and  $v_{eff}$  ( $\text{ms}^{-1}$ ) an effective velocity due to currents and waves:

$$v_{eff} = \sqrt{v_R^2 + U_{on}^2} \quad (B10)$$

Here,  $v_R$  is the magnitude of an equivalent depth-averaged velocity computed from the velocity in the bottom computational layer, assuming a logarithmic velocity profile.  $U_{on}$  is the near-bed peak orbital velocity in the direction of wave propagation.

Hence, the effect of vegetation on bed load transport is modelled only indirectly through the reduction of the velocity in the bottom layer that gives a lower  $v_R$ , consequently a lower  $v_{eff}$  and lower sediment mobility.



## Dankwoord

Zo, dit is eigenlijk het leukste stukje om te schrijven: het gaat over mensen in plaats van water, planten of onderzoek. Voor sommigen zal dat vreemd klinken; die hebben afgelopen jaren zo weinig van mij gehoord dat ze haast wel moeten denken dat dit boekje toch het allerbelangrijkst is. Dat is het niet, maar soms moeten dingen gewoon af om verder te kunnen met iets anders, iets leukers.

Bij het bedanken van mensen, omdat ze iets voor je hebben gedaan, omdat je lol met ze hebt gehad, of gewoon omdat ze er zijn, is het logisch om met de belangrijkste te beginnen: Marieke. Nu zouden hier twintig kantjes kunnen volgen over waarom precies, maar ik houd het kort: Omdat je er altijd was, ook als ik ver weg in mijn coconnetje zat. Ik hoop dat je nog heel lang blijft en dat we samen lèuke dingen kunnen doen.

Ruud en Jannie, bedankt voor het opgemaakte bed, de lekkerste spaghetti en de discussies vanaf 'mijn plek tegen de schoorsteen' tijdens een week rustig schrijven in Vlissingen –en vele jaren daarvoor. Nog meer dank voor het er niet-altijd-maar-soms-wel naar vragen, en zeggen dat het helemaal niet erg is als ik het niet afmaak. Ook jullie telefonische vreugdedansje is me dierbaar. Fer, je hebt het van grotere afstand gevolgd, maar wel een fijne bijdrage aan mijn Engels geleverd toen dat nodig was.

Ook belangrijk: paranimfen. Kristel en Joost, jullie zijn tijdens die verdediging het meest zichtbaar voor anderen, maar in alle jaren daarvoor hebben jullie me ook altijd met raad –en wanneer nodig met daad of plaksnor- terzijde gestaan. Edwin, bedankt voor de kaft, daar ga ik nog vaak glimlachend naar kijken, en voor alle fietsavonturen. Dolf, Frank, Gerrit, Janwillem: laten we OLRE op peil houden.

Andere leuke dingen, waarvan het jammer is dat ze er zo weinig van gekomen zijn: Doeschka die leuke dingen regelt, Gert-Jan om na het sowieso hardlopen in slecht weer Holland Sport mee te kijken, en Joline die directe vragen stelt. Wat er wel veel van kwam is spelen met de Wilde Spinazies. Bedankt voor de afleiding en de onovertroffen zeegras-imitaties. Als Sjaak, Bas of dr. Lex was ik dat boekje meestal wel gauw vergeten.

Koos, eind 2004 was je de eerste aan wie ik vertelde dat ik ging promoveren. Niks voor jou, maar je vond het wel heel mooi dat je grote broer 'doctor' ging worden. Dat heeft even geduurd. Nu zit je vast op een wolkje te kijken naar zo'n gekke dag als van de verdediging. Je zou mij uitgelachen hebben om mijn rare pinguïnpak, en gezegd hebben dat ik al die mensen die lastige vragen stellen maar gewoon in elkaar moest slaan. Anders kwam je daar wel even bij helpen. Daarna zou je met mijn vrienden grapjes over mij maken, en soms trots naar me kijken.

Nikki, rondjes fietsen is leuker dan postzegels plakken –toch was het erg fijn dat je daar mee hielp. Caroline, je bedrijfslogo is erg treffend, al dacht ik soms meer aan een bulldozer dan een kruiwagen. Gelukkig begint de universiteit steeds meer te erkennen dat mensen als jij soms hard nodig zijn voor studenten en aio's.

Marcel, jij hebt mij de gelegenheid gegeven om te doen wat ik zelf nodig vond, er op vertrouwend dat het met de juiste mensen erbij wel goed komt. Je zorgvuldige en positieve herformuleringen van mijn nog twijfelende teksten neem ik als voorbeeld. Wim, je interesse en

positieve uitstraling hebben sommige onderwerpen een stuk helderder gemaakt. Martin, ik vond het erg jammer dat je naar Texel verhuisde: zoveel voorbeelden of sparringpartners op biogeomorfologisch gebied zijn er helaas niet aan de TU. Ik ben nog wel steeds blij dat je ooit een leuk afstudeeronderwerp in de aanbieding had, en dat je deze promotieplek iets voor mij vond. Zonder biologie is morfologie niet compleet.

Inhoudelijk wil ik vooral Rob bedanken. Jouw kennis van hydrodynamica en wiskunde, plus een deel van je vrije tijd, liggen aan de basis van het plantbuigingsmodel. Ik heb veel van je geleerd, en gelukkig heb je een enorm geduld met uitleggen. Tjeerd, ook van jou heb ik veel geleerd: goede vragen stellen, in plaats van in oplossingen denken bijvoorbeeld. En hoe ingenieurs en ecologen iets voor elkaar kunnen betekenen. Die samenwerking en discussie, ook met Marieke, Peter en Tjisse, was leuk en leerzaam.

Ook binnen de TU was het vaak leuk werken, niet alleen vanwege het buiten lunchen in bij de 'vloestofvijver', de vrijdagmiddag beats van Ruben & Jaap of een bottertocht. Bas, je was een fijne kamergenoot – niet alleen vanwege je matlabkennis. Walter, dat gezamenlijk tentamens afnemen was best leuk, maar aan die conferentie in Esperance heb ik toch betere herinneringen. Nog bedankt voor één van de beste adviezen die ik in deze jaren kreeg: 'Ga op vakantie man.' Marije, Bianca, jullie waren een belangrijke sociale factor op de 3e verdieping. En Mexico was een mooi terrein voor een surf/road trip. Sierd, Matthieu: veel dank voor jullie hulp bij het soms middernachtelijke meten vanuit ons privé-kasteel in Dinard (Jérôme Fournier et Laurent Godet du Muséum national d'Histoire naturelle, merci beaucoup!). Wim, het voetballen was leuk, net als het met een bakkie filosoferen over hoe van alles beter zou kunnen. Tomo, toen je begon kon ik je nog een beetje op weg helpen, daarna ging jij veel sneller.

Naast alle andere collega-aio's ook dank aan Adeeba, Chantal, Inge, Judith en Mark voor het regelen van allerlei dingen en zorgen dat alles loopt. Wilfred en Ad: bedankt voor de plant-gerelateerde artikelen in mijn postvak. Leuke dingen buiten Delft: voetballen met Twentse aio's tijdens de NCK-summarschool op Texel, door Luxemburgse riviertjes struinen tijdens een veldwerkweek van de afdeling Watermanagement, en enigszins met geografen-ogen leren kijken tijdens een week Denemarken met geografen uit Utrecht.

Tot slot wil ik mijn Deltares collega's bedanken voor hun hulp, interesse, flexibiliteit, afleiding of samenwerking: Bas, Bregje, Ellis, Harriëtte, Luca, Mindert, Paul, Sharon met name, maar de rest net zo goed.

## Curriculum Vitae

I was born on August 10<sup>th</sup> 1978 in Vlissingen, where I grew up and graduated from secondary school, the Stedelijke Scholengemeenschap Scheldemond (VWO), in 1996. Fascinated by how things work, I started studying Civil Engineering at Delft University of Technology. Given the environment in which I grew up –next to the sea–, Hydraulic Engineering was a natural interest. Especially when combined with biology, as I discovered during my M.Sc. graduate research on ‘The effect of vegetation on scroll-bar formation’ that involved fieldwork in the Allier and Volga Rivers in 2003.

After a year of teaching Infrastructure and Environmental Engineering at Mondriaan College (MBO), I started the PhD research leading to this thesis, with the Hydraulic Engineering section of Delft University of Technology. During this research I co-operated with Deltares and the Centre for Estuarine and Marine Ecology of the Netherlands Institute for Ecology (NIOO-CEME, now NIOZ Yerseke), conducting experiments in their laboratory flume and using their equipment for a fieldwork campaign France.

Since 2008 I work as a consultant/researcher at the Water Quality and Ecology department of the Marine and Coastal Systems unit of Deltares.